DOI: 10.1070/RCR4865

Non-classical covalent bonds

Vladimir A. Starodub, Tatyana N. Starodub

Institute of Chemistry, Jan Kochanowski University,
G Świętokrzyska st. 15, 25-406 Kielce, Poland

The possibility of multiple bond formation between Periodic Table Group 13 – 15 elements is considered. The ways of triple bond formation between these elements are discussed; particular attention is paid to the B≡B triple bonds. New non-linear compounds with triple bonds and their molecular structures are considered. The causes are given for the formation of compounds with unusually short distances between chemically non-bonded atoms. The grounds of the theory of two-centre three-electron bonds are presented and conditions of existence of isolated square planar carbon clusters are analyzed. The bibliography includes 181 references.

Contents

1. Introduction 717
2. Multiple bonds between atoms of Group 13 and 15 elements 718
3. Multiple bonds B – X (X = O, F) and B – B 723
4. Triple bonds between atoms of Group 13 and 14 elements 736
5. Unusually short distances between chemically non-bonded atoms 738
6. Two-centre three-electron bonds 740
7. Isolated square planar carbon complexes 744
8. Conclusion 746

1. Introduction

The development of foundations of quantum mechanics in 1925 – 1926 allowed chemists to understand for the fist time the nature of chemical bonding in simple molecules such as, for example, a hydrogen molecule. The study of Heitler and London [1] published in 1927 laid the ground of the valence bond (VB) method. In 1931, Pauling [2] developed the concept of orbital hybridization to interpret the equivalence and the tetrahedral geometry of bonds formed by carbon atoms in alkanes. A convenient tool of the VB method is the so-called theory of valence shell electron pair repulsion proposed by Sidgewick and Powell [3] and further developed by Gillespie and Nyholm.[4] (It is more appropriate to call it a model rather than a theory.) Despite the simplicity, this model is very useful in inorganic chemistry for structural data analysis; it also has some predictive power. For example, the hybridization concept and the valence shell electron pair repulsion model (VSEPM) easily explain the linear geometry of the acetylene molecule (H – C≡C – H) and non-linear geometry of the diazene molecule.

Diazene structures



Indeed, acetylene is formed by sp-hybridized orbitals arranged at an angle of 180°, while diazenes are composed of unhybridized p orbitals the angle between which is 90°. According to VSEPM, the linear geometry of the acetylene molecule is caused by tendency to minimize the repulsion of three bonds, the C≡C triple bond and two C – H single bonds, whereas in the case of diazene, repulsion of three bonds and two lone pairs takes place. There are numerous molecules and/or ions, the structures and the mere existence of which cannot be explained by the VB method. The best known examples of such molecules and ions are boron hydrides, polyhalide anions (Br_3^-, I_n^-, $n = 3-9$), noble gas compounds (XeF_2, XeF_4, XeF_6, HArF) and sulfur nitrides such as N_2S_2, N_4S_4 and poly(sulfur nitride) $(SN)_x$. A concept of hypervalence was developed as an extension of the VB method in order to describe these molecules [the molecular orbital (MO) method does not require this extension].[5, 6]

V.A.Starodub. Doctor of Chemical Sciences, Professor of the Chemical Engineering Department of the Institute of Chemistry, Jan Kochanowski University.
Telephone: +48(041)349 – 7058, e-mail: starodub@ujk.edu.pl
T.N.Starodub. Candidate of Chemical Sciences, Adjunct at the same Department.
Telephone: +48(041)349 – 7058, e-mail: starodub@ujk.edu.pl
Current research interests of the authors: synthetic metals and semiconductors, molecular magnets, coordination compounds, radical ion salts.

Received 9 October 2018
Translation: Z.P.Svitanko

© 2019 Uspekhi Khimii, Russian Academy of Sciences and Turpion Ltd.

Despite the wide use of the alternative MO theory, the VB method still remains popular in chemistry, first of all, owing to good visual presentation.

According to the VB method, all Period 2 elements can be divided into electron-deficient (Li, Be and B) and electron-rich (N, O, F, Ne) ones. In this context, carbon holds a unique position: this is the only element the valency of which, defined by the number of valence electrons, is equal to its coordination number, defined by the number of valence orbitals. Proceeding from their electronic structures, beryllium and boron cannot form multiple bonds with like atoms. However, multiple bonds can arise between (electron-deficient) boron atoms and (electron-rich) nitrogen atoms.

Currently, complexes with multiple bonds between Group 13 atoms have also been synthesized, although quite recently this was considered impossible. The relevance of this line of research is indicated by reviews,[7–16] which consider particular aspects and problems of the modern chemical bond theory. This review addresses the possibility of formation of multiple bonds between Group 13–15 elements. The consideration also includes compounds with unusually short distances between atoms that are not chemically bonded and compounds with two-centre three-electron bonds. Conditions of formation of isolated square planar carbon complexes synthesized in 2000 are discussed.[17]

The following abbreviations and designations are used in the review:

AO — atomic orbital,
CAAC — 1-(2,6-diisopropylphenyl)-3,3,5,5-tetamethylpyrolidin-2-ylidene,
Cp — cyclopentadienyl,
Dipp — 2,6-diisopropylphenyl,
Dis — bis(trimethylsilyl)methyl,
DME — dimethoxyethane,
DFT — density functional theory,
Dur — 2,3,5,6-tetramethylphenyl,
Eind — 1,1,3,3,5,5,7,7-octaethyl-*s*-hydroindacen-4-yl,
H_3(OOO) — 2,6-bis(3-*tert*-butyl-2-hydroxy-5-methylbenzyl)-4-*tert*-butylphenol,
HOMO — highest occupied molecular orbital,
Idip — 1,3-bis(2,6-diisopropylphenyl)imidazol-2-ylidene,
IMe — 1,3-dimethylimidazolin-2-ylidene,
IRR — irreducible representation,
Mes — 2,4,6-timethylphenyl (mesityl),
MO — molecular orbital,
Naph — naphthyl,
NHC — N-heterocyclic carbene,
NICS — nucleus independent chemical shift,
(*p*-methyl)form — *N*,*N*′-bis(4-methylphenyl)formamidinate,
(*p*-methoxy)form — *N*,*N*′-bis(4-methoxyphenyl)formamidinate,
r_e — internuclear distance,
SOMO — singly occupied molecular orbital,
Tbt — 2,4,6-tris[bis(trimethylsilyl)methyl]phenyl,
TfO — trifluoromethylsulfonate (triflate),
tmeda — tetramethylethylenediamine,
Trip — 2,4,6-triisopropylphenyl,
US — ultrasound,
VB — valence bonds,
VSEPM — valence shell electron pair repulsion model,
WBI — Wiberg bond index.

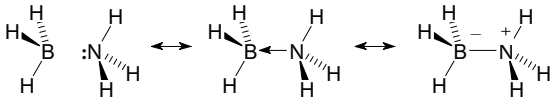
2. Multiple bonds between atoms of Group 13 and 15 elements

The reaction of diborane dissolved in tetrahydrofuran with ammonia gives the salt $[H_2B(NH_3)_2]^+(BH_4)^-$,[18] whereas borane reacts with ammonia to yield a complex [reaction (1)].

$$BH_3 + NH_3 \longrightarrow [H_3B{\leftarrow}NH_3] \quad (1)$$

In this complex, a donor-acceptor π-bond is formed with participation of the vacant orbital of the boron atom and the lone pair of nitrogen. The length of this bond is 1.58 Å. Despite the formal structural similarity of this complex with ethane, their properties are considerably different. Indeed, ethane is a gas, while the complex $[H_3BNH_3]$ is a solid with a melting point of 97.6 °C. The differences are due to highly polar bonds in the complex (Scheme 1).

Scheme 1



The difference is also manifested in the dehydrogenation [reactions (2) and (3)]: ethane dehydrogenation is an endothermic reaction, while dehydrogenation of the cpmplex $[H_3B{\leftarrow}NH_3]$ is exothermic.[19]

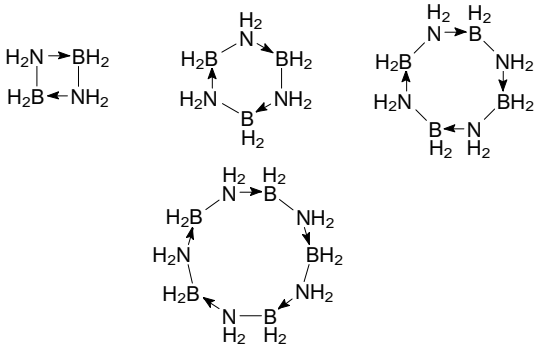
$$H_3C-CH_3 \longrightarrow H_2C{=}CH_2 + H_2; \quad (2)$$
$$\Delta H_{298} = 32.6 \text{ kcal mol}^{-1}$$

$$[H_3B{\leftarrow}NH_3] \longrightarrow H_2B{=}NH_2 + H_2; \quad (3)$$
$$\Delta H_{298} = -5.1 \text{ kcal mol}^{-1}$$

This difference is caused by the fact that the weak donor-acceptor B←N bond is replaced by the stronger covalent σ-bond arising from overlap of the sp^2-hybrid orbitals of nitrogen and boron, while the donor-acceptor bond is strengthened because of the decrease in the B–N distance.

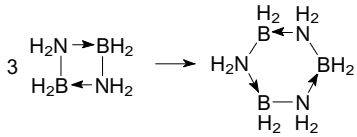
Aminoborane H_2BNH_2 is an isoelectronic analogue of ethylene; however, unlike ethylene, it has a higher dipole moment (1.84 D) and low stability and forms cyclic oligomers or polymers.[20] Aminoborane, as well as cycloborazanes $(H_2BNH_2)_n$, $n = 2-5$, were obtained by reactions of sodium amide ($NaNH_2$) with the salt $[H_2B(NH_3)_2]^+(BH_4)^-$ in liquid ammonia.[21]

Cycloborazane structures



Cycloborazanes are stable up to 100 °C, but in solutions, the dimer is slowly converted to the trimer (Scheme 2).[21]

Scheme 2

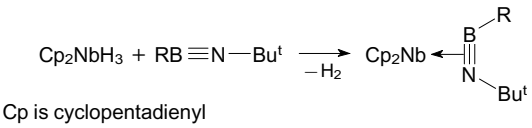


The geometric parameters determined by microwave spectroscopy[22] confirm the presence of a double bond in the aminoborane molecule: the B–N bond length is 1.39 Å (*versus* 1.58 Å in [$H_3B{\leftarrow}NH_3$]).

The unstable HBNH molecule was studied by spectroscopy.[23] The boron–nitrogen bond length (1.2381 Å) corresponds to a triple bond between these elements: HB≡N–H. The atomic orbitals (AOs) in this molecule are sp-hybridized; both hybrid orbitals are involved in the formation of σ-bonds with hydrogen atoms and the boron–nitrogen bond. The p orbitals form π-bonds, one common covalent bond and one donor-acceptor bond.

Iminoboranes RB≡NR′ (here and below, unless stated otherwise, the characters R and R′ stand for an organic group such as alkyl, aryl, *etc.*) are isoelectronic to acetylenes, while their structure and reactivity are similar to those of substituted acetylenes, *e.g.*, RC≡CF. The coordination of iminoboranes to transition metals may be accompanied by dimerization to give tetrahapto-bonded four-membered BNBN rings similar to cyclobutadiene.[24] Like for acetylenes, coordination of the B≡N bond is possible (Scheme 3).[24]

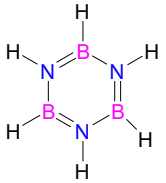
Scheme 3



Cp is cyclopentadienyl

As opposed to acetylene, unsubstituted iminoborane H–B≡N–His readily trimerizes to borazine.

Borazine structure



Borazine can also be prepared by thermolysis of [H_3BNH_3] according to reaction (4).

$$3\,[H_3B{\leftarrow}NH_3] \longrightarrow (HBNH)_3 + 6\,H_2 \qquad (4)$$

Borazine is an isostructural and isoelectronic analogue of benzene. Its physical properties (phase ranges, density) are similar to those for benzene. However, the chemical properties of these compounds are considerably different.

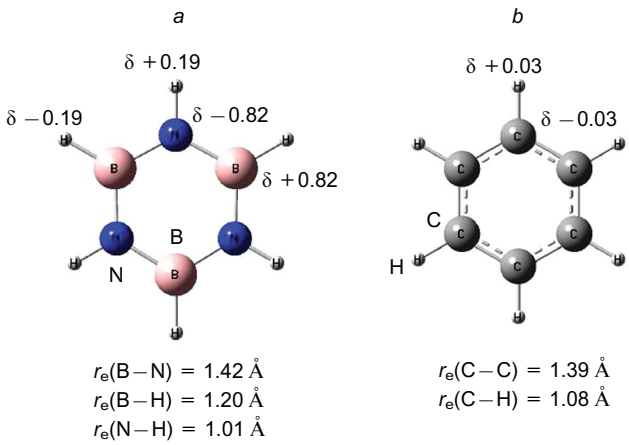
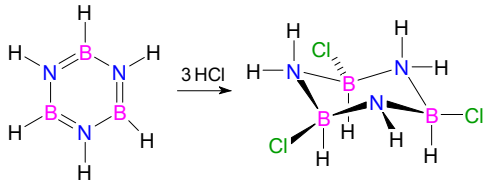


Figure 1. Distribution of the partial conventional charge (δ) and internuclear distances (r_e) for borazine (*a*) and benzene (*b*) (see http://ifasonline.com/theme/images/ChemicalScience/topic-30_image-11_mobile.png, accessed May 8, 2019).

Due to large electronegativity difference (the Pauling electronegativity is 2.0 for boron and 3.0 for nitrogen), the charge distribution in the borazine molecule is favourable for the nucleophilic attack on boron atoms and electrophilic attack on nitrogen atoms (Fig. 1).

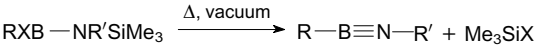
Although the borazine molecular orbitals resemble benzene MOs, there are still differences: for bonding MOs, the electron density is higher on nitrogen atoms and for antibonding MOs, it is higher on boron atoms.[25] Borazine is more reactive than benzene and is more prone to addition reactions (Scheme 4).

Scheme 4



The substituted aminoboranes and iminoboranes are more stable; therefore, they were structurally characterized (Fig. 2). The substituted iminoboranes R–B≡N–R′ (**1**) can be obtained by pyrolysis of (trimethylsilylamino)boranes (Scheme 5).[26,27]

Scheme 5



X = Br, Cl, F, OMe

Compounds **1** are stable only at low temperatures, while under ambient conditions, they undergo cyclodi-, cyclotri- and cyclotetamerization and polymerization to give products **2**–**5** as shown in Scheme 6.[28] It can be seen that the course of the reaction (pathways *a*–*e*) and the structure of products depend on the size of substituents R and R′: in the case of bulky branched substituents, four-membered rings resembling cyclobutadiene are formed, non-branched R and R′ groups result in product mixtures formed according to

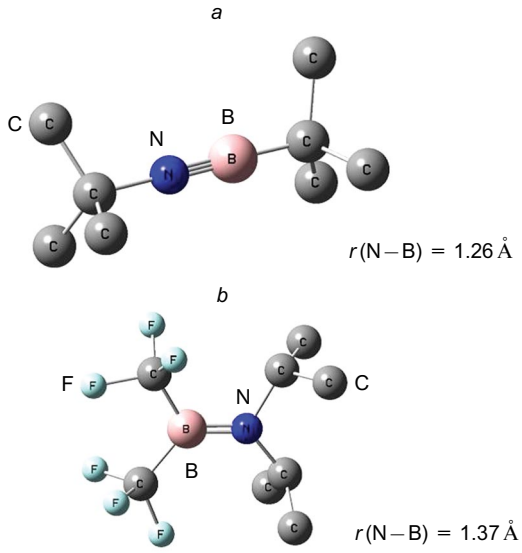
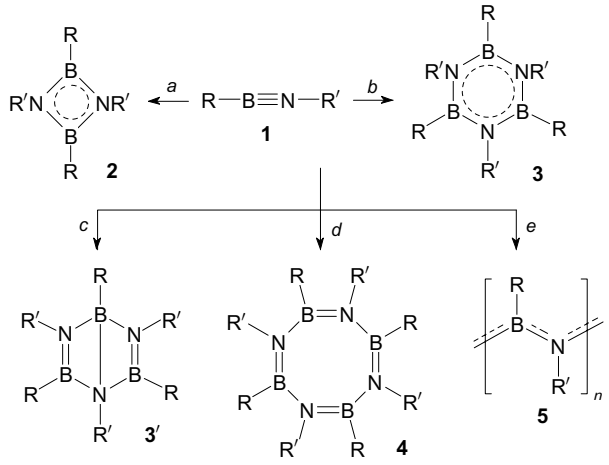


Figure 2. Structural models of amino- (*a*) and iminoboranes (*b*). The hydrogen atoms are omitted for the sake of simplicity (see http://ifasonline.com/theme/images/ChemicalScience/topic30_image15_mo-bile.png, accessed May 8, 2019).

Scheme 6



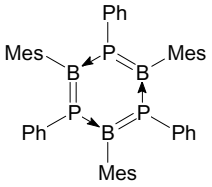
2: R = R′ = Bu^s,[29] Bu^t;[30] R = Bu^t: R′ = SiMe$_3$,[31] Mes;[31] R = C_6F_5, R′ = Bu^t;[32] **3**: R = R′ = Me,[33] Et,[33] Pr^n,[29] Pr^i,[29] Bu^n,[29] Bu^i,[29] Bu^s;[29] R′ = Bu^t: R = Me,[34] Et,[26] Pr^n,[26] Bu^n;[26] **3′**: R = Bu^t: R′ = Ph,[31] Pr^i,[35] Bu^s;[31] **4**: R = Bu^t, R′ = Me;[31] **5**: R = R′ = Et,[33] Pr^n,[29] Bu^n,[29] Bu^i;[30] Mes is 2,4,6-trimethylphenyl (mesityl)

pathways *c* and *d*, while borazines (pathway *b*) are produced with substituents of medium size.

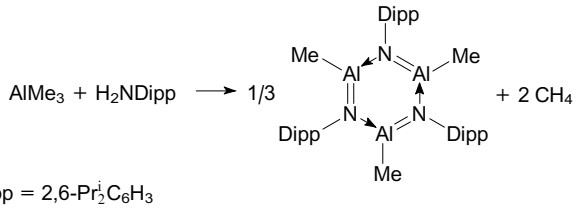
Double bonds can also exist in $H_2A{=}XH_2$ type molecules, where A is Group 13 element and X is Group 15 element. For example, double bonds exist in $R_2B{=}PR'_2$ and $R_2B{=}AsR'_2$, where R, R′ are alkyl or aryl.[36] The B–P bond lengths in the $Mes_2B{-}PMes_2$ and $Mes_2B{-}PBu^t_2$ molecules are 1.839 and 1.844 Å, respectively, which is less than the sum of the boron and phosphorus covalent radii (0.82 and 1.10 Å). The cyclic molecule $(PhPBMes)_3$ is the P-analogue of borazine.[36]

The reaction shown in Scheme 7 was used to prepare Al analogues of borazine called alumazenes.[8,36]

Structure of P-analogue



Scheme 7



Dipp = 2,6-Pr$^i_2$C$_6$H$_3$

The aromaticity of alumazene is confirmed by the fact that the $Al_3N_3C_6$ moiety is planar. In this case, the sp^2-hybrid orbitals of aluminium and nitrogen form a system of σ-bonds and the vacant p orbitals of aluminium and the lone pairs of nitrogen form a system of donor-acceptor π-bonds.

The $H_2A{=}XH_2$ molecules should be planar (C_{2v} symmetry), which is optimal for the donor-acceptor π-bond to form. The configuration twisted by 90° has no π-bond. The energy difference between the planar and twisted forms can be considered to be equal to the internal rotation barrier (Fig. 3). Quantum chemical calculations using the *ab initio* CCSD(T) method with the complete basis set (CBS) were carried out[19] for the two conformations of the $H_2B{=}NH_2$, $H_2Al{=}NH_2$, $H_2B{=}PH_2$ and $H_2Al{=}PH_2$ molecules. The bond energies for the $[H_3A{\leftarrow}XH_3]$ donor-acceptor complexes are summarized in Table 1.

Table 1. Energy of the donor-acceptor σ-bond in the complexes $[H_3A{\leftarrow}XH_3]$ (kcal mol^{-1}).[19]

Complex	T = 0 K	T = 298 K	Ref.[a]
$[H_3B{\leftarrow}NH_3]$	25.9	27.2	37
$[H_3Al{\leftarrow}NH_3]$	26.1	27.3	38
$[H_3B{\leftarrow}PH_3]$	21.1	22.5	38
$[H_3Al{\leftarrow}PH_3]$	14.0	14.7	38

[a] References are given to papers describing the preparation of complexes.

Dehydrogenation of these complexes yields the products $H_2A{=}XH_2$, in which sp^2-hybrid orbitals form the A–X σ-bonds, while the donor-acceptor π-bonds are formed by the vacant orbitals of element A and lone pairs of element X. The results of calculation of the rotation barriers (π-bond energies) and dissociation energy of $H_2Al{=}XH_2$ molecules are summarized in Table 2.[19]

As can be seen from Table 2, the σ- and π-bond energies regularly decrease with increasing atomic size. The highest rotation barrier (29.9 kca mol^{-1}) in the $H_2B{=}NH_2$ molecule is still considerably lower than that for ethylene (65 kcal mol^{-1}).[39] Note that the $H_2B{=}PH_2$ and $H_2Al{=}PH_2$ molecules are non-planar and have C_s symmetry. This unexpected result obtained by Douglas *et al.*[39] was

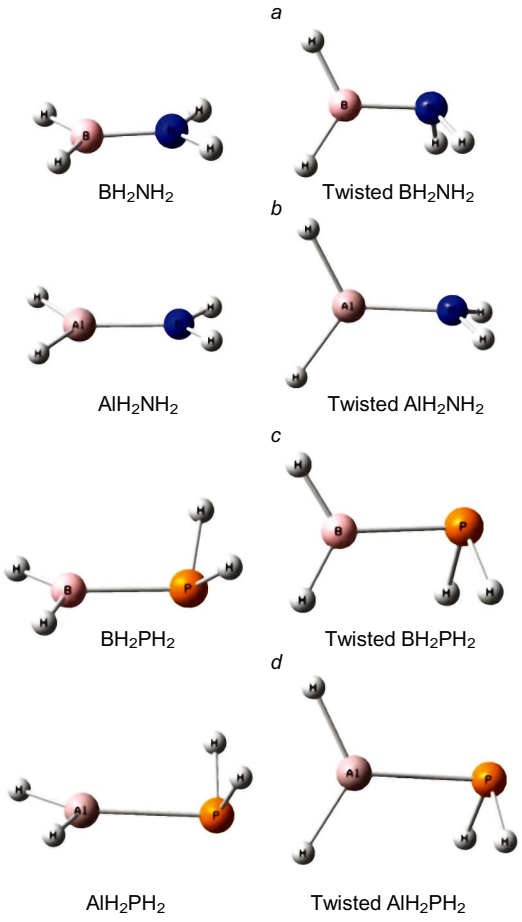


Figure 3. Optimized molecular structures of $H_2B{=}NH_2$ (*a*), $H_2Al{=}NH_2$ (*b*), $H_2B{=}PH_2$ (*c*), $H_2Al{=}PH_2$ (*d*) (on the left) and the corresponding structures without π-bond (on the right).[19]

Table 2. Rotation barriers (π-bond energies) and dissociation energies of the $H_2A{=}XH_2$ molecules (kcal mol^{-1}).[19]

Molecule	Total dissociation energy	Dissociation energy of σ-bonds	Rotation barrier
$H_2B{=}NH_2$	139.7	109.8	29.9
$H_2Al{=}NH_2$	109.3	98.8	10.5
$H_2B{=}PH_2$	86.8	77.6	9.2
$H_2Al{=}PH_2$	71.0	68.3	2.7

confirmed by other studies of the $H_2A{=}XH_2$ and $HA{\equiv}XH$ molecules (see below).

Since the π-bond energy between the A and X atoms in $H_2A{=}XH_2$ rapidly decreases with increasing atomic number of the elements, the existence of compounds $H_2B{=}XH_2$ with antimony or bismuth is unlikely. Nevertheless, analogous molecules with a triple bond — $HB{\equiv}XH$ — can exist.

It was shown [7, 40] that the $B{\equiv}P$ and $B{\equiv}Sb$ triple bonds are possible in compounds $RB{\equiv}PR$ and $RB{\equiv}SbR$. The authors carried out density functional theory (DFT) calculations for the $RB{\equiv}SbR$ molecules, where R = H, OH, F, Me, SiH_3, $SiMe(SiBu^t_3)_2$, $SiPr^iDis_2$ [Dis = $CH(SiMe_3)_2$], NHC (NHC is N-heterocyclic carbene). According to the

Table 3. Wiberg bond indices for $RB{\equiv}SbR$.[40]

R	WBI	R	WBI
H	1.944	SiH_3	2.129
OH	1.763	$SiMe(SiBu^t_2)_2$	2.349
F	1.756	$SiPr^iDis_2$	2.177
Me	1.988	NHC	2.126

Note. The WBI of acetylene is 2.99.

results, the triple bond in these molecules is very weak [this can be evaluated in terms of the Wiberg bond index (WBI), which characterizes the chemical bonds in closed-shell molecules, if their structures have been calculated within the zero differential overlap approximation [41]]. Table 3 presents the calculated Wiberg bond indices for some $RB{\equiv}SbR$ molecules with small or bulky substituents.[40]

The bonds in the $RB{\equiv}SbR$ molecules have been described using two models: model *A* implies the presence of a donor-acceptor σ-bond and two donor-acceptor π-bonds, with boron being the donor atom for the σ-bond and antimony being the donor atom in the π-bonds; according to the second model (model *B*), the molecule is

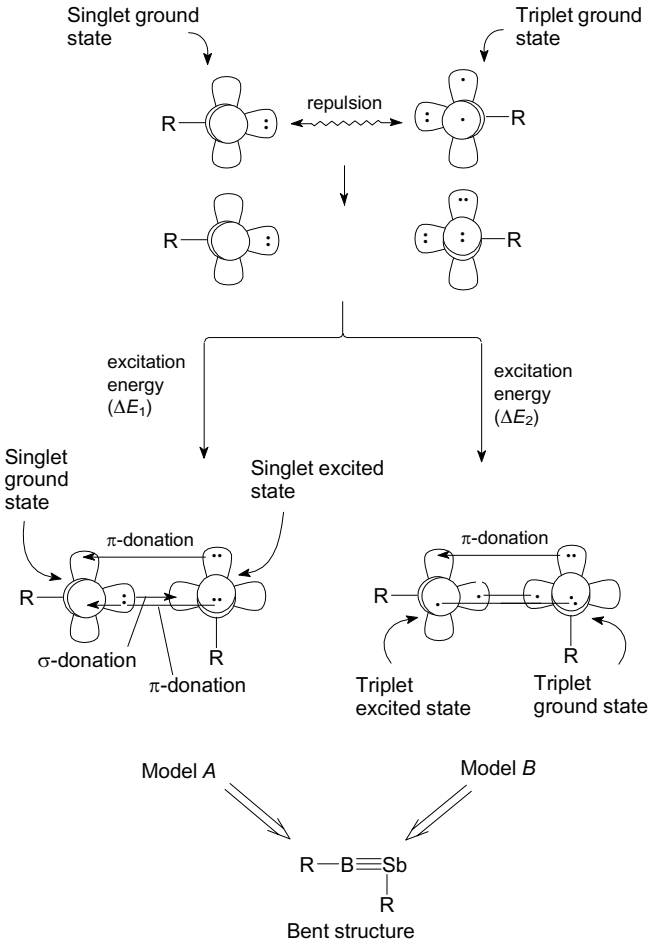


Figure 4. Models *A* and *B* corresponding to triple bond formation in the $RB{\equiv}SbR$ molecules.[7, 40]

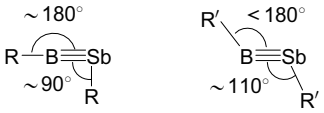
formed by a common B – Sb covalent bond and two donor-acceptor bonds, with antimony being the donor.

The details of triple bond formation are shown in Fig. 4.[7, 40] It can be seen that in model *A*, the boron atom is sp-hybridized, one sp-hybrid orbital is used to form the covalent bond with the group R, while the other one, being more stable than unhybridized p orbitals, bears a lone electron pair (singlet ground state, see Fig. 4). The antimony atom uses the 5p orbital for the bond with the substituent R, while the remaining two 5p electrons occupy one of the two 5p orbitals (singlet excited state, see Fig. 4). This gives rise to a donor-acceptor B→Sb σ-bond and two donor-acceptor π-bonds. In model *B*, the boron atom is in the triplet excited state (one electron in the sp-hybrid orbital and one is in the 2p orbital), while the antimony atom is in the triplet ground state (two unpaired electrons in the 5p orbitals and one lone pair, $5s^2$). This results in the formation of the covalent B – Sb σ-bond, one covalent π-bond and one donor-acceptor π-bond. It is worth noting that according to both models, RB≡SbR molecules are non-linear! (This result is at variance with the commonly accepted model of a triple bond.)

The results of calculations[40] confirm this conclusion: molecules with small substituents exist as form **6a**, while those with bulky substituents R′ occur as form **6b**.

In any case, the triple bond in RB≡SbR is weak, as indicated by the Wiberg bond indices. The electronic structures of these molecules with small substituents are more adequately described by model *A*, whereas molecules with large substituents are better described by model *B*. Irrespective of the nature of the substituent R, the RB≡SbR molecules are non-linear.

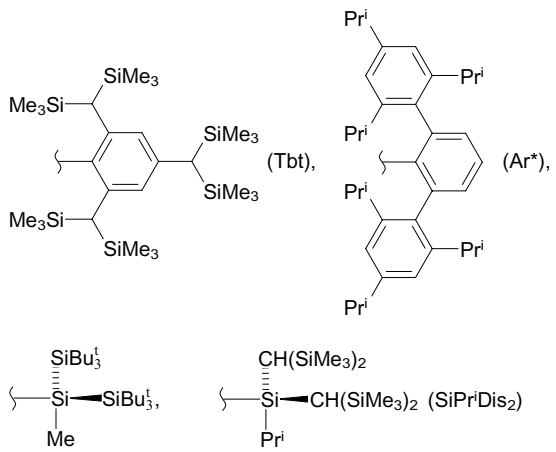
Structures 6



6a **6b**

The data of some studies[7, 40] seemingly rule out the existence of RB≡BiR (too large difference between the sizes of valence orbitals — boron 2p orbitals and bismuth 6p orbitals). Nevertheless, the possibility of synthesizing these compounds was demonstrated in 2016.[42] The authors carried out DFT calculations for the RB≡BiR molecules, where R = H, OH, F, Me, SiH_3 or the bulky substituents depicted below.

Substituent structures



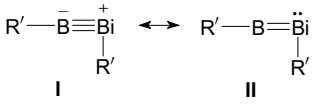
The results are similar to those obtained for RB≡SbR, particularly, the RB≡BiR molecules are non-linear and WBI > 2 for bulky substituents confirm the presence of a triple bond (Table 4).

Table 4. Wiberg bond indices for RB≡BiR (**6a**).[42]

R	WBI	R	WBI
H	2.016	$SiMe(SiBu^t_3)_2$	2.34
OH	1.720	$SiPr^iDis_2$	2.37
F	1.705	Ar*	2.25
Me	1.944	Tbt	2.19
SiH_3	2.135		

The compounds R′B≡BiR′ with bulky substituents are kinetically more stable (polymerization is hampered by steric factors). The WBI ranging from 2.19 to 2.37 clearly point to triple bonds. According to Lu *et al.*,[42] the electronic structures of the R′B≡BiR′ molecules are described by resonance forms I and II.

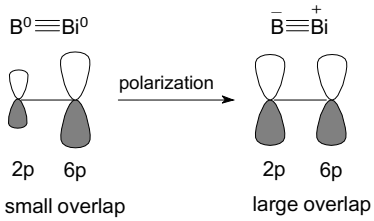
Resonance forms I and II



I **II**

The bond polarization in form I is due to the electronegativity difference between boron and bismuth (boron is more electronegative). The increased electron density in the boron orbitals leads to orbital expansion, whereas the decrease in the electron density in the bismuth orbitals results in orbital contraction. As a consequence, the orbital sizes become equal (Scheme 8).

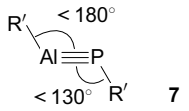
Scheme 8



It is noteworthy that this explanation is too cumbersome: the electronegativity difference between boron and bismuth is not so large to cause this effect: boron has a Pauling electronegativity of 2.04 and an Allred – Rochow electronegativity of 2.01; the Pauling and Allred – Rochow electronegativities of bismuth are 2.02 and 1.67, respectively (Ref. 43, p. 214).

Lu *et al.*[44] theoretically demonstrated the possibility of synthesis of compounds with an Al≡P triple bond. In the compounds R′Al≡PR′ (**7**), the aluminium and phosphorus atoms are linked by one σ-bond, one π-bond and one donor-acceptor π-bond. Typically, all these molecules are non-linear.

Structures 7



7

In 2018, compounds with the indium – antimony triple bond were shown to exist.[45] According to calculations, the R – In≡Sb – R molecules containing small substituents (R = H, F, OH, Me, SiH_3) are unstable. However, if the R′ – In≡Sb – R′ molecules contain bulky, sterically hindered groups {R′ = $SiMe(SiBu^t_3)_2$, $SiPr^i Dis_2$, $C_6H_2[CH(SiMe_3)_2]_3$-2,4,6, $C_6H_3(C_6H_2Pr^i_3$-2,4,6$)_2$-2,6}, there is a global minimum in the potential energy surface of the singlet state of the molecule; therefore, such indium antimonides are thermodynamically stable. The most probable type of bonding in these molecules corresponds to the formula R′In⇇SbR′, *i.e.*, one common σ-bond, one common π-bond and one donor-acceptor π-bond are present. Hence, the R′ – In≡Sb – R′ moieties are non-linear (Fig. 5).

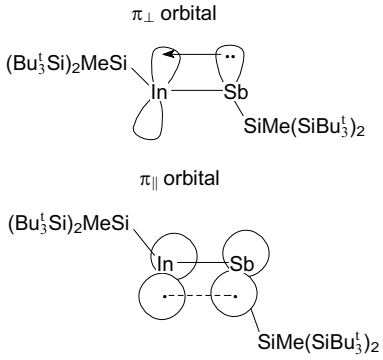
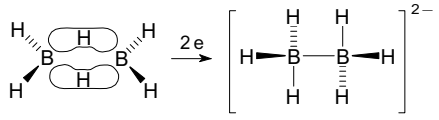


Figure 5. π-Orbitals of the In≡Sb moiety in the [(Bu$^t_3$Si)$_2$MeSi]In≡Sb[SiMe(SiBu$^t_3$)$_2$] molecule.[45]

3. Multiple bonds B – X (X = O, F) and B – B

Diborane B_2H_6, in which the boron atoms are bonded *via* two bridging hydrogen atoms (three-centre two-electron bond), forms the $[B_2H_6]^{2-}$ dianion isoelectronic to the ethane molecule. Indeed, each of these species has 12 valence electrons and, according to the isoelectronic principle, they should have identical structures. The reduction of diborane with sodium or potassium amalgam is accompanied by cleavage of the B – H – B bridging bonds to give a B – B covalent bond (Scheme 9).[46]

Scheme 9

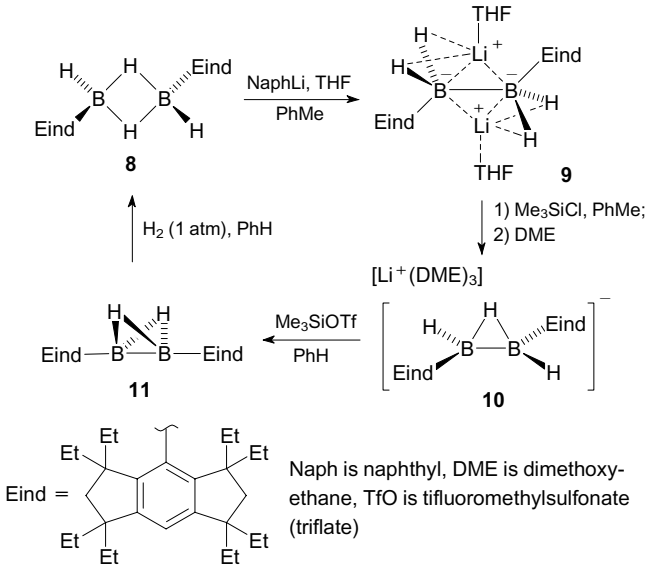


Similarly, the B=B double bond with a 1.613 Å length exists in the $[B_2H_4]^2$ dianion, which is isoelectronic to ethylene.[47]

The reduction of Mes_2B – BPhMes with lithium in a diethyl ether – hexane mixture affords a compound with the B=B double bond, namely, [{$(Et_2O)Li$}$_2$(Mes_2B=BPhMes)].[48] The dihedral angle between the planes of the Mes_2B and BPhMes moieties decreases from 79.1 to 7.3°, while the boron – boron bond length varies from 1.706 to 1.636 Å, which corresponds to the length of the B=B double bond. Thus, the Mes_2B – BPhMes molecule is virtually planar and its double bond is formed upon two-electron reduction.

In 1935, Stock *et al.*[46] described the salts $Na_2[B_2H_6]$ and $K_2[B_2H_6]$. However, for a long time, researchers failed to confirm the presence of the σ-bond in the $[B_2H_6]^{2-}$ dianion. The reason is its low stability; therefore, this anion should rather be regarded as an intermediate of diborane reduction, while $[BH_4]^-$ and $[B_3H_8]^-$ are the stable reduction products.[49] Only 76 years after the Stock's study, the description of $[B_2H_6]^{2-}$ as anion containing a B – B σ-bond was proved to be correct. This was done by using bulky 1,1,3,3,5,5,7,7-octaethyl-s-hydroindacen-4-yl substituents (Eind) in the diborane molecule (Scheme 10).[50]

Scheme 10



As indicated by Scheme 10, two-electron reduction of the sterically protected diborane (Eind)HB(μ-H)$_2$BH(Eind) (**8**) gives the ionic pair [Li^+(THF)]$_2$[(Eind)H_2BBH_2(Eind)]$^{2-}$ (**9**) with a stable σ-bond between the boron atoms.

The boron – boron distance equal to 1.924 Å is somewhat longer than the internuclear distance corresponding to the B – B single bond (1.72 Å) and longer than the distance between the boron atoms in diborane (1.82 Å). Hence, only weak interaction occurs between the (Eind)$H_2B^{-\bullet}$ radical anions, which is enhanced by B – H- - -Li^+ bonds.

On treatment with chlorotri(methyl)silane, compound **9** is partially dehydrogenated to yield hydrogen bridged compound **10** in which the σ-bond between the boron atoms is retained (see Scheme 10). The length of this bond in molecule **10** is typical of boron compounds with the B=B bonds, although it is longer than the bond in the salt [Li^+(THF)]$_2$[(Eind)HBBH(Eind)]$^{2-}$ in which this length is 1.616 Å.

Further dehydrogenation of compound **10** affords product **11** with two hydrogen bridges — (μ-H)$_2$(Eind)BB(Eind). The structure of deuterated compound **11** is shown in

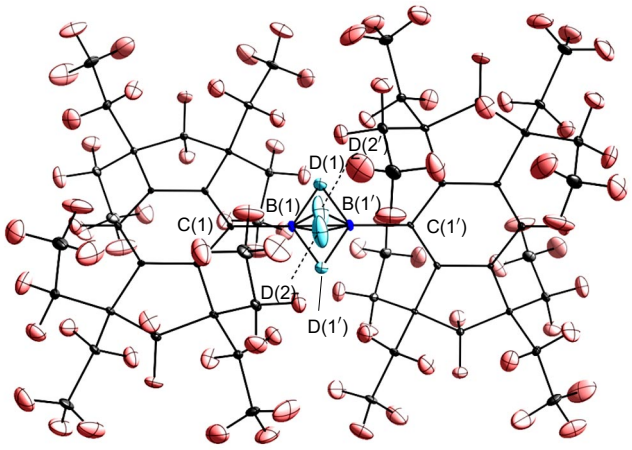
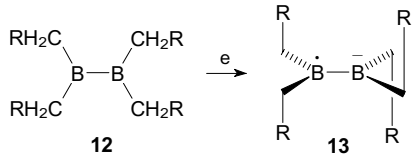


Figure 6. Molecular structure of (μ-D)$_2$(Eind)BB(Eind).[50] The B–B bond length is 1.483 Å.

Fig. 6. Treatment of **11** with hydrogen in benzene recovers the initial substituted diborane (Eind)HB(μ-H)$_2$BH(Eind) (**8**). Thus, the formation of a common B–B σ-bond upon cleavage of the three-centre two-electron B–H–B bond is possible when the diborane molecule contains bulky substituents.

The single-electron reduction of tetra(neopentyl)diborane (**12**) generates radical anion **13** with a single-electron π-bond (Scheme 11).[51]

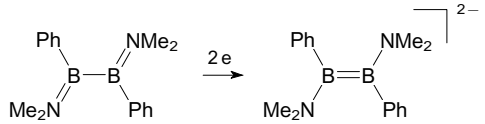
Scheme 11



R = Bu^t

The structure of this radical anion is similar to that of its isoelectronic analogue, tetra(neopentyl)ethylene radical cation. The latter is formed upon oxidation of tetra(neopentyl)ethylene with antimony pentachloride.[51] The substituted diboranes R(R$'_2$N)B–B(NR$'_2$)R (R = Ar or Alk) are analogues of substituted buta-1,3-dienes (Scheme 12).[52]

Scheme 12



As can be seen in Scheme 12, the boron atom uses its sp^2 hybrid orbitals to form three σ-bonds and the vacant 2p orbital of boron forms a π-bond with a nitrogen lone pair. The two-electron reduction generates a B=B double bond *via* overlap of boron 2p orbitals, each bearing one electron. In the initial diborane R(R$'_2$N)B–B(NR$'_2$)R, the B–N and B–B bond lengths are 1.399 and 1.714 Å, respectively. Upon reduction to the dianion according to Scheme 12, the B–N bond length increases to 1.560 Å, while the B–B bond length decreases to 1.623 Å.

A similar effect is observed in the reduction of tetraamino-substituted diboranes:[53] the length of the bond between boron atoms decreases from ~1.72 (in diboranes with B–B a single bond) to ~1.60 Å (in tetraamino-substituted diborane anions with the B=B bond). Note that the difference between the C–C and C=C bond lengths is greater and equals 0.2 Å. The smaller difference between the B–B and B=B bond lengths can be attributed to the electrostatic repulsion between negatively charged boron atoms in dianions.[53] Perhaps, the absence of electrostatic repulsion accounts for the fact that the B–B bond length in {Li(Et$_2$O)$_2$}[MeO(Mes)BB(Mes)OMe] with a π-bond order of 0.5 is only 1.636 Å, which is only slightly greater than that in diborane anions with a true double bond.[54]

The same effect was detected for the single-electron reduction of the substituted diborane (Mes)$_2$BBPhMes with potassium graphite (KC_8).[55] The B–B bond length in the [(Mes)$_2$BBPhMes]$^{-\bullet}$ radical anion is 1.654 Å. Thus, in the radical anions based on diboranes, the single-electron B–B π-bond (the bond order is 1.5) is only slightly longer than the usual two-electron bond (the B–B bond order is 2). This is caused by Coulombic repulsion between the likely charged boron atoms in dianions and the absence of this repulsion in radical anions.

As noted in Section 2, the electron-deficient borane BH_3 reacts with electron-rich ammonia to form the [$H_3B{\leftarrow}NH_3$] donor-acceptor complex (diborane does not react with ammonia). In 1937, the first boron-based carbonyl, borane carbonyl [$H_3B{\leftarrow}CO$], was prepared by the direct reaction between diborane and carbon monoxide.[56] This reaction, however, does not proceed to completion, but reaches equilibrium (5).

$$B_2H_6 + 2\,CO \rightleftharpoons 2\,[H_3B{\leftarrow}CO] \quad (5)$$

Gordy *et al.*[57] suggested that the reaction includes two steps depicted as reactions (6) and (7).

$$B_2H_6 \rightleftharpoons 2\,BH_3 \quad (6)$$

$$BH_3 + CO \rightleftharpoons [H_3B{\leftarrow}CO] \quad (7)$$

In the authors' opinion, this hypothesis is supported by the fact that trimethylamine easily and completely replaces carbon monoxide to give the stable complex [$(H_3C)_3N{\rightarrow}BH_3$].

$$[H_3B{\leftarrow}CO] + (H_3C)_3N \longrightarrow [(H_3C)_3N{\rightarrow}BH_3] + CO \quad (8)$$

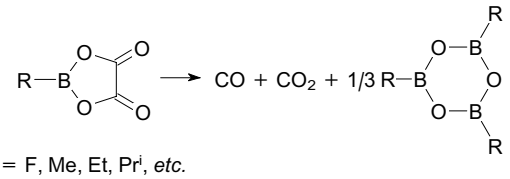
Unlike borane carbonyl, the complex with trimethylamine is highly stable: on heating for several hours at a temperature of 125 °C, no signs of decomposition are observed.

Due to the lack of stability of [$H_3B{\leftarrow}CO$], only in 1950, was it possible to determine its structural characteristics by microwave spectroscopy.[57] The bond lengths in the complex are 1.194 (B–H), 1.540 (B–C), and 1.131 Å (C–O). In 1976, an isomer of this complex, boroxine $(H_3CBO)_3$, and its derivatives were synthesized by thermolysis of boron oxalates (Scheme 13).[58]

The R–B≡O monomer readily trimerizes; in the case of R = F at a temperature of 1000 K, only traces of the monomer were detected.

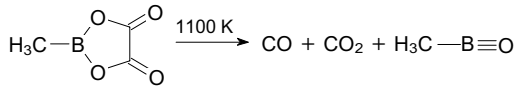
$$(FBO)_3 \rightleftharpoons 3\,F{-}B{\equiv}O \quad (9)$$

Scheme 13



Thirteen years later, Bock *et al.*[59] demonstrated the formation of monomeric $H_3C-B{\equiv}O$ upon thermolysis of an oxalate, 2-methyl-1,3,2-dioxaborolane-4,5-dione, at 1100 K (Scheme 14).

Scheme 14



It is noteworthy that the $H_3C-B{\equiv}O$ molecule is isoelectronic to the acetonitrile molecule ($H_3C-C{\equiv}N$), which suggests the existence of the $B{\equiv}O$ triple bond. This assumption was confirmed[59] by X-ray electron spectroscopy. The possibility of existence of the $B{\equiv}O$ triple bond was stated in a study[60] dealing with oxo(2,4,6-tri-*tert*-butylphenyl)borane — (sym-Bu^{t}Ph)$-B{\equiv}O$. In 1994, the isomeric $[H_3B{\leftarrow}CO]$ and $H_3C-B{\equiv}O$ molecules were studied by a quantum chemical method at the (U)MP2/6-3 lG* level using the Gaussian 92 program.[61] The results were in good agreement with experimental data (Fig. 7).

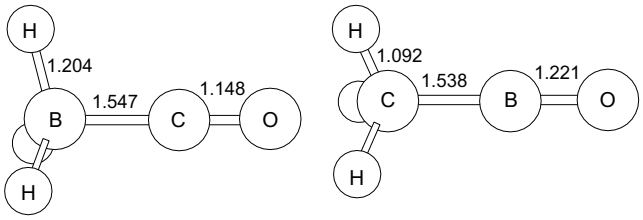


Figure 7. Calculated bond lengths (Å) in $[H_3B{\leftarrow}CO]$ and $H_3C-B{\equiv}O$.[61] The experimental bond lengths in the complex $[H_3B{\leftarrow}CO]$ are 1.540 (B – C) and 1.131 Å (C – O).

The B – O distance equal to 1.221 Å unambiguously indicates the presence of a triple bond. According to calculations,[61] the $H_3C-B{\equiv}O$ molecule is approximately 43 – 55 kcal mol^{-1} more stable than the borane carbonyl molecule (the scatter of energies is due to the use of different methods: MNDO, MP2/4-31G and MP2/6-31G*). In the VB model, the triple bond involves the boron sp-hybrid orbitals. One of them is used to form the bond with hydrogen, while the other forms the σ-bond with oxygen. The third valence electron of boron, being located in the 2p orbital, forms a π-bond with oxygen, while the vacant 2p orbital of boron is involved in the donor-acceptor π-bond with the oxygen lone pair.

In 2002, the stable complex $[(F_3C)_3B{\leftarrow}CO]$ was synthesized. The complex melted at 9 °C without decomposition and, hence, its structure was studied not only in the gas phase, but also in the crystal (Fig. 8).[62]

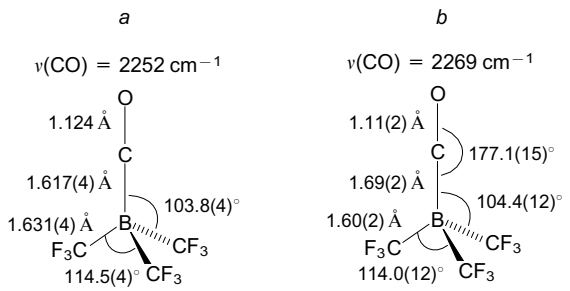


Figure 8. Molecular structure of $[(F_3C)_3B{\leftarrow}CO]$ in the gas phase (*a*) and in the crystalline state (*b*).[62]

As can be seen from Fig. 8, the C – O bond length in this complex is somewhat shorter than that in the CO molecule — 1.131 Å.[63] However, the B – C bond in $[(F_3C)_3B{\leftarrow}CO]$ is longer than that in $[H_3B{\leftarrow}CO]$ by 0.077 Å, which corresponds to a weaker donor-acceptor bond. The ν(CO) stretching frequency of $[(F_3C)_3B{\leftarrow}CO]$ is 2252 cm^{-1}, *i.e.*, it is higher than that of gaseous CO (2143 cm^{-1}). The authors attributed this difference to polarization of the coordinated ligand. In the stronger complex $[H_3B{\leftarrow}CO]$, the ν(CO) stretching frequency is 2165 cm^{-1} (Ref. 64).

Boron trifluoride does not react with carbon monoxide or nitrogen in the gas phase. However, at about 24 K, weakly bound complexes $[F_3B{\leftarrow}CO]$ and $[F_3B{\leftarrow}N_2]$ are formed.[65] The ν(CO) frequency of $[F_3B{\leftarrow}CO]$ is 2150.5 cm^{-1}, which slightly exceeds the vibrational frequency of uncoordinated CO. The ν(CO) frequency of $[(F_2B)_3B{\leftarrow}CO]$ is somewhat higher: 2162 cm^{-1} (Ref. 66), which is very close to ν(CO) of $[H_3B{\leftarrow}CO]$.

The highly exothermic reaction of atomic boron with oxygen in the gas phase gives only BO$^{\bullet}$ (boronyl) radicals.[67] The formation of the radical was confirmed by IR spectroscopy, with vibrational frequencies of oxygen – boron bond being $\nu(^{11}BO)$ = 1850 cm^{-1} and $\nu(^{10}BO)$ = 1903 cm^{-1}. The boronyl is isoelectronic to the CN$^{\bullet}$ cyanide radical. It was noted[68] that this radical contains the $B{\equiv}O$ triple bond. Note that both the VB and MO methods predict the bond order in boronyl to be 2.5 (see, for example, Ref. 69). According to quantum chemical calculations,[70] the ground state electronic configuration of boronyl is $(\sigma_1)^2(\sigma_1^*)^2(\sigma_2)^2(\sigma_2^*)^2(\pi_x,\pi_y)^4(\sigma_3)^1$. According to Pauling, this corresponds to the bond order of 2.5. The ground state term of boronyl is $^2\Sigma^+$. Nevertheless, the B – O bond length present in boronyl is typical of $B{\equiv}O$ triple bond, being 1.2049 Å in the ground state (Refs 71, 72), while in the ^2P excited state, which has a 2.96 eV higher energy (418.8 nm), the internuclear distance increases to 1.3553 Å.[72] Using microwave and laser IR spectroscopy data for the ^{11}BO molecule, Osiac *et al.*[73] determined the internuclear distance in boronyl with high accuracy: $r_e(^{11}BO)$ = 1.204068 Å. According to the data of Zhai *et al.*,[72] the stretching frequency of this molecule is 1886.7 cm^{-1} in the ground state and decreases to 1260.7 cm^{-1} in the excited state.

Being the electronic analogue of the cyanide radical and having half-filled bonding MO, boronyl is expected to have a high electron affinity. Indeed, according to Zhai *et al.*,[72] the electron affinity of boronyl is 2.510 ± 0.015 eV (earlier,[74] a value of 2.719 eV was found by the *ab initio* method at the MP4SDQ level with the Gaussian basis set). The

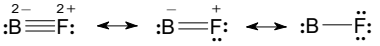
ground state term of the BO^- anion is $^1\Sigma^+$; this is an isoelectronic analogue of N_2, CO and CN^- and, hence, it should contain a triple bond. However,[74,75] the addition of an electron to boronyl induces an increase in the internuclear distance to 1.227 Å, which means weakening of the bond. Note that the bond length in the $CN^{\bullet}$ radical virtually does not change upon attachment of an electron: $r_e(CN^{\bullet}) = 1.162$ Å, $r_e(CN^-) = 1.161$ Å.[75]

Boronyl surpasses the cyanide radical in the acceptor properties. Therefore, the chemistry of boronyl and the BO^- anion is expected to resemble the CO and CN^- chemistry. According to the data of Pyykkö,[76] the existence of salts containing BN^{2-} and BO^- anions, such as Ca(BN) and K(BO), is quite possible. The enthalpy of formation of the salt Na(BO) was estimated[76] to be -408 kJ mol^{-1}.

Note that VB approach is able to predict the presence of a triple bond in the BF molecule. In particular, the boron atom uses one 2p orbital to form the σ-bond with fluorine, while two vacant 2p orbitals are involved in the formation of two donor-acceptor π-bonds. In this case, one can expect that the BF molecule would have an inverted dipole moment (with respect to that expected considering the electronegativity concept): B⇇F.

This was confirmed experimentally:[77] the bond length in the BF molecule is 1.2625 Å (the sum of the boron and fluorine covalent radii is 1.54 Å); the dipole moment of the molecule determined by microwave spectroscopy[77] is 0.5 ± 0.2 D, with the negative end of the dipole being concentrated on the boron atom. Several Lewis structures were proposed to describe the BF molecule (Scheme 15).

Scheme 15



Quite a few quantum chemical calculations were carried out for BF;[78–86] some of them confirmed the presence of the triple bond. The dipole moment of this molecule considerably depends on the calculation method (in D): 2.16,[78] 1.13,[78] 0.62,[80] 1.40,[81] 0.23[83] and 0.89.[84] It was shown[84] that the dipole moment is very sensitive to the B–F bond length; an increase in the bond length by approximately 0.2 Å leads to a change in the sign of the dipole moment: $B^-F^+ \rightarrow B^+F^-$.

The dissociation energy of the BF radical is also sensitive to the calculation method. For example, the dissociation energies of the BF and CO molecules were reported[78] to be approximately equal (120.83 and 124.06 kcal mol^{-1}). According to another study,[85] the values were 204.02 and 278.66 kcal mol^{-1} (for comparison, a value of 221.60 kcal mol^{-1} was found for N_2). The most accurate determination of the BF internuclear distance was done[86] by emission IR spectroscopy; the resulting value was 1.262712 Å.

Fantuzzi *et al.*[87] found the ground state dipole moment to be 0.920 D, while in the excited state, the sign of the dipole moment changes as $B^-F^+ \rightarrow B^+F^-$ and the value becomes 0.573 D. The B–F bond length increases from 1.2627 Å to 1.3081 Å upon excitation,[86] *i.e.*, the increase is only 0.0454 Å. However, this is sufficient for inversion of the dipole moment (this effect was predicted[84] for increasing the internuclear distance by 0.2 Å). The bond order in the BF molecule indicated by Fantuzzi *et al.*[87] is close to unity. The inversion nature of the dipole moment is attributable to the fact that the boron atom employs one sp-hybrid orbital to form the σ-bond with fluorine, while the second such orbital pointing to the opposite direction bears an electron pair, which accounts for strong polarization: BF^+ (Fig. 9).

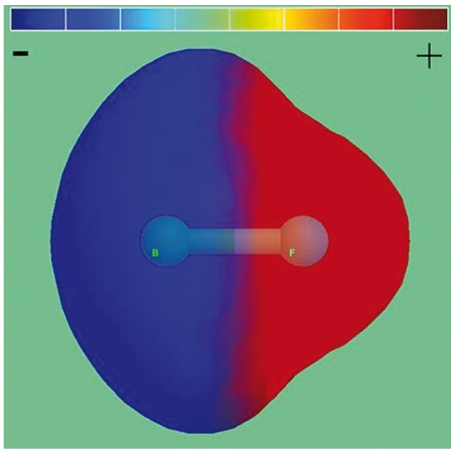


Figure 9. Formation of the dipole moment of the BF molecule.[87]

Diboryne H–B=B–H is the simplest molecule with the B=B double bond. This compound was detected upon laser vaporization of boron in a hydrogen atmosphere.[88] The primary product of reaction between atomic boron and hydrogen, BH, subsequently reacts with hydrogen or dimerizes.

$$BH + H_2 \longrightarrow BH_3, \Delta H = -93 \text{ kcal mol}^{-1} \quad (10)$$

$$BH + BH \longrightarrow HBBH, \Delta H = -117 \text{ kcal mol}^{-1} \quad (11)$$

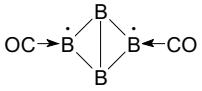
Diboryne was identified by IR spectroscopy: the ν(BH) stretching frequency is 2679.9 cm^{-1}. It was shown[89] that it is actually a biradical, with the ground state term being $^3\Sigma_g^-$. The bond length between the boron atoms is 1.509 Å, which confirms the presence of the B=B double bond. Diboryne can be considered to be an analogue of the acetylene molecule in which an electron has been removed from each π-bond. Thus, the boron atom forms two σ-bonds (one with hydrogen and one with boron) and one π-bond [two electrons in the doubly degenerate (π_x, π_y)-level occupy orbitals in conformity with Hund's rule]. According to this model, the HBBH molecule is linear. Note that B=B double bonds are very rarely encountered[12] and their 'collection' was markedly expanded in recent years.[8,9,14–16,90–102]

A progress in the synthesis of compounds with B=B and B≡B multiple bonds was attained in 2002 in a study of laser vaporization of boron in a carbon monoxide atmosphere.[103,104] A new coordination compound, [O≡C→B≡B←C≡O], was matrix-isolated in argon at 8 K and studied by IR spectroscopy.[104] This complex was also investigated by quantum chemical (DFT) calculations. The calculated B–B bond length is 1.453 Å, which is considerably shorter than the B=B double bond. The structure of this complex can be conceived as follows: the boron atom uses sp-hybrid orbitals; one of them is involved in B–B σ-bond formation, while the other one remains vacant and forms a donor-acceptor bond with the C≡O molecule. Two boron 2p orbitals are involved in the

formation of two π-bonds. Thus, the electron excitation and transition from a more stable sp-hybrid orbital to a higher 2p orbital is counterbalanced by the energy release upon formation of the coordination bond with carbon monoxide. This interpretation implies that the same effect would also be observed upon coordination of other strong electron donors.

Under analogous conditions, laser vaporization of boron in a CO + Ar atmosphere (~0.05 vol.% – 0.1 vol.% CO) resulted in the formation of the $B_4(CO)_2$ cluster biradical.[103]

Biradical structure



Qualitatively, the structure of this cluster is described as follows: the terminal boron atoms have sp^2-hybrid orbitals, the electrons of two of these orbitals are involved in two B – B σ-bonds, and the possibility of formation of a strong donor-acceptor bond with CO is ensured by transition of the third electron from the hybrid orbital to the less stable 2p orbital. The electrons of the terminal boron atoms remain unpaired, since the distance between the terminal atoms is too large for a π-bond to exist between them.

Quantum chemical calculations[103] revealed the unusual structure of the $B_4(CO)_2$ cluster. Its symmetry group is D_{2h}; therefore, all of the electronic states should be non-degenerate. However, the orbital ($2b_{2g}$) and orbital ($9a_g$) energies are so similar that these frontier MOs are singly occupied (so-called SOMOs). Therefore, the $B_4(CO)_2$ cluster is a rare example of a σ – π-biradical. Figure 10 depicts the highest occupied molecular orbitals (HOMOs) of this cluster ($2b_{2g}$ and $2b_{3g}$ are π-orbitals).

The $9a_g$ orbital provides the diagonal B – B binding, while $2b_{2g}$ participates in the B – C bond and is non-bonding for the B_4 cluster. The occupied bonding $2b_{3g}$ orbital embraces all four atoms of the B_4 cluster. Thus, the cluster contains three π-electrons. Using the nucleus independent chemical shift (NICS) method, it was shown[103] that the $B_4(CO)_2$ cluster containing three π-electrons is aromatic, contrary to Hund's rule. This may be caused by the fact that one π-electron is located in the non-bonding $2b_{2g}$ orbital.

Laser vaporization of boron in a CO + Ar atmosphere with matrix isolation in the solid argon resulted in the formation of the following compounds: BCO, BBCO, OCBBCO, $B(CO)_2$ and $B_4(CO)_2$. It was shown[105] that irradiation of OCBBCO induces its photoisomerization according to reactions (12) and (13).

$$OCBBCO + h\nu \longrightarrow OBBCCO \quad (12)$$

$$OBBCCO + h\nu \longrightarrow OBCCBO \quad (13)$$

Considering the structural data presented in Fig. 11, the following types of bonds can be proposed for isomeric molecules: O≡C–B≡B–C≡O, O≡B–B≡C–C≡O and O≡B–C≡C–B≡O, which was confirmed[105] by IR spectroscopy (Table 5).

Quantum chemical calculations[106] demonstrated the possibility of existence of aromatic boron carbonyls — analogues of aromatic hydrocarbons (benzene, cyclopropenylium cation, cyclopentadienyl anion and tropylium cation).

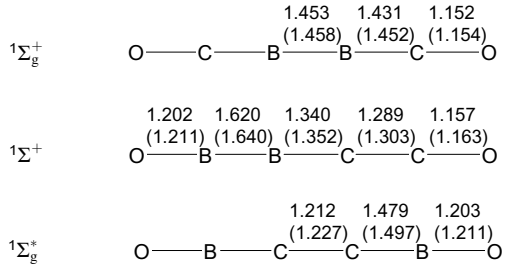


Figure 11. Results of structural studies of isomeric OCBBCO, OBBCCO and OBCCBO molecules by the B3LYP6-311 + G* and CCSD(T)/6-311 + G* (in parentheses) methods.[105]
The bond lengths are given in Å.

Table 5. IR absorption bands of the products of laser vaporization of boron in a CO + Ar atmosphere (cm^{-1}).[105]

$^{12}C^{16}O$	$^{13}C^{16}O$	$^{12}C^{18}O$	Assignment
2216.6	2140.0	2197.8	$O^{10}B^{10}BCCO$, ν(CO) [a]
2215.7	2147.0	2196.9	$O^{11}B^{10}BCCO$
2209.0	2144.3	2190.4	$O^{11}B^{11}BCCO$
2064.6	2062.1	2034.9	$O^{10}BCC^{10}BO$, ν_{as}(BO)
2040.2	2034.5	2010.1	$O^{10}BCC^{11}BO$
1999.3	1996.8	1965.6	$O^{11}BCC^{11}BO$
1942.7	1936.1	1916.9	$O^{10}BCC^{11}BO$, ν_s(BO)
934.0	912.0	919.5	$O^{10}BCC^{10}BO$, ν_{as}(BC)
930.9	909.5	917.1	$O^{10}BCC^{11}BO$
928.1	906.8	914.9	$O^{11}BCC^{11}BO$
490.1	486.7	487.5	$O^{10}BCC^{10}BO$, π_{as}(OBC) [b]
480.7	477.0	478.1	$O^{10}BCC^{11}BO$
473.7	470.2	471.1	$O^{11}BCC^{11}BO$

[a] Stretching vibrations; [b] Bending vibrations.

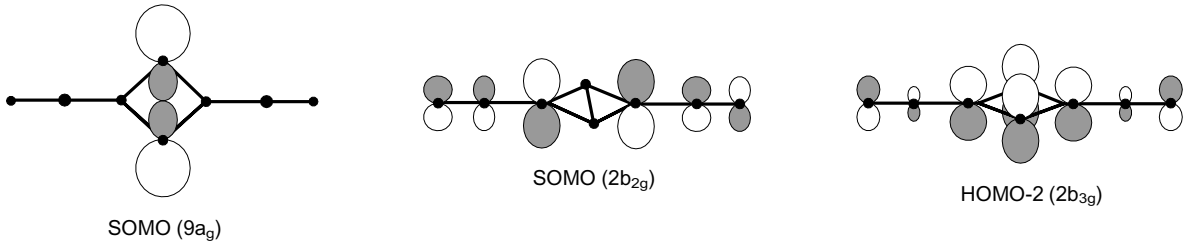
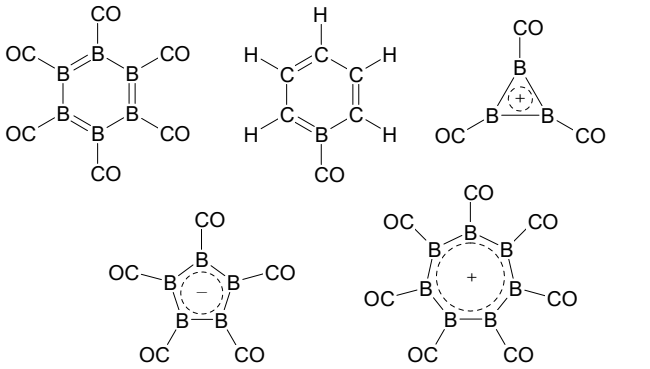


Figure 10. Highest occupied molecular orbitals of the $B_4(CO)_2$ cluster.[103]

Boron carbonyl structures



In the same publication,[106] a correlation was obtained between the stretching frequencies [ν(CO)] and charges on the boron atom [q(B)] in boron carbonyls $(BCO)_n$ (Fig. 12). As can be seen in Fig. 12, the charges on the boron atoms are negative. The higher the charge on the boron atom, the greater the ν(CO) stretching frequency. For example, in the $(BCO)_4$ tetramer, the charge on the boron atom is the greatest (−0.090), while that in $(BCO)_5$ is the lowest (−0.294); the ν(CO) vibrational frequency is 2232 cm^{-1} in the former and 1962 cm^{-1} in the latter.

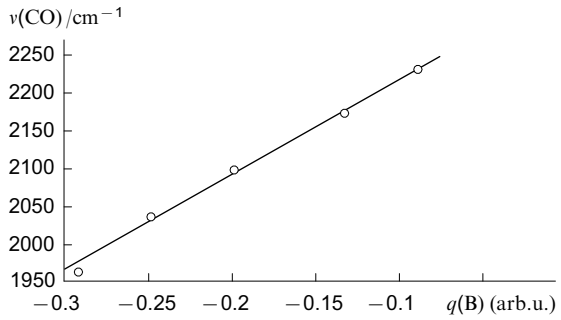


Figure 12. Linear dependence of the wave number corresponding to CO vibrations on the boron atom charge.[106]

It was shown [107] that isomeric carbon boronyls $(CBO)_n$ are thermodynamically more stable than the boron carbonyls $(BCO)_n$ and also can form quasiaromatic structures. In this connection, synthesis of cyclic carbon boronyls may be expected in the near future.

The fact that the CO molecule and the BO^- anion are isoelectronic suggests the existence of the $[O{\equiv}B{-}B{\equiv}B{-}B{\equiv}O]^{2-}$ anion analogous to the carbonyl $O{\equiv}C{-}B{\equiv}B{-}C{\equiv}O$. In 2008, the clusters B_4O_2, $B_4O_2^-$ and $B_4O_2^{2-}$ were detected by photoelectron spectroscopy upon laser vaporization of boron in an $He + O_2$ atmosphere (0.01 vol.% O_2).[68] The line at 355 nm has a vibrational structure, the vibrational frequencies being 350 ± 40, 1530 ± 30 and 2040 ± 30 cm^{-1}, respectively. According to DFT and *ab initio* calculations, all these molecules are linear and correspond to D_h symmetry group. The ground state of the B_4O_2 cluster is the $^3\Sigma_g^-$ triplet (biradical) and the order of the central bond is two: $O{\equiv}B{-}B{=}B{-}B{\equiv}O$. The $[O{\equiv}B{-}B{\equiv}B{-}B{\equiv}O]^-$ monoanion is a radical, the ground state term is $^2\Pi_u$ and the order of the central bond is 2.5. The

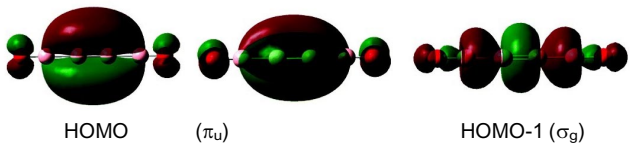


Figure 13. Electron density distribution in the $[O{\equiv}B{-}B{\equiv}B{-}B{\equiv}O]^{2-}$ dianion.[68]

attachment of one more electron to the cluster gives the closed-shell $B_4O_2^{2-}$ dianion, $^1\Sigma_g^+$, with a bond order of three (Fig. 13).

Thus, the $B_4O_2^{2-}$ dianion is indeed an analogue of $B_2(CO)_2$. However, unlike the latter, it is stable and corresponds to a global minimum of the potential energy function. Meanwhile, as noted above, $B_2(CO)_2$ isomerizes to more stable OBBCCO (the energy release is about 2.6 eV) and then to OBCCBO (~4.1 eV more stable). For this reason, the existence of stable salts, such as $Li_2(B_4O_2)$, is quite probable. Table 6 summarizes the Wiberg bond indices for different boron compounds with multiple bonds between boron atoms.

Table 6. Wiberg bond indices for the multiple (WBI) and single (WBI_{B-B}) bonds between boron atoms and index sums for the central boron (WBI_B) or carbon (WBI_C) atoms.[68]

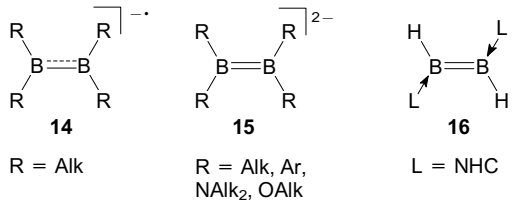
Species	WBI	WBI_{B-B}	WBI_B(WBI)
$B_2(BO)_2$	1.44	1.07	2.57
$B_2(BO)_2^-$	1.97	1.14	3.27
$B_2(BO)_2^{2-}$	2.43	1.24	3.96
$Li_2(B_4O_2)$ [a]	2.61	1.13	3.97
$B_2H_2^-$	1.50	–	2.49
$B_2H_2^{2-}$	2.25	–	3.24
B_2H_2	3.00	–	4.00
$Li_2(B_2H_2)$ [a]	2.90	–	4.00
C_2H_2	3.00	–	3.95

[a] D_{2h} point group of symmetry.

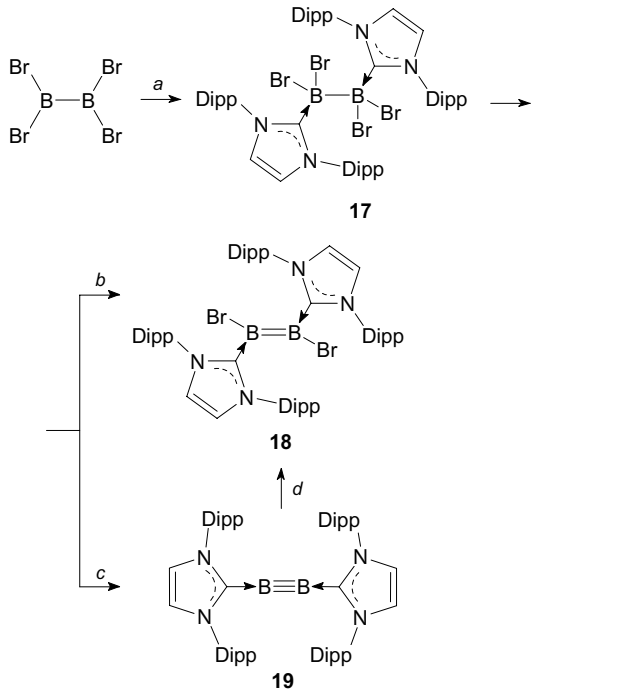
All of the above compounds with the B≡B triple bonds were detected only in the gas phase or were matrix-isolated in crystalline argon. However, a breakthrough along this line was made in 2012, in particular, the first stable carbene complex with B≡B triple bonds was synthesized.[108] Shown below are previously known compounds with boron–boron multiple bonds (**14**–**16**), conversion of complex **17** to boron carbene complexes with double B=B bonds (**18**) and triple B≡B bonds (**19**) (Scheme 16) as well as structures of the synthesized complexes (Fig. 14).

It can be seen from Fig. 14 that the C(1)–B(1)–Br(1)–B(2)–Br(2)–C(2) central moiety of compound **18** is virtually planar, as was to be expected in

Structures 14–16



Scheme 16



(*a*) Idip (2 equiv.), pentane, −78 °C; (*b*) NaphNa (2 equiv.), THF, −78 °C; (*c*) NaphLi (4 equiv.), THF, −78 °C; (*d*) **17** (1 equiv.), C_6D_6, rt; Idip is 1,3-bis(2,6-diisopropylphenyl)imidazol-2-ylidene

the case of sp^2-hybridization of boron atoms. The central moiety of complex **19** — C(1)–B(1)–B(2)–C(2) — is nearly linear, which corresponds to sp-hybridization of boron. Complex **19** is green-coloured; the colour is due to pronounced absorption at 385 nm [the absorption coefficient (ε) is 26 426 litre (mol cm)$^{-1}$] and at 600 nm [ε = 17 685 litre (mol cm)$^{-1}$]. The ν(B≡B) stretching frequency is 1339 cm^{-1}.

In 2013, an unusual reductive coupling of carbon monoxide with complex **19** was found.[109] In this reaction, the formally zero-valent boron atom is oxidized to B^{III}, thus lending six electrons to CO molecules. Previously, examples

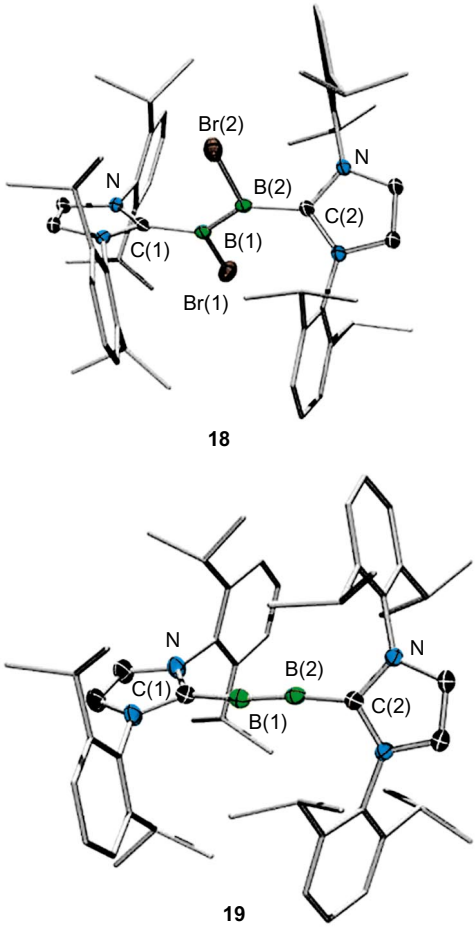
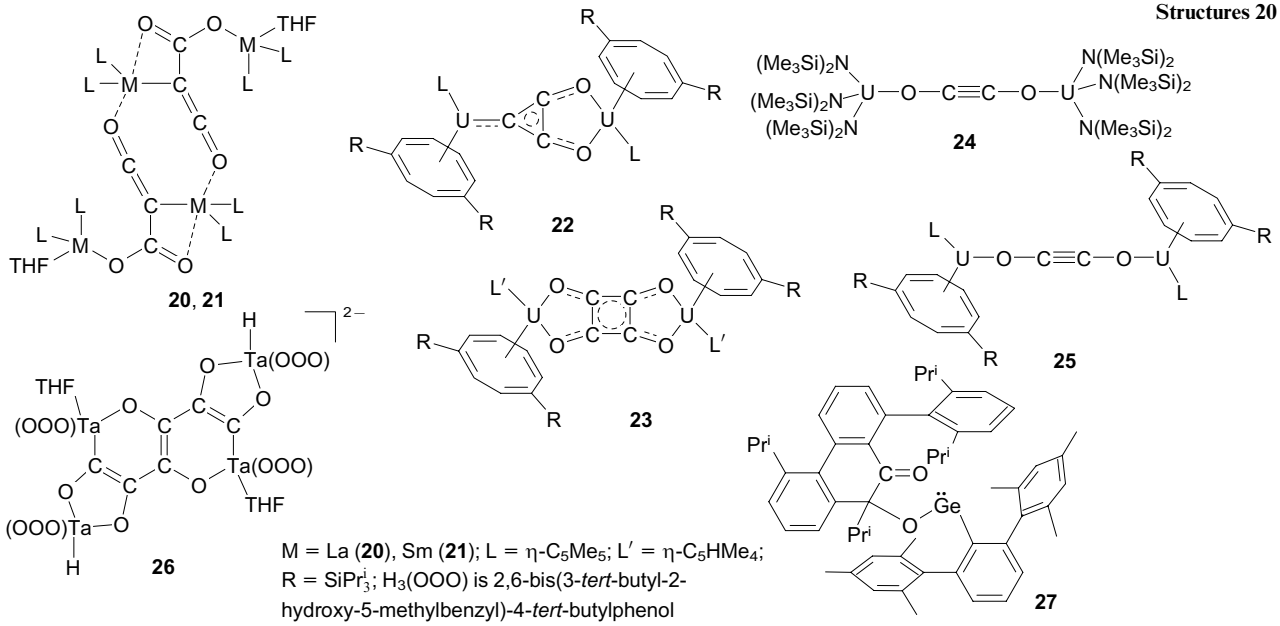


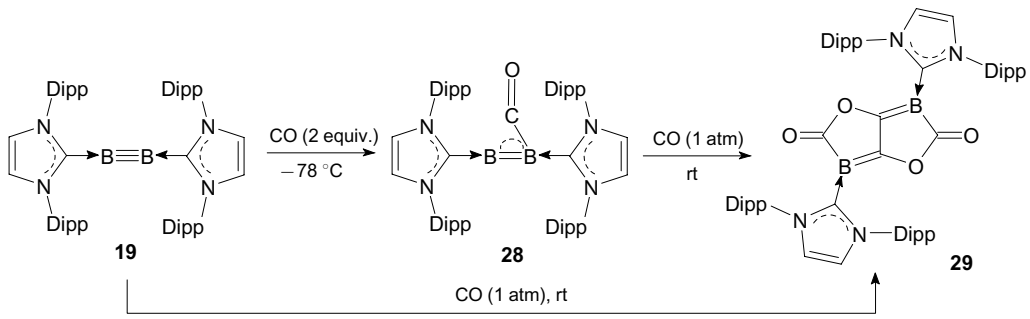
Figure 14. Molecular structures of carbene boron complexes with double (**18**) and triple bonds (**19**) between the B atoms.[108] Selected bond lengths (Å) and bond angles (deg): for **18**, 1.546 [B(1)–B(2)], 1.569 [B(1)–C(1)], 2.030 [B(1)–Br(1)], 1.586 [B(2)–C(2)], 2.046 [B(2)–Br(2)]; 128.6 [B(2)–B(1)–C(1)], 120.2 [B(2)–B(1)–Br(1)], 132.0 [B(1)–B(2)–C(2)], 116.2 [B(1)–B(2)–Br(2)]; for **19**, 1.449 [B(1)–B(2)], 1.487 [B(1)–C(1)], 1.495 [B(2)–C(2)]; 173.0 [B(2)–B(1)–C(1)], 173.3 [B(1)B(2)–C(2)].

Structures 20 – 27



M = La (**20**), Sm (**21**); L = η-C_5Me_5; L′ = η-C_5HMe_4; R = $SiPr^i_3$; H_3(OOO) is 2,6-bis(3-*tert*-butyl-2-hydroxy-5-methylbenzyl)-4-*tert*-butylphenol

Scheme 17



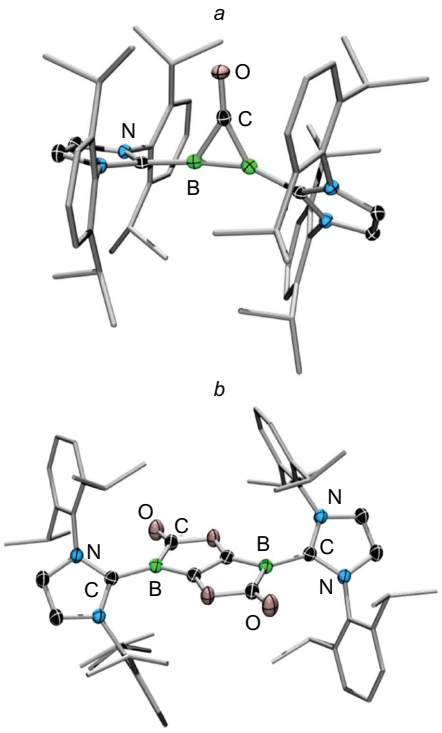


Figure 15. Molecular structures of complexes **28** (*a*) and **29** (*b*).[109]

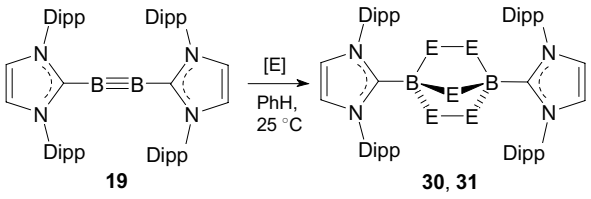
were reported of reductive coupling of carbon monoxide with complexes of rare earth metals — lanthanum and samarium (**20**, **21**), uranium (**22**–**25**), tantalum (**26**), germanium (**27**), yttrium, niobium and rhenium.

Braunschweig *et al.*[109] isolated two complexes resulting from reductive coupling of one (**28**) or four (**29**) carbon monoxide molecules to a carbene boron complex. The attachment of four CO molecules leads to complete cleavage of the B≡B triple bond (Scheme 17). The structures of the brown-orange $B_2CO(Idip)_2$ complex (**28**) and the red-orange complex $B_2C_4O_4(Idip)_2$ (**29**) are depicted in Fig. 15.

On treatment with excess CO at room temperature, $B_2CO(Idip)_2$ is converted to $B_2C_4O_4(Idip)_2$. Thus, compound **28** is an intermediate of the reaction of $B_2(Idip)_2$ with carbon monoxide. Cleavage of the triple bond affords carbene-stabilized planar bicyclic bis(borolactone).

It follows from the above that the complex $B_2(Idip)_2$, which is in essence a carbene-stabilized B_2 molecule, is a strong reducing agent. For this reason, it is quite expected that it woud react with elemental chalcogens (sulfur and selenium) to give complexes **30** and **31**. This reaction was described.[110, 111] The reductive coupling of elemental chalcogens affords [2.2.1]bicyclic systems in which boron atoms

Scheme 18



E = S (**30**), Se (**31**)

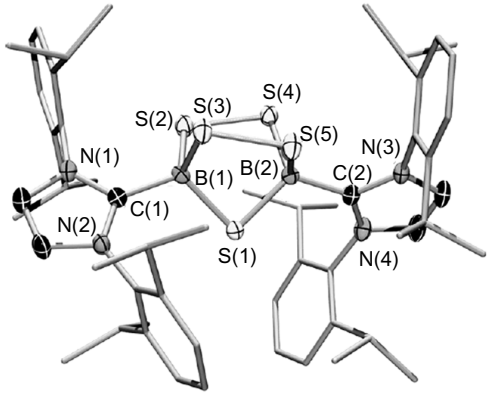


Figure 16. Molecular structure of complex **30**.[110]
Selected bond lengths (Å) and bond angles (deg.): 1.614 [B(1)–C(1)], 1.618 [B(2)–C(2)], 1.923 [B(1)–S(2)], 1.875 [B(1)–S(3)], 2.080 [S(2)–S(4)], 2.092 [S(3)–S(5)]; 115.1 [C(1)–B(1)–S(1)], 111.4 [C(1)B(1)–S(2)], 106.1 [C(1)–B(1)S(3)].

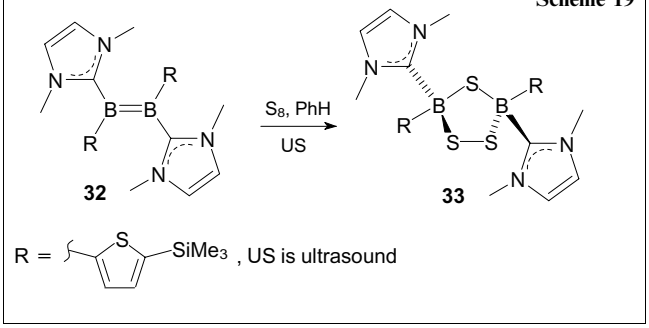
are linked by chalcogen bridges (Scheme 18). Figure 16 shows the molecular structure of complex **30**. The selenium analogue **31** has a similar structure.

The reaction of carbene-stabilized complexes **32** containing a B=B double bond involves the reductive insertion of three sulfur atoms giving complexes **33** with two chalcogen bridges (Scheme 19).[110]

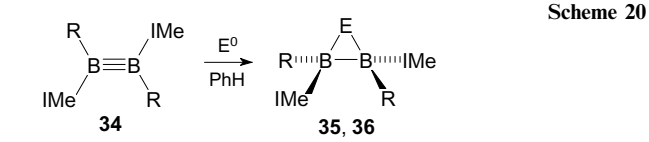
The insertion of one chalcogen atom, selenium or tellurium, into the B=B double bond of compound **34** is also possible; this gives complex **35** or **36** (Scheme 20, Fig. 17).[111]

Analogous complexes with the B≡B triple bond react with dichalcogenides, which are weaker oxidants than chalcogens. In this case, the bond in the dichalcogenide is cleaved to give π-complexes **37**, **38** (Scheme 21).[111] Meanwhile, the reaction of di-*tert*-butylacetylene with $[PhTe]^+[SbF_6]^-$ produces salts **39**. As can be seen in

Scheme 19



Scheme 20



R = SiMe3 ; E = Se (**35**), Te (**36**);

IMe is 1,3-dimethylimidazolin-2-ylidene

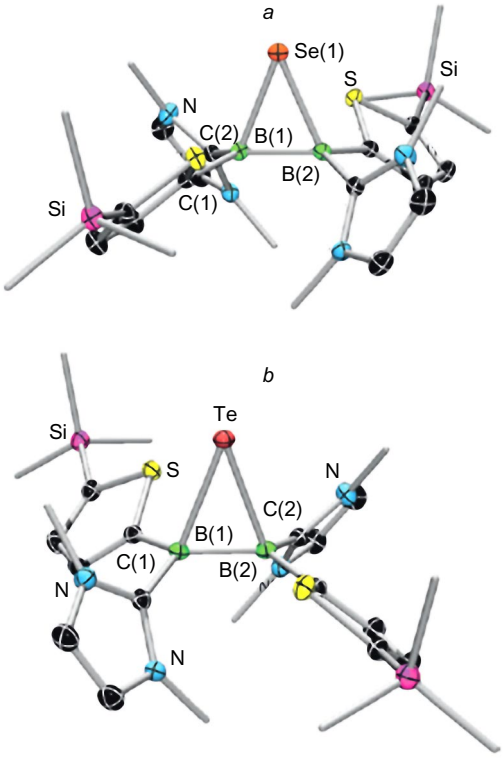
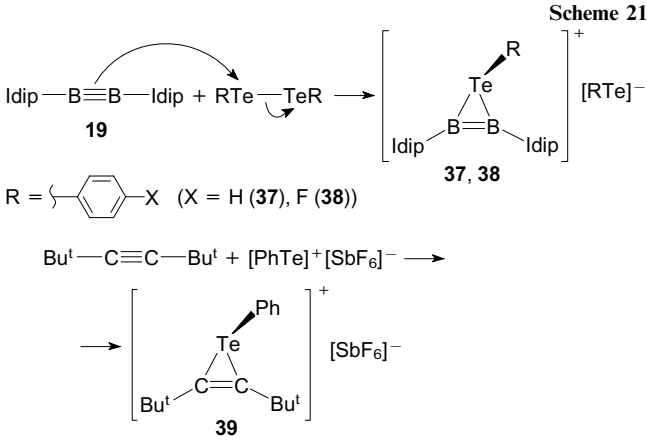


Figure 17. Molecular structures of chalcogen-bridged boron complexes **35** (*a*) and **36** (*b*).[111]

Selected bond lengths (Å): for **35**, 1.707 [B(1)–B(2)], 1.604 [C(2)–B(1)], 1.586 [C(1)–B(1)], 2.115 [B(1)–Se(1)]; for **36**, 1.713 [B(1)–B(2)], 1.584 [C(1)–B(1)], 1.598 [C(2)–B(1)], 2.360 [B(1)–Te(1)].

Scheme 21, both reactions give similar products, but have different mechanisms. The reactions of substituted acetylenes are accompanied by oxidative bond cleavage in the ditelluride to give the $PhTe^+$ cation, which is then coordinated to the C≡C triple bond. The electronegativity of

Scheme 21



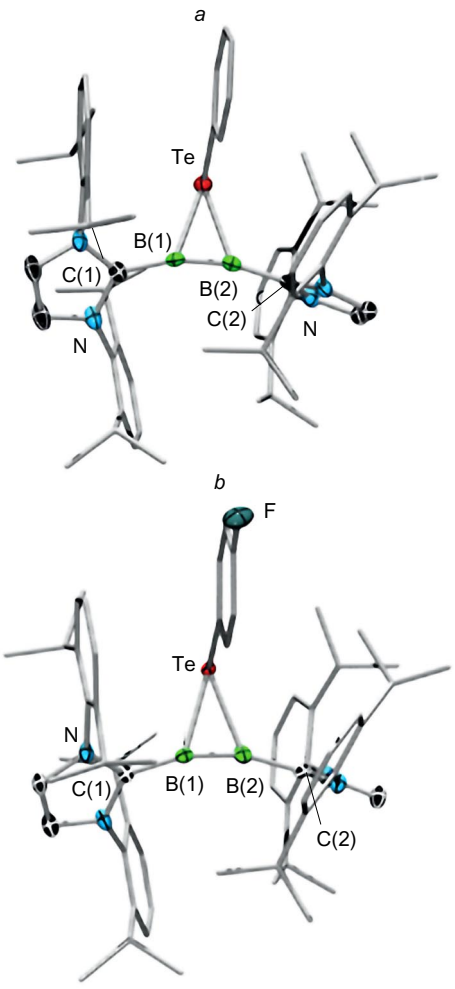


Figure 18. Molecular structures of the cations of salts **37** (*a*) and **38** (*b*).[111]

Selected bond lengths (Å) and bond angles (deg.): for **37**, 1.490 [B(1)–B(2)], 1.551 [C(1)–B(1)], 1.552 [C(2)–B(2)], 2.260 [B(1)–Te(1)], 2.247 [B(2)–Te(1)]; 165.0 [C(1)–B(1)–B(2)], 164.1 [C(2)B(2)–B(1)], 123.9 [C(1)–B(1)Te(1)], 124.8 [C(2)–B(2)–Te(1)]; for **38**: 1.494 [B(1)–B(2)], 1.545 [C(1)–B(1)], 1.559 [C(2)–B(2)], 2.254 [B(1)Te(1)], 2.243 [B(2)–Te(1)]; 164.7 [C(1)–B(1)—B(2)], 163.6 [C(2)–B(2)–B(1)], 123.7 [C(1)–B(1)–Te(1)], 125.4 [C(2)–B(2)–Te(1)].

carbon (2.55 in the Pauling scale) is higher than that of tellurium (2.10 in the Pauling scale). However, the electronegativity of boron (2.04 in the Pauling scale) is lower than that of tellurium. While reacting with diaryl ditelluride, $B_2(Idip)_2$ acts as a nucleophile by attacking the tellurium atom; this promotes heterolytic cleavage of the Te–Te bond with generation of the $PhTe^-$ anion as the leaving group.

It is noteworthy that the tellurium atoms in compounds **37** and **38** have a pyramidal rather than planar configuration (Fig. 18). The formation of a planar configuration of the B(1)B(2)–Te(1)–Ph moiety is prevented by the formation of the antiaromatic three-membered ring with four π-electrons, since the tellurium atom provides two π-electrons to the π-system. When the tellurium configuration is pyramidal, the tellurium p orbital slightly overlaps with the boron π-orbitals.

The bond lengths between the boron atoms in salts **37** and **38** are 1.490 and 1.494 Å, respectively (see Fig. 18). This is slightly longer than the bond in $B_2(Idip)_2$ (1.449 Å), but is considerably shorter than the B=B double bond (1.58–1.61 Å). A similar effect is produced by coordination of the $PhTe^+$ cation to bis(*tert*-butylacetylene): in complex **39**, the bond length between the carbon atoms is 1.288 Å, while in the starting acetylene it is 1.202 Å.

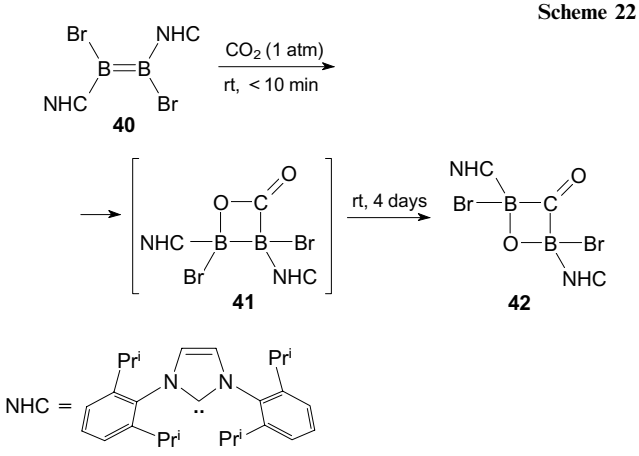
Stoy *et al.*[92] discovered the insertion of one or two carbon dioxide molecules into the (B=B) double bond or (B≡B) triple bond. The [2+2]-cycloaddition reactions at room temperature and ambient pressure proceed as shown in Schemes 22 and 23.

As shown in Scheme 22, diborene **40** reacts with CO_2 to give dibora-β-lactone in which two boron atoms have added a carbon atom and one of oxygen atoms. The C–O bond length with the second, uncoordinated oxygen is 1.20 Å, which is somewhat greater than the bond length in the starting CO_2 (1.163 Å[63]).

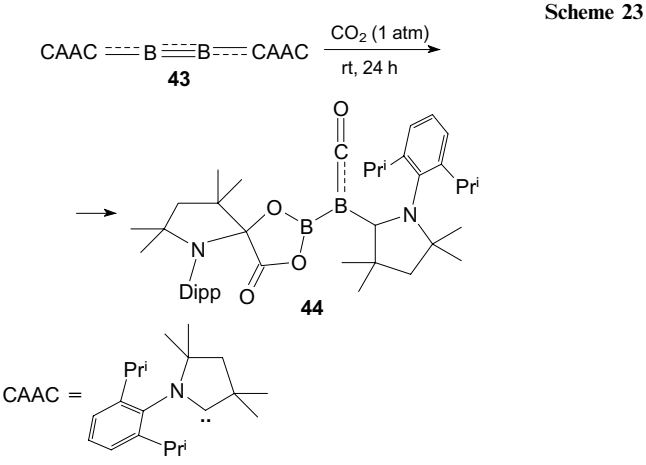
Thermally unstable lactone **41** (characterized by NMR spectroscopy and X-ray diffraction) easily isomerizes to more stable compound **42**. The C=O bond length in it is 1.212 Å, *i.e.*, it is somewhat shorter than the common bond length in organic ketones. The *ν*(CO) vibrational frequency is 1706 cm^1, which is typical of aliphatic ketones.[112] The structures of compounds **40** and **41** are shown in Fig. 19.[92]

Diboracumulene **43** reacts with carbon dioxide to give compound **44** (see Scheme 23, Fig. 20). Its IR spectrum exhibits two strong lines at 1987 and 1777 cm^{-1}. The former can be assigned to vibrations of the boraketene group, while the latter is attributable to carboxyl vibrations. The former vibrational frequency is close to the *ν*(CO) mode (1928 and 1929 cm^{-1}) of diboryne dicarbonyl adducts (CAAC)(CO)BB(CO)(CAAC) [CAAC is 1-(2,6-diisopropylphenyl)-3,3,5,5-tetramethylpyrrolidin-2-ylidene] or mono-

Scheme 22



Scheme 23



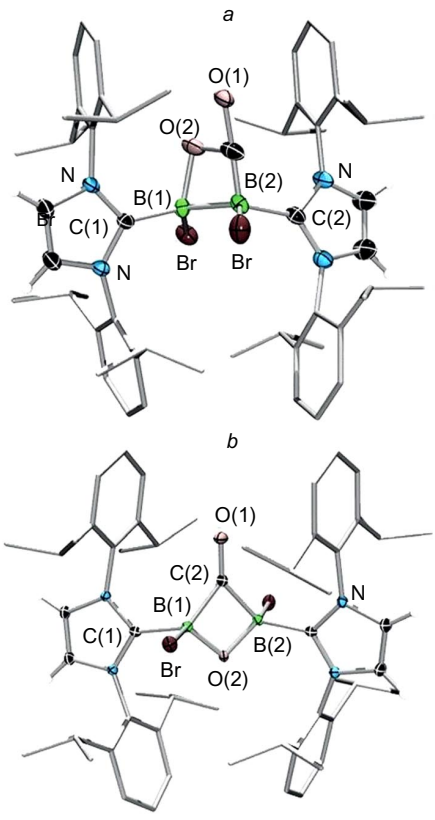


Figure 19. Molecular structures of products **41** (*a*) and **42** (*b*).[92] Selected bond lengths (Å) and bond angles (deg.): for **41**, 1.800 [B(1)–B(2)], 1.690 [B(2)–C(2)], 1.200 [C(2)–O(1)], 1.346 [C(2)O(2)], 1.490 [B(1)–O(2)]; 73.7 [B(1)–B(2)–C(2)], 136.2 [B(2)–C(2)–O(1)], 124.5 (O(1)–C(2)–O(2)]; for **42**, 1.436 [B(1)–O(2)], 1.445 [B(2)–O(2)], 1.642 [B(1)–C(2)], 1.641 [B(2)–C(2)], 1.212 [C(2)–O(1)]; 95.5 [B(1)–O(2)B(2)], 81.0 [B(1)–C(2)–B(2)].

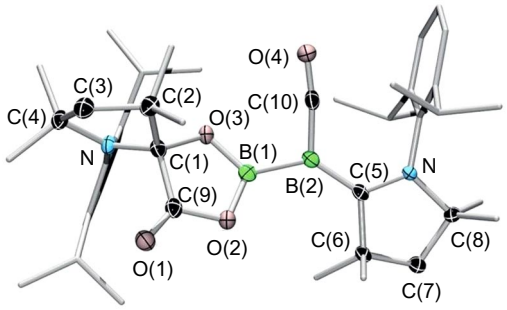


Figure 20. Molecular structure of the product of reaction between diboracumulene **43** and carbon dioxide.[92]
Selected bond lengths (Å) and bond angles (deg.): 1.660 [B(1)–B(2)], 1.417 [B(1)–O(2)], 1.380 [B(1)–O(3)], 1.202 [C(9)–O(1)], 1.366 [C(9)–O(2)], 1.466 [B(2)–C(10)], 1.157 [C(10)–O(4)], 1.497 [B(2)–C(5)]; 171.6 [B(2)–C(10)O(4)].

carbonyl compounds (CAAC)B(CO) (1921 and 1962 cm^{-1}).[113, 114]

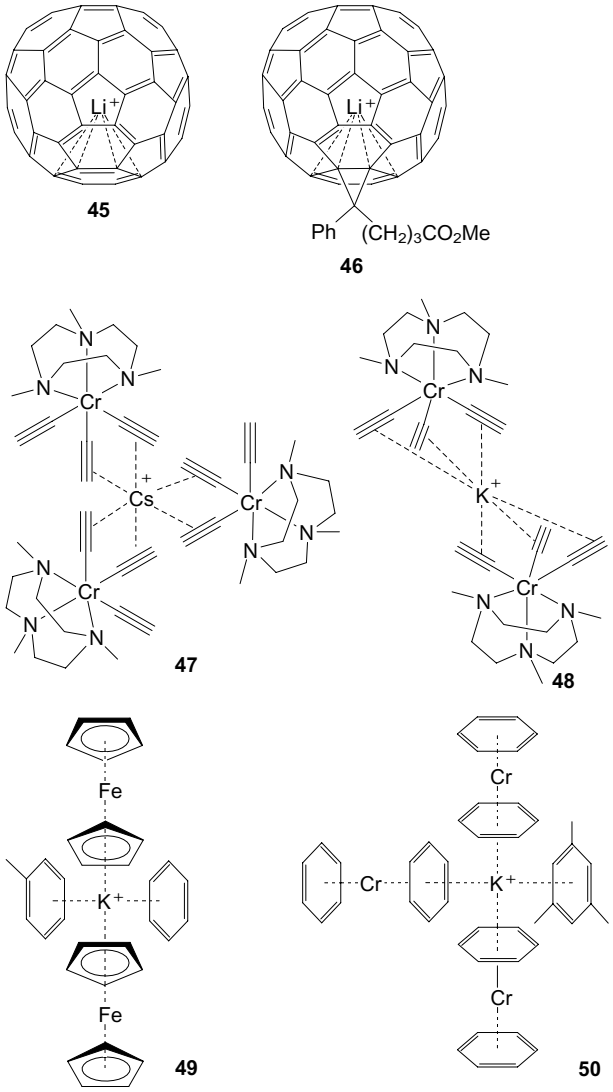
Hering-Junghans [115] discovered the ability of borylenes to fix molecular nitrogen.

Lately, researchers' interest has been attracted by compounds in which cation–π-bond type interaction is present.[116–118] These non-covalent contacts play an important role in biology, chemistry and materials science. In most systems, they occur together with strong covalent or dative bonds. Cases where these contacts exist by themselves are rather rare. The known examples of these contacts are present in structurally characterized complexes **45**–**50** with alkali metal–π-bond contacts.[119]

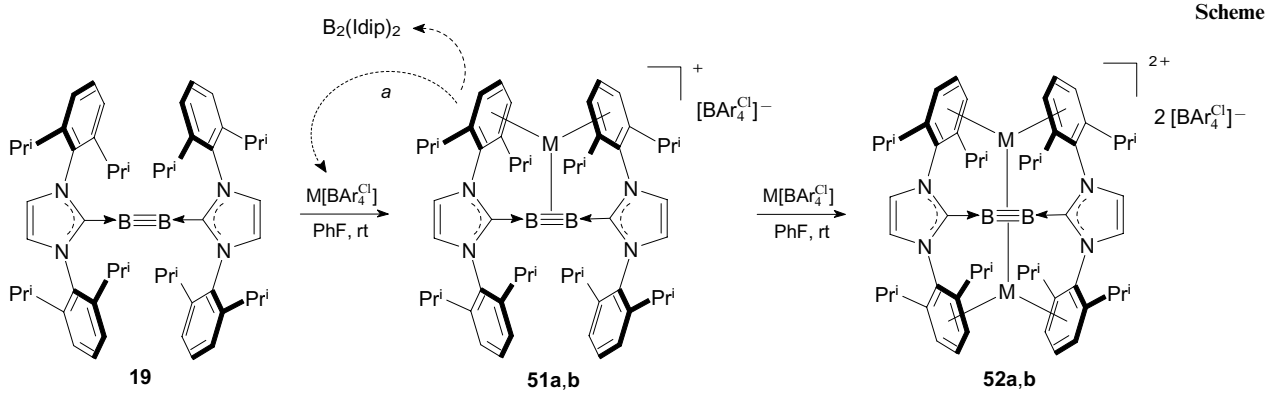
It was shown [119] that encapsulated complexes of alkali metal ions **51a**,**b** (not isolated in a solid state) and **52a**,**b** are produced from $B_2(Idip)_2$ (**19**). The addition of two equivalents of the solid lithium or sodium tetrakis(3,5-dichlorophenyl)borate salt ($[BAr^{Cl}_4]^-$) to a solution of diboryne **19** in fluorobenzene followed by ultrasonic treatment yielded a homogeneous solution with a colour varying from dark green to pink (**51a**) or violet (**51b**), respectively (Scheme 24). Using the difference between the solubilities of these complexes, the authors isolated the crystals of **52a** and **52b** and studied them by X-ray diffraction (Fig. 21).

According to IR and ^{11}B NMR spectroscopy, the interaction between the π-system of $B_2(Idip)_2$ (**19**) and the Li^+ or Na^+ cation is weak. However, the coordination of these cations induces a considerable change in the $B_2(Idip)_2$ structure and electronic properties: in the starting $B_2(Idip)_2$, the planes of N-heterocyclic carbenes are rotated through 56.7° relative to each other, whereas in complexes **52a**,**b**, they are coplanar. The coordination also changes considerably the electronic spectra of $B_2(Idip)_2$ (Fig. 22). Thus, the

Structures 45 – 50



Scheme 24



(*a*) crystallization, partial conversion, recovery of the starting compounds; M = Li (**a**), Na (**b**)

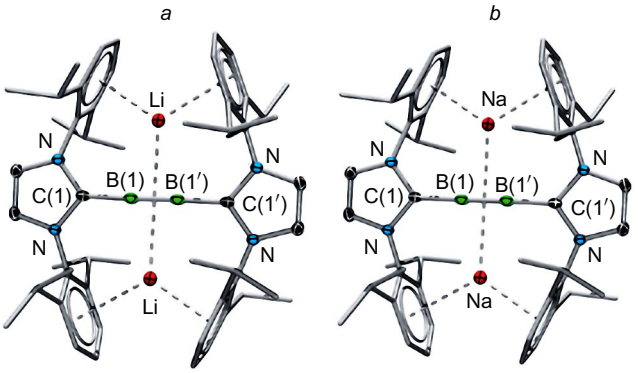


Figure 21. Molecular structures of dications **52a** (*a*) and **52b** (*b*).[119] Selected bond lengths and interatomic distances (Å): for **52a**, 1.452 [B(1)–B(1′)], 1.523 [B(1)–C(1)], 2.764 (B–Li), 2.806 and 2.978 (LiC); for **52b**, 1.459 [B(1)–B(1′)], 1.516 [B(1)–C(1)], 2.514 (BNa), 2.863 and 2.933 (Na–C).

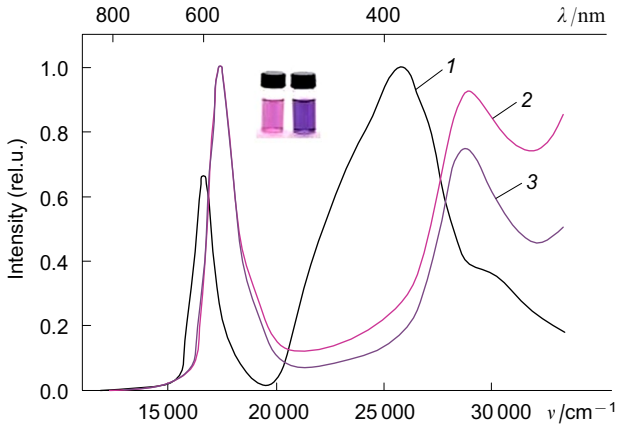


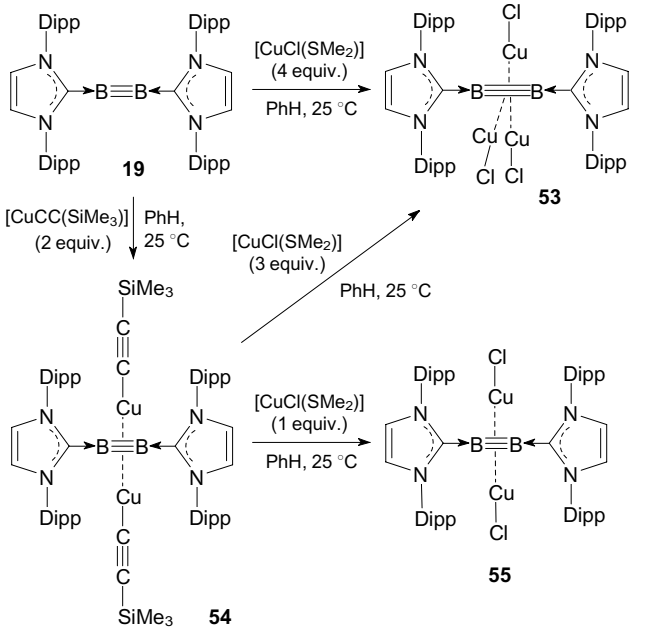
Figure 22. UV spectra of complexes **19** (*1*), **52a** (*2*) and **52b** (*3*).[119]

cation–π-bond contact is an important factor, which is to be taken into account for the development of functionalization methods for boron-containing materials.

It is known[120] that acetylene derivatives are prone to form π-complexes with cations such as Cu^+, Ag^+, Au^+, Zn^{2+}, Cd^{2+} and Hg^{2+}. Presumably, similar properties are inherent in boron complexes with B≡B bonds. In 2017, the first π-complex of $B_2(Idip)_2$ with Cu^+ cations was obtained.[121] The addition of $[CuCl(SMe_2)]$ to $B_2(Idip)_2$ (**19**) in different ratios (Scheme 25) affords $\{[B_2(Idip)_2](CuCl)_3\}$ (**53**) in 8% yield. The low yield is attributable to the reducing capacity of complex **19**, which leads to reduction of Cu^+ ions to metallic copper. When the complex $[CuCC(SiMe_3)]$, which is more stable against reduction, is used, the reaction gives $\{[B_2(Idip)_2][CuCC(SiMe_3)]\}$ (**54**) in 86% yield. It is worth noting that treatment of complex **54** with an equivalent amount of $[CuCl(SMe_2)]$ results in replacement of the coordinated ligand rather than in the insertion of the third copper atom and gives $\{[B_2(Idip)_2](CuCl)_2\}$ (**55**) in 48% yield (see Scheme 25).

The molecular structures of π-complexes **53**–**55** are shown in Fig. 23. As can be seen, the boron–boron bond in complex **53** (1.526 Å) is longer than that in the starting

Scheme 25



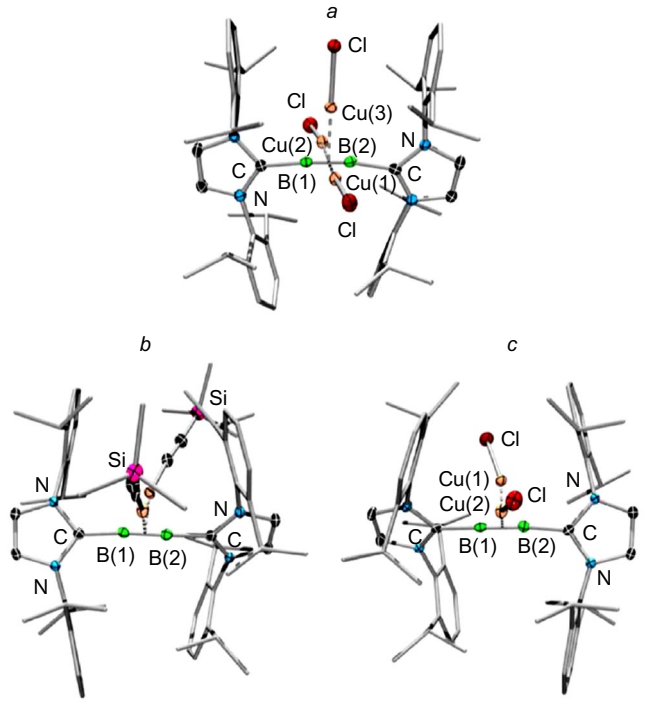
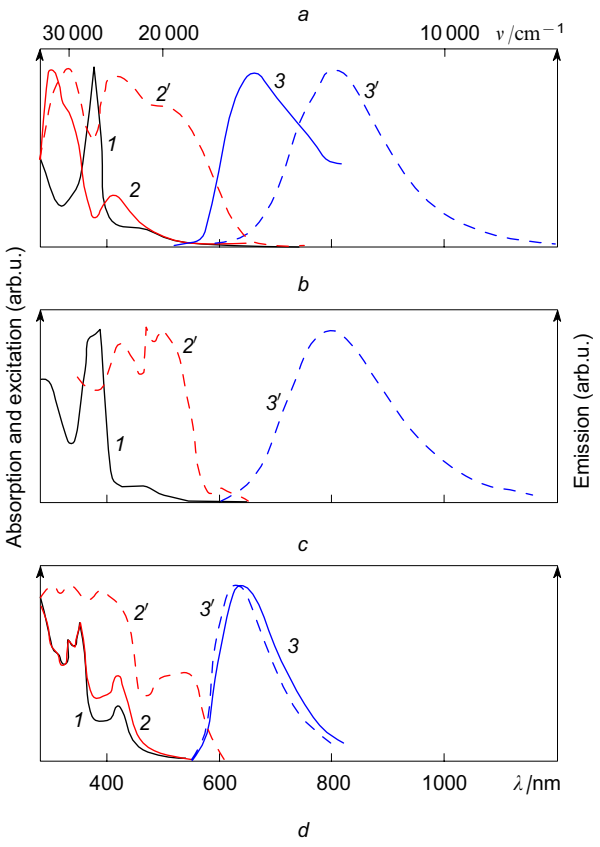


Figure 23. Molecular structures of complexes **53** (*a*), **54** (*b*) and **55** (*c*). [121] Selected bond lengths, interatomic distances (Å) and bond angles (deg.): for **53**, 1.526 [B(1)–B(2)], 2.056 [B(1)–Cu(1)], 2.068 [B(2)–Cu(1)], 2.107 [B(1)–Cu(2)]; 81.03 [Cu(1)–B(1)–Cu(2)], 90.13 [Cu(1)–Cu(2)–Cu(3)]; for **54**: 1.478 [B(1)–B(2)], 2.087 [B(1)–Cu(1)], 2.087 [B(1)–Cu(2)], 2.085 [B(2)–Cu(2)], 2.087 [B(2)–Cu(1)]; 104.53 [Cu(1)–B(1)–Cu(2)]; 104.15 [Cu(1)–B(2)–Cu(2)]; for **55**: 1.486 [B(1)–B(2)], 2.087 [B(1)–Cu(1)], 2.079 [B(1)–Cu(2)], 2.078 [B(2)–Cu(2)], 2.075 [B(2)–Cu(1)]; 102.6 [Cu(1)–B(1)–Cu(2)], 103.0 [Cu(1)B(2)–Cu(2)].

$B_2(Idip)_2$ (1.449 Å). The coordination of a CuCl molecule also leads to elongation of the B – C bonds from 1.487 and 1.495 Å in $B_2(Idip)_2$ to 1.562 Å in complex **53**. The B≡B bond length in complex **54** (1.478 Å) is intermediate between these values for complexes **19** and **53**, like the B – C bond length in compound **54** (1.535 Å). The structure of complex **55** is similar to that of **54**.

The coordination of copper ions leads to a substantial contribution of d orbitals to the frontier orbitals of complex **19**. As a result, π-complexes **53** – **55** exhibit phosphorescent properties in the red and near-IR range with a quantum yield of up to 0.58 (Fig. 24). The contribution of the copper d orbitals induces strong spin – orbit coupling, which ensures effective $S_1 \rightarrow T_n$ conversion and $T_1 \rightarrow S_0$ phosphorescence transition.



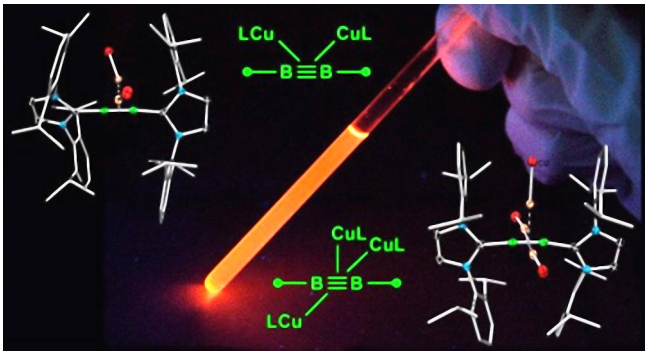


Figure 24. Absorption (*1*), excitation (*2*) and emission (*3*) spectra of complexes **55** (*a*), **54** (*b*) and **53** (*c*) in deaerated toluene (continuous lines *1* – *3*) and in the solid state (dashed lines *2′*, *3′*) under argon and phosphorescence of diborynes (*d*).[121]

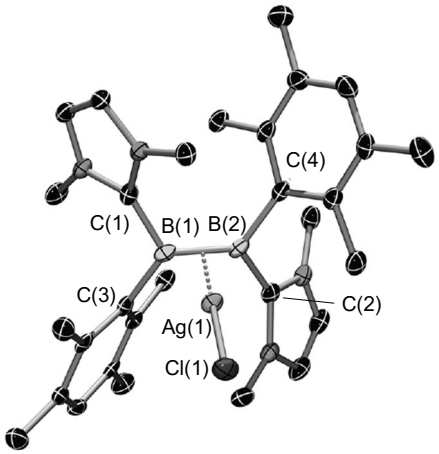
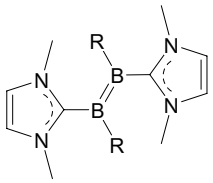


Figure 25. Molecular structure of the complex $B_2(Idip)_2(Dur)_2(AgCl)$.[122] Selected bond lengths, interatomic distances (Å) and bond angles (deg.): 1.645 [B(1) – B(2)], 1.594 [B(1) – C(1)], 1.629 [B(1) – C(3)], 1.588 [B(2) – C(2)], 1.614 [B(2) – C(4)], 2.318 [B(1) – Ag(1)], 2.366 [B(2) – Ag(1)], 2.410 [Ag(1) – Cl(1)]; 41.10 [B(1) – Ag(1) – B(2)], 159.03 [B(2) – Ag(1) – Cl(1)], 159.69 [Cl(1) – Ag(1) – B(1)].

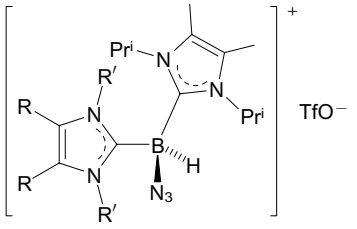
Substituted diborenes $B_2(Idip)_2R_2$ are also able to form π-complexes with transition metal salts.[122, 123] Indeed, treatment of $B_2(Idip)_2(Dur)_2$ (Dur is 2,3,5,6-tetramethylphenyl) with silver chloride gives rise to the π-complex $[B_2(Idip)_2(Dur)_2]AgCl$ (Fig. 25).[121]

The complex $[B_2(Idip)_2(Dur)_2](AgCl)$ is stable in the crystalline state and in solution at temperatures not exceeding −25 °C; however, it is light-sensitive and rapidly decomposes either at room temperature or in the light to give silver. Coordination of silver ions leads to an insignificant increase in the B=B bond length [in the starting complex $B_2(Idip)_2(Dur)_2$, it amounts to 1.590 Å]. The structure of $[B_2(Idip)_2(Dur)_2](CuCl)$ is similar.[123] Both complexes show fluorescent properties in solutions (the quantum yield is virtually 100%). Unlike complexes **53**, **54** and **55** and despite the presence of d-metals, the spin – orbit

Diborene structure



Azidoborane structure



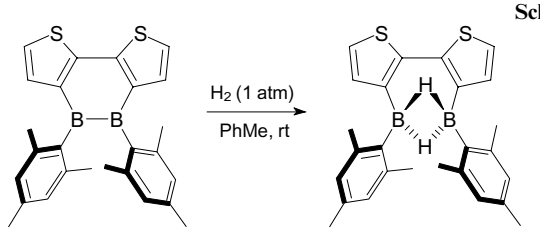
R = H, Me;
R′ = Pr^i, Dipp

coupling in diborene complexes is very weak; therefore, virtually no $S_1 \rightarrow T_n$ conversion takes place.

Thermolysis of azidoboranes stabilized by coordination to carbenes gives donor-acceptor complexes HBNH[124] and the azidoborane $[HBN_3]^+$ cation.

B,B-Dimesityl-substituted dithieno-1,2-diborin is an antiaromatic compound (4 π-electrons). Due to strong electron deficiency, it can induce homolytic bond cleavage in the hydrogen molecule under ambient conditions. This gives rise to hydrogen-bridged diborane (Scheme 26).[125] The reaction is accompanied by a sharp change in the solution colour from dark green to yellow and by fluorescence (Fig. 26).[125]

Scheme 26



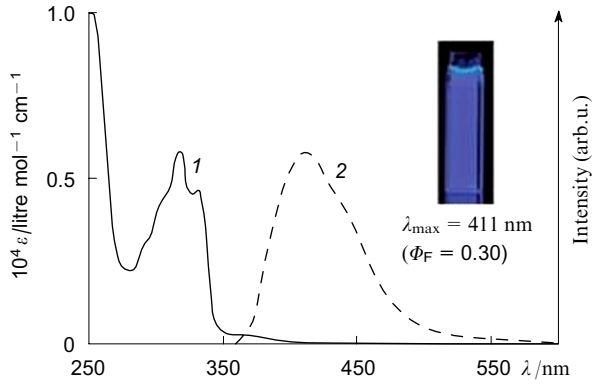


Figure 26. UV/Vis absorption spectra (*1*) and fluorescence spectra (*2*) of the hydrogen-bridged complex (see Scheme 26).[125]
ε is the absorption coefficient; Φ_F is quantum yield.

4. Triple bonds between atoms of Group 13 and 14 elements

Triple bonds were detected in clusters based on Group 13 metals. For example, sodium reduction of alkyl gallium dichlorides $RGaCl_2$ (R = 2,6-$Mes_3C_6H_3$) gave the cyclotrigallene cluster $Na_2[RGa]_3$.[11,126,127] This cluster, which contains two π-electrons, formally meets Hückel's rule and should be aromatic, which has been confirmed experimentally. The cluster $Na_2[RGa]_3$ (Fig. 27) is a structural analogue of the triphenylcyclopropenyl cation.

It is worth noting that the gallium cluster is one of the few known metal aromatic systems. The sodium reduction of alkyl gallium dichloride $RGaCl_2$ [R = 2,6-$(Tipp)_2C_6H_3$, where Tipp = 2,4,6-$Pr^i_3C_6H_2$] gave the unique cluster $Na_2[RGa{\equiv}GaR]$.[128] The uniqueness of this cluster is that gallium occurs there in zero oxidation state and the coordination number of gallium is two. This complex is the first cluster with a metal–metal triple bond in which the metal is a p-block element. The Ga≡Ga bond length is 2.319 Å. By

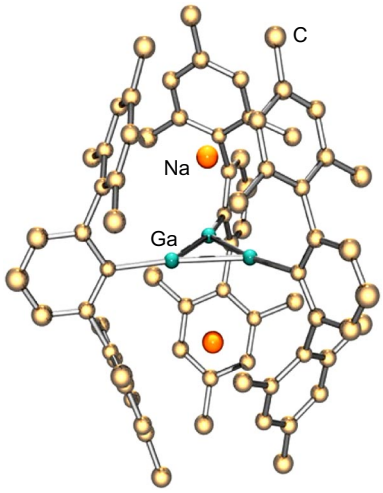


Figure 27. Molecular structure of the $Na_2[(2,6\text{-}Mes_2C_6H_3)Ga]_3$ cluster.[10]

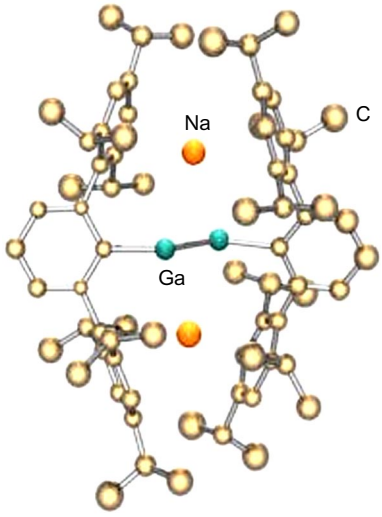


Figure 28. Molecular structure of the $Na_2[RGa{\equiv}GaR]$ cluster, R = 2,6-$(Tipp)_2C_6H_3$.[10]

analogy with alkynes, the cluster $Na_2[RGa{\equiv}GaR]$ can be called digallyne. An unusual feature of digallyne is the nonlinear geometry of the C–Ga≡Ga–C moiety (Fig. 28).

It is known that formation of the triple bond in alkynes requires sp-hybridization of AOs. One of the hybrid orbitals serves for σ-bond formation with the other atom of the bond, while unhybridized p orbitals form two π-orbitals located in mutually perpendicular planes. That is why the

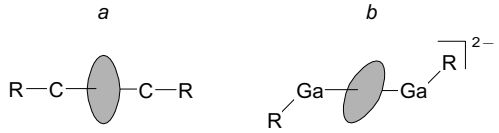


Figure 29. Classical linear (*a*) and non-classical bent (*b*) triple bonds.[10]
The R–Ga–Ga bond angle is 131°.

non-linearity of the R – Ga≡GaR moiety was unexpected by theoretical chemists (Fig. 29).

For the description of such non-classical triple bonds, the model of bent σ-bonds was proposed.[10, 11, 129, 130] These bonds are weaker than π-bonds. They are similar to so-called banana bonds, which were defined earlier to describe bonding in alkenes. As can be seen in Fig. 30, each sp-hybrid orbital of one gallium atom, out of the two atoms forming the bond overlaps with the p orbital of the other atom, the p orbital of which overlaps with the sp orbital of the first atom. The pure π-bond is formed in the plane perpendicular to the plane of the C – Ga≡Ga – C moiety in the *trans*-configuration.

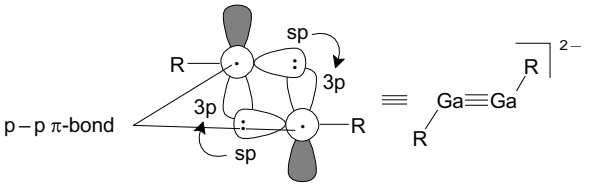


Figure 30. Scheme of formation of non-classical triple bonds in gallium clusters.[11]

Non-classical triple bonds were also detected in the cluster $Na_2[RGa{\equiv}GaR]$ (R = 2,6-$Ph_2C_6H_3$) (Ref. 128) and, according to calculations,[131] they should also occur in the simple cluster $Na_2[HGa{\equiv}GaH]$.

In 2006, dialuminyne — the cluster $Na_2[RAl{\equiv}AlR]$, where R = 2,6-$(Dipp)_2C_6H_3$ — was synthesized (Fig. 31).[132]

The non-classical triple bonds were also detected in compounds based on Group 14 elements.[11] For example, disilyne RSi≡SiR [R = $SiMe(SiBu^t_3)_2$] was prepared in 2002;[133] however, this product proved to be very unstable. The first stable disilyne with a triple bond was described two years later[134] (Scheme 27).

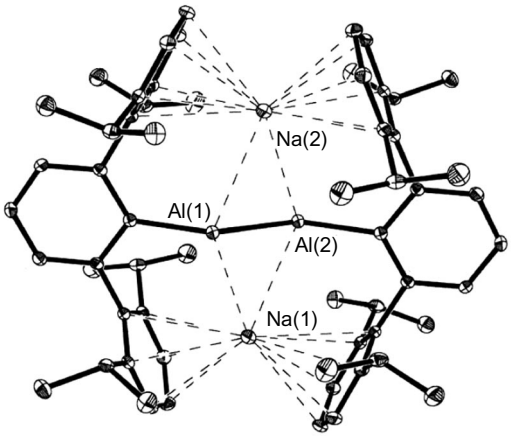
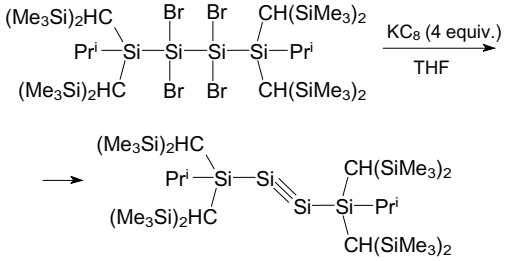


Figure 31. Structure of dialuminyne (digallyne analogue) $Na_2[RAl{\equiv}AlR]$, where R = 2,6-$(Dipp)_2C_6H_3$.[132]
The Al – Al bond length is 2.428 Å.

The Si – Si≡Si – Si moiety is non-linear; the length of the Sii≡Si triple bond is 2.0622 Å, while the Si – Si≡Si bond angle is 137.44°.[134] Apparently, this structure is stabilized by bulky substituents, which prevent polymerization of disilyne, as can be seen in Fig. 32. The disilyne crystals are green-coloured, as their long-wavelength absorption band occurs at 483 nm. DFT calculations con-

Scheme 27



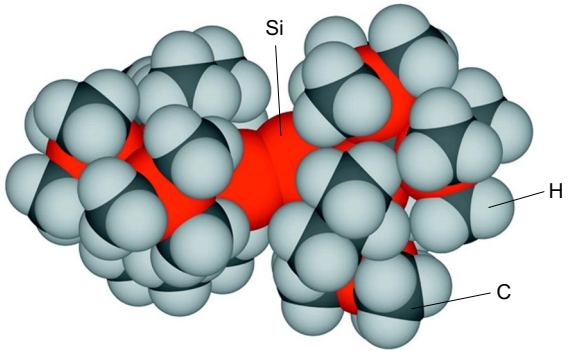


Figure 32. Model of the disilyne molecule $(Me_3Si)_2CHPr^iSi - Si{\equiv}Si - SiPr^iCH(SiMe_3)_2$.[134]

firm the presence of a triple bond: the Wiberg index is 2.618.[134]

According to *ab initio* and DFT calculations,[135] the linear structure of disilynes can be stabilized by covalent bonds with magnesium. Figure 33 presents the optimized structure of a disilyne with a porphyrin complex of magnesium. It can be seen that the triple bond in the classical linear Mg – Si≡Si – Mg moiety is somewhat longer than that in the non-classical bent moiety, although the Wiberg bond index is greater for the linear version: 2.92 *vs.* 2.618.

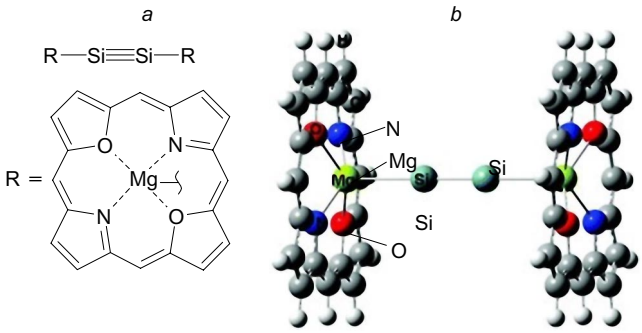


Figure 33. Optimized disilyne structure with modified Mg porphyrin complex.[135]
The Si≡Si bond length is 2.092 Å and the Mg – Si bond length 2.639 Å.

The digermyne R – Ge≡Ge – R [R = 2,6-$(Dipp)_2C_6H_3$],[136, 137] distannyne R – Sn≡Sn – R [R = 2,6-$(Dipp)_2C_6H_3$][137, 138] and diplumbyne R – Pb≡Pb – R [R = 2,6-$(Trip)_2C_6H_3$][139] were also synthesized. Digermyne forms red-coloured crystals (λ_{max} = 501 nm) and the molecule has a centre of symmetry, with the

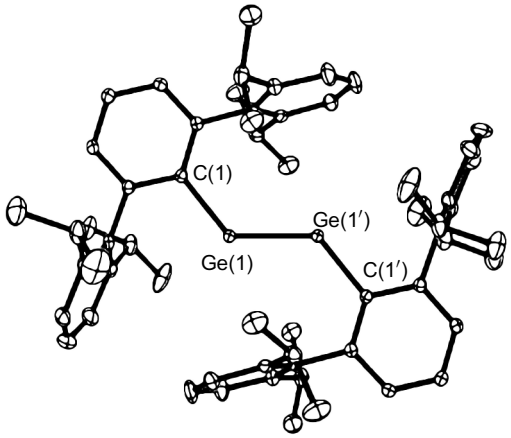


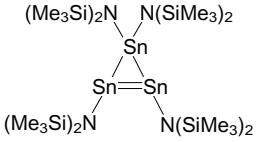
Figure 34. Molecular structure of digermyne R–Ge≡Ge–R [(R = 2,6-(Dipp)$_2$C$_6$H$_3$].[136]
The Ge(1)–Ge(1′) bond length is 2.285 Å, the Ge(1′)–Ge(1)–C(1) bond angle is 128.67°.

C(1′)–Ge(1′)–Ge(1)–C(1) moiety being non-linear (Fig. 34).

Structural data [136] confirm the presence of a triple bond in digermyne: the distance between the germanium atoms in the molecule (2.285 Å) is markedly shorter than that in compounds with a Ge–Ge single bond (2.44 Å) and shorter than the Ge=Ge double bond in digermenes — germanium analogues of alkenes. In the digermene 2,6-(Trip)$_2$C$_6$H$_3$(Me)Ge=Ge-(Me)C$_6$H$_3$(Trip)$_2$-2,6, the Ge=Ge bond length is 2.317 Å.[136] The conclusion about the presence of a triple bond in digermyne was also confirmed by the results of DFT quantum chemical calculations.[137]

The C–Sn≡Sn–C moiety in distannyne is also non-linear, the Sn(1′)–Sn(1)–C(1) angle is noticeably smaller than 180°. The Sni≡Sn bond in distannyne (2.6675 Å) is shorter than the Sn=Sn bonds in so-called distannenes. In the distannene Sn$_2$R$_4$ [R = CH(SiMe$_3$)$_2$], the bond length between the tin atoms is 2.768 Å,[140] although the usual length of this bond ranges from 2.77 to 2.91 Å.[141] However, in cyclic tristannene [(Me$_3$Si)$_2$N]$_4$Sn$_3$, the length of the Sn=Sn double bond is even shorter than that in distannyne and amounts to 2.601 Å.[141]

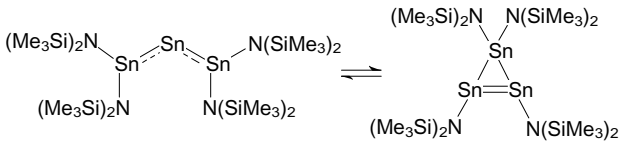
Tristannene structure



A possible cause of this pronounced shortening of the bond is highly efficient overlap of the 5p orbitals of tin in the three-membered ring. Nevertheless, it should be admitted that the bond order in distannyne is definitely less than three. This is confirmed by easy isomerization of cyclotristannene to tristannaallene (Scheme 28).[141]

The C–Pb–Pb–C moiety in diplumbyne is also non-linear (Fig. 35). However, the distance between the lead atoms (3.1881 Å) is markedly greater than the bond lengths in typical diplumbanes: for example, the Pb–Pb bond length in Ph$_3$PbPbPh$_3$ is 2.84 Å.[142] Meanwhile, the unusually small C(1)–Pb(1)–Pb(1′) bond angle suggests the

Scheme 28



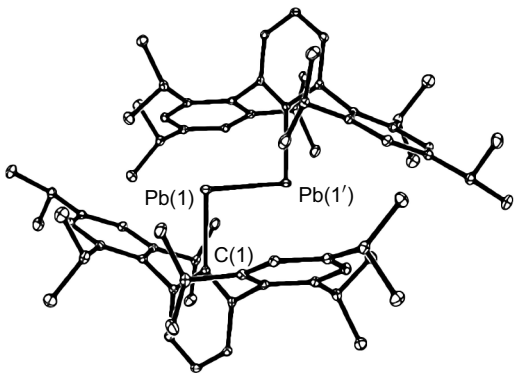
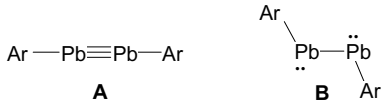


Figure 35. Molecular structure of diplumbyne 2,6-(Trip)$_2$C$_6$H$_3$Pb≡PbC$_6$H$_3$(Trip)$_2$-2,6.[139]
The Pb(1)–Pb(1′) bond length is 3.1881 Å; the C(1)–Pb(1)–Pb(1′) bond angle is 94.26°.

absence of sp-hybridization and the presence of lone pairs on lead atoms. In this connection, the bent form **B** with a Pb–Pb single bond rather than linear structure **A** with a Pb–Pb triple bond was considered to be preferable for this compound.[139]

Diplumbyne structure



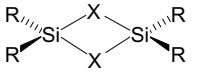
Probably, the π-bond formed upon the overlap of 6p orbitals of lead atoms is too weak. Thus, in the series C≡C, Si≡Si, Ge≡Ge, Sn≡Sn and Pb≡Pb, the strength of the triple bond regularly decreases.

5. Unusually short distances between chemically non-bonded atoms

In 1987, Jemmis *et al.*[143] reported MINDO calculations for the cyclic molecules (R$_2$SiX)$_2$ (**56a–d**) and (R$_2$CX)$_2$ (**57a,b**).

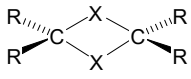
The experimentally determined Si–X–Si angles (deg.) in these molecules differ little from the values calculated by the extended Hückel method and are, respectively, 86.0 and 90.5 (for compound **56a**), 91.0 and 91.6 (**56b**), 91.0 and 85.8 (**56c**), and 82.5 and 81.5 (**56d**).

Structures 56, 57



56a–d

R = H; X = O (**a**), NH (**b**), CH$_2$ (**c**), S (**d**)



57a,b

R = H; X = O (**a**), S (**b**)

Table 7. Lengths of the Si – Si bonds in cyclic molecules **56**.[143]

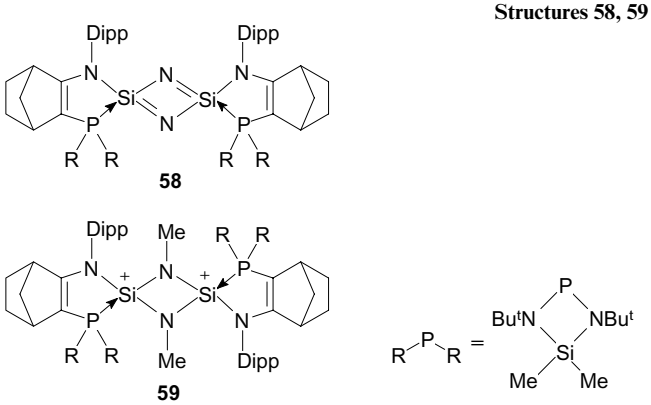
Compound **56**	X	Si – Si bond length /Å			
		experiment	MINDO	extended Hückel method	3-21G (*ab initio*)
a	O	2.31	2.61	2.40	2.54
b	NH	2.49	2.63	2.51	2.62
c	CH_2	2.70	2.56	2.58	2.74
d	S	2.84	2.88	2.72	3.13

The calculations showed that molecules **56** contain unusually short Si – Si bonds (about 2.3 Å), with their length being in the range of Si=Si double bond lengths and depending on the group X (Table 7).

The data obtained by MINDO and extended Hückel method indicate the existence of weak antibonding interaction between the silicon atoms, although the silicon – silicon distances correspond to the length of the Si=Si double bonds! Meanwhile, the carbon – carbon distances are substantially longer than twice the carbon covalent radius (r) and exceed 2 Å.[143] The authors attributed this result to purely geometric factors: the closer the r_X/r_A ratio to the critical value $\sqrt{2}-1$, the shorter the difference between atoms of the element (in this case, carbon or silicon). For example, $r_O/r_C = 0.96$ and $r_O/r_{Si} = 0.66$. Therefore, in the $(H_2GeX)_2$ molecule, short distances between germanium atoms should also be expected ($r_O/r_{Ge} = 0.61$).

In 2016, Jemmis *et al.*[143] synthesized 1,3-disila-2,4-diazacyclobutadiene **58** and analogous dication **59** in which the distances between silicon atoms were 2.23 Å and the Si=Si bond lengths were in the 2.15 – 2.23 Å range (Fig. 36).

Structures 58, 59



The four-membered Si(1) – N(1′) – Si(1′) – N(1) ring is antiaromatic (four π-electrons, all belonging to nitrogen atoms); therefore, distortion of the rhombic structure of the ring due to the Jahn – Teller effect is unavoidable. Thus the nitrogen atoms move apart, which results in the silicon atoms moving towards each other. The electron density distribution in the ring derived from high-resolution X-ray diffraction attests to the absence of a diagonal Si – Si bond (Fig. 37).

The considerable electronegativity difference between the nitrogen and silicon atoms (1.2 in the Pauling scale[63]) accounts for the pronounced polarization of the Si – N bond. As a result, the negatively charged nitrogen atoms move apart, despite the fact that the positive charges on the silicon atoms are markedly lower (in magnitude) due to the coordination of phosphorus atoms. This is responsible for the unusually short distances between silicon atoms that are not connected by covalent bonds.

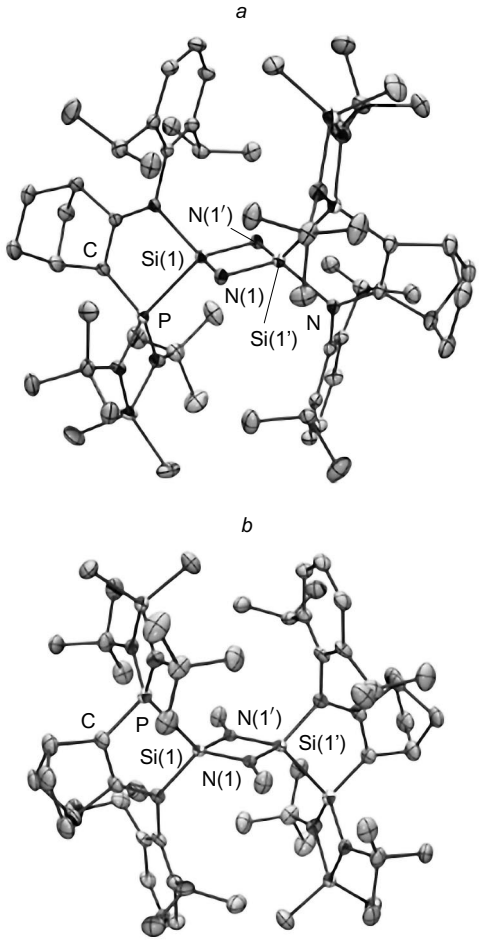


Figure 36. Molecular structures of *trans*-1,3-diaza-2,4-disilacyclobutadiene **58** (*a*) and *N*,*N*′-dimethylcyclodisilazane dication **59** (*b*).[144]
Selected bond lengths (Å) and bond angles (deg.): for **58**, 2.23502 [Si(1) – Si(1′)], 2.6055 [N(1) – N(1′)], 1.7114 [Si(1) – N(1)], 1.7213 [Si(1) – N(1′)]; 81.247 [Si(1) – N(1) – Si(1′)], 98.756 [N(1) – Si(1) – N(1′)]; for **59**, 2.518 [Si(1) – Si(1′)], 2.368 [N(1) – N(1′)], 1.730 [Si(1) – N(1)]; 93.51 [Si(1) – N(1) – Si(1′)], 86.49 [N(1) – Si(1) – N(1′)].

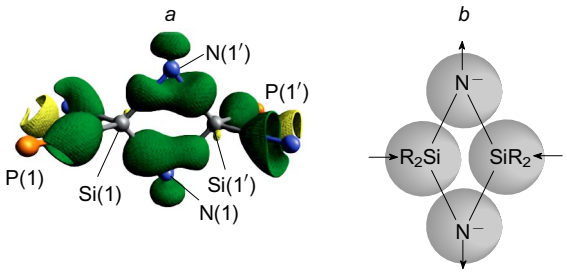
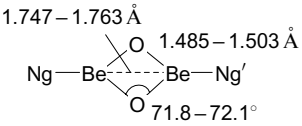


Figure 37. Deformation electron density distribution in the Si(1) – N(1′) – Si(1′) – N(1) ring of *trans*-1,3-diaza-2,4-disilacyclobutadiene (*a*) and scheme of electrostatic repulsion between two nitrogen atoms (*b*).[144]
The green and yellow colour denotes the electron-rich and electron-deficient regions, respectively.

The N-methylation of the four-membered ring decreases the charges on nitrogen atoms and, as a result, sharply decreases the distances between them, from 2.6055 Å in compound **58** to 2.368 Å in dication **59**. The repulsion between the silicon cations in compound **59** accounts for a considerable increase in the bond length between silicon atoms with respect to that in compound **58** (from 2.235 to 2.518 Å).

The examples of 1,3-disila-2,4-diazacyclobutadienes do not exhaust the range of compounds containing unusually short bonds between atoms not bonded by covalent bonds. The preparation of beryllium oxide complexes with noble gas atoms, $Ng_2Be_2O_2$, (Ng = Ne, Ar, Kr, Xe) was reported in 2017.[145]

Structures of $Ng_2Be_2O_2$



An unusual feature of these compounds is that the Be–Be internuclear distance is in the 1.747–1.763 Å range, whereas the length of the Be=Be double bond is 1.80 Å and the length of the Be≡Be triple bond is ~1.70 Å. However, the electron density distribution in these complexes indicates the absence of bonds between beryllium atoms! Furthermore, the Be–OBe–O ring is antiaromatic (four π-electrons from two oxygen atoms) and the Be–O bonds are highly polarized (the Pauling electronegativity difference between beryllium and oxygen is 1.87). The coordination of noble gas atoms decreases the positive charge on the beryllium atoms. Therefore, the Be–Be distances should be expected to decrease with increasing donor ability of the noble gas atoms. According to the data of Zhang *et al.*,[145] the positive charge on the noble gas atoms in the complexes varies in the following order: 0.07 (Ne), 0.16 (Ar), 0.18 (Kr), 0.21 (Xe). In accordance with this, the shortest Be–Be distance (1.747 Å) is found in $Xe_2Be_2O_2$, while the longest distance is in $Ne_2Be_2O_2$ (1.763 Å) (Fig. 38).

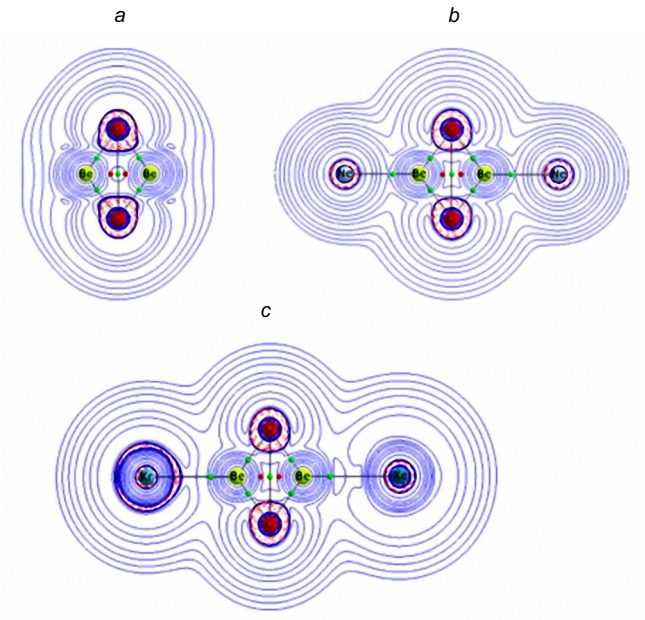


Figure 38. Electron density Laplacian $\Delta\rho(r)$ for Be_2O_2 (*a*), Ne–Be_2O_2–Ne (*b*), Kr–Be_2O_2–Xe (*c*) molecules in the Be_2O_2 ring plane; the calculation was done at the MO6-2X/def2-QZVPP level.[145]
The red dashed lines indicate the charge concentration regions [$\Delta\rho(r) < 0$], the continuous blue lines show the regions of charge depletion [$\Delta\rho(r) > 0$]. Continuous lines connect the atomic nuclei; green dots correspond to bond critical points and red dots show the ring critical points.

6. Two-centre three-electron bonds

In 1931, Pauling[146] introduced the notion of three-electron bonds to describe the electronic structures of paramagnetic molecules such as NO, NO_2 or O_2. An example of species with a three-electron bond is the He_2^+ cation in which three electrons occupy σ-bonding and σ-antibonding (σ*) orbitals (Fig. 39 *a*).

The electronic configuration of the He_2^+ cation is $(\sigma_s)^2(\sigma_s^*)^1$; therefore, the He–He bond order is 1/2. Note that in the hydrogen molecular cation H_2^+, the bond is also a half bond. However, the bond in the helium cation is weaker, since unlike the bond in the H_2^+ cation, the strength of the half bond is affected by pronounced repulsion of three electrons. Therefore, according to quantum chemical calculations,[148,149] the order of σ-bond in the case of two-centre three-electron (2c–3e) bond is less than 1/2.

The 2c–3e-bonds are commonly designated by '∴'. These bonds can be formed by s-block (in particular, alkaline earth metals), p-block (in this case, 15 valence electrons are necessary) and d-block elements (d^{10} electronic configuration). In particular, for the crystallographically characterized Xe_2^+ cation in the $[Xe_2]^+[Sb_4F_{21}]^-$ salt, the Xe∴Xe bond length is unusually great, 3.09 Å,[150] which is much longer than twice the covalent radius of xenon (2.80 Å).[151] Abnormal features of this type are rarely encountered; an example is the carbonyl $Re_2(CO)_{10}$ in which the Re–Re bond length (3.04 Å) is also greater than twice the covalent radius of rhenium (3.02 Å).[63] The fact that the Xe∴Xe bond is weak is indicated by its minor dissociation energy of 0.975 eV.[150]

The dihalide anions X_2^- and dichalcogenide trianions E_2^{3-} are isoelectronic analogues of the Xe_2^+ cation. The X_2^- molecular ions were investigated back in 1957 [152] using X-ray irradiation of crystals of alkali metal halides (LiF, NaCl, KCl, KBr). This type of radiolysis induces to radiation damages (see, for example, a monograph [153]). Dichalcogenide trianions were unknown until recently.

As regards the half bonds between d-elements, in the case of M_2^{n+} cluster ions, the D-term of the atom is split in the field of D_h symmetry into three terms: term (corresponding to d_z^2 orbital), doubly degenerate Π_g term (d_{xz} and d_{yz} orbitals) and doubly degenerate Δ_g term ($d_{x^2-y^2}$ and d_{xy} orbitals). According to general selection rules, non-zero overlap is possible only for orbitals of identical symmetry. The linear combination of Σ_g^+ orbitals gives a bonding σ orbital and an antibonding σ* orbital. The linear combination of atomic orbitals of the Π_g term gives π and π* orbitals, while the combination of atomic orbitals of the Δ_g term gives δ and δ* orbitals (see Fig. 39). In this case, the electronic configuration is $(\sigma)^2(\pi)^4(\delta)^4(\delta^*)^4(\pi^*)^4(\sigma)^1$. This configuration is possible for palladium with $4d^{10}$ valence configuration; indeed, in the Pd_2^+ cation, the Pd∴Pd bond is present. Figure 39 shows some compounds that may have half bonds E_2^{3-} and M_2^{5+}.

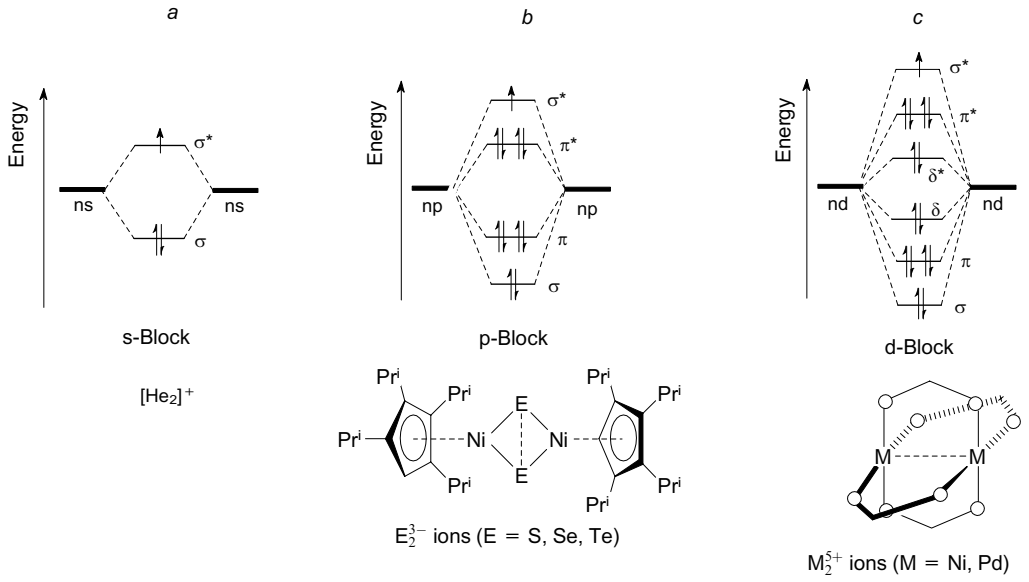


Figure 39. Half (two-centre three-electron) bonds for s- (*a*), p- (*b*) and d-block (*c*) elements.[147]

In tetragonally coordinated complexes shown in Fig. 40, the symmetry has decreased to D_{4h}. In this case, the d_{z^2} orbitals are transformed according to the A_{1g} irreducible representation; d_{xz} and d_{yz} orbitals are transformed according to the E_g irreducible representation (*i.e.*, the Π_g term is converted to E_g), while the Δ_g term is split into B_{1g} (including $d_{x^2y^2}$ orbital) and B_{2g} (d_{xy} orbital).

Finally, two MOs are excluded from the sets of δ and δ* orbitals, namely, the δ and δ* MOs formed by the $d_{x^2-y^2}$ orbitals pointing directly to the ligands. These orbitals are used to form donor-acceptor bonds with equatorial groups. Therefore, the number of electrons needed to form the M∴M bonds equals 15, which corresponds to a (d^8-d^7) pair of atoms (Fig. 40 *b*, the dashed lines point to the corresponding ligands). This is attained by either reduction of (d^7-d^7) dimer or oxidation of (d^8-d^8) dimer.

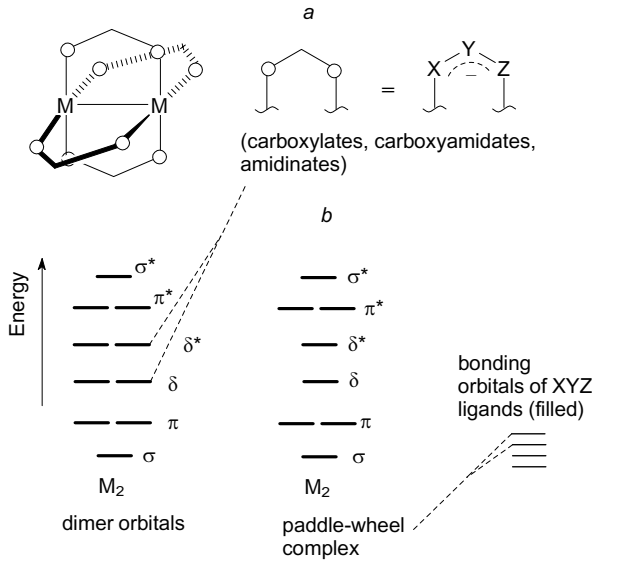


Figure 40. Tetragonally coordinated d-block metal complexes (*a*) and their system of orbitals (*b*).[68]

The oxidation of (d^8-d^8) dimer was described in 1988.[154] The authors studied the $M_2^{II,II}$ complexes (M = Ni^{II}, Pd^{II}) with bidentate bridging ligands, *N*,*N*′-bis(4-methylphenyl)formamidinates [(*p*-methyl)form] designated by XYZ, where X = Z = NAr, Y = CH (see Fig. 40 *a*).

According to the 2c – 3e bond model, the neutral complex $[M_2((p\text{-methyl})form)_4]$ contains no M – M bond (16 valence electrons fully occupy bonding and antibonding orbitals). Its oxidation to $[M_2((p\text{-methyl})form)_4]^+$ should yield the M∴M bond (15 valence electrons). However, the outcome was unexpected. The oxidation of $[Ni_2((p\text{-methyl})form)_4]$ to $[Ni_2((p\text{-methyl})form)_4]^+$ results in a decrease in the distance between the nickel atoms by only 0.07 Å, whereas in the analogous palladium complex, the bond length between the palladium atoms increases by 0.015 Å. The EPR data attest to localization of the unpaired electron on the nickel atom; nevertheless, according to quantum chemical calculations,[154] this electron occurs in the δ* orbital rather than in the σ* orbital, as implied by the diagram shown in Fig. 40.

The replacement of the methyl group in (*p*-methyl)form by a methoxy group gives (*p*-methoxy)form ligands. The analogous complex, $[Ni_2((p\text{-methoxy})form)_4]$, has a considerably lower oxidation potential and the corresponding $Ni_2^{II,II}$ complexes are more stable. Figure 41 shows the molecular structures of neutral and cationic complexes with the (*p*-methoxy)form ligand. The oxidation of neutral complex is accompanied by a decrease in the distance between the nickel atoms by 0.11 Å, which exceeds the expected reduction of the bond length upon removal of an electron from the δ* orbital (0.03 – 0.07 Å). The EPR spectroscopy data and DFT calculations[155] confirm that the cluster Ni_2^{5+} has the $(\sigma^*)^1$ configuration and, hence, it contains the Ni∴Ni bond.

Analogous DFT calculations for the complexes $[Pd_2((p\text{-methoxy})form)_4]$, $[Pd_2((p\text{-methoxy})form)_4]^+[BF_4]^-$ (Ref. 156) predict the $(\sigma^*)^1$ ground state for the cation; therefore, these compounds also have a Pd∴Pd half σ-bond.

In 2005, Brown *et al.*[157] prepared an unusual cluster cation, $[Cu_3S_2(tmeda)_3]^{3+}$ (tmeda is tetramethylethylenedi-

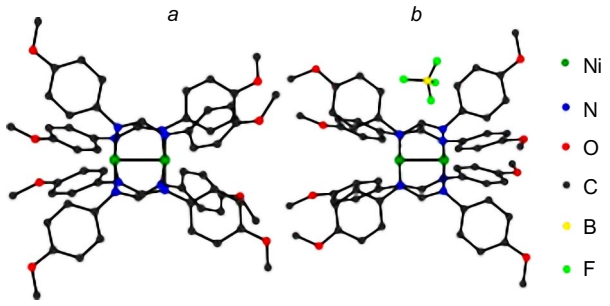


Figure 41. Molecular structures of $[Ni_2((p\text{-methoxy})form)_4]$ (*a*) and $[Ni_2((p\text{-methoxy})form)_4]^+[BF_4]^-$ (*b*).[147]

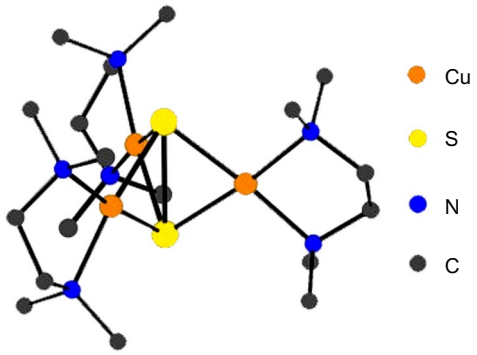


Figure 42. Molecular structure of the $[Cu_3S_2(tmeda)_3]^{3+}$ trication.[147]
Hydrogen atoms are omitted for clarity.

amine). The structure of this cluster (Fig. 42) attracted researchers' attention due to the fact that in this case, chemists faced, for the first time, the situation where the structural features of a cluster cannot be unambiguously interpreted in terms of the common crystallographic views.

In 2009, a paper eloquently entitled 'A Bonding Quandary — or — A Demonstration of the Fact That Scientists Are Not Born With Logic' was reported by three co-authors [158] (Fig. 43). The paper addressed the problem of either presence or absence of a bond between the sulfur atoms in the cluster $[Cu_3S_2(tmeda)_3]^{3+}$ and in clusters **60a**,**b** reported by Isobe and co-workers.[159, 160] In these clusters for M = Ir, the d_1 bond is long (> 2.7 Å) and the d_2 bond is short (< 2.1 Å); for M = Rh, the d_1 bond is short and the d_2 bond is long. In particular, the cluster cation $[\{Rh_2Cp^*_2(\mu\text{-}CH_2)_2\}_2(\mu\text{-}S_4)]^{2+}$ was described.[159] Formally,

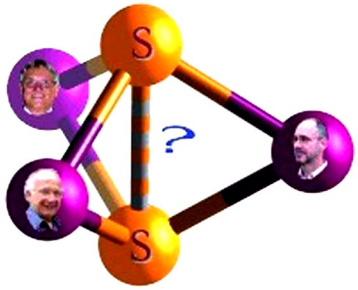
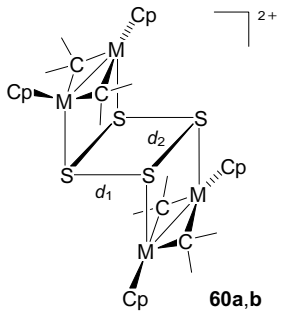


Figure 43. Co-authors of Ref. 158: Carlo Mealli (right), Santiago Alvarez (top left) and Nobel Prize Laureate Roald Hoffmann (bottom left).

Structure 60



60a,**b**

M = Ir (**a**), Rh (**b**)

this cation contains a coordinated tetrasulfide ion, a fragment of which is shown below (the short bonds between the sulfur atoms are depicted by a continuous and a dashed line, while the long bonds are shown by only dashed lines). The cluster has both short (1.979 Å) and long (2.702 Å) bonds. An opposite situation occurs in the similar complex $[\{(IrCp^*)_2\text{-}(\mu\text{-}CH_2)_2\}_2\text{-}(\mu\text{-}S_4\text{-}S{:}S'{:}S''{:}S''')]Cl_2$ (Cp* is pentamethylcyclopentadienyl): the short bonds between the sulfur atoms (2.049 Å) are parallel to the bonds between iridium atoms and long sulfur–sulfur bonds (2.895 Å) are perpendicular to the bonds between iridium atoms (Fig. 44).[160]

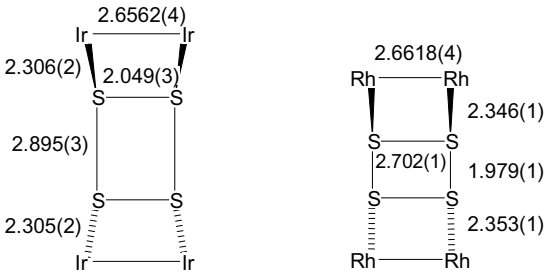
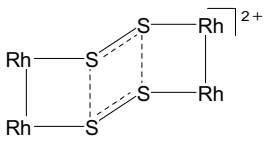


Figure 44. Structural motifs in iridium (**60a**) and rhodium (**60b**) clusters.[160]

Hoffmann and co-workers [158] tend to believe that the Jahn–Teller distortion of the S_4^{2-} cyclic ion gives rise to two single and two S–S half bonds in the iridium- and rhodium-based cluster ions. As regards the structure of $[Cu_3S_2(tmeda)_3]^{3+}$ and similar clusters, opinions of the three authors [158] were different: they did not agree about evidence for coordination of either two sulfide ions ($2 \times S^{2-}$) or one disulfide ion S_2^{2-}. However, the structures of all these clusters can be described in terms of the 2c–3e-bond model (see Figs 39 and 45), which implies the coordination of the S_2^{3-} anion.

Structure of the S_4 fragment



According to quantum chemical calculations,[147] ~50% of the molecular orbitals of the Ni_2S_2 moiety are antibonding σ* orbitals of the S_2 group. Thus, it can be stated that the coordinated S_2^{3-} species contain 2c–3e S∴S bonds.

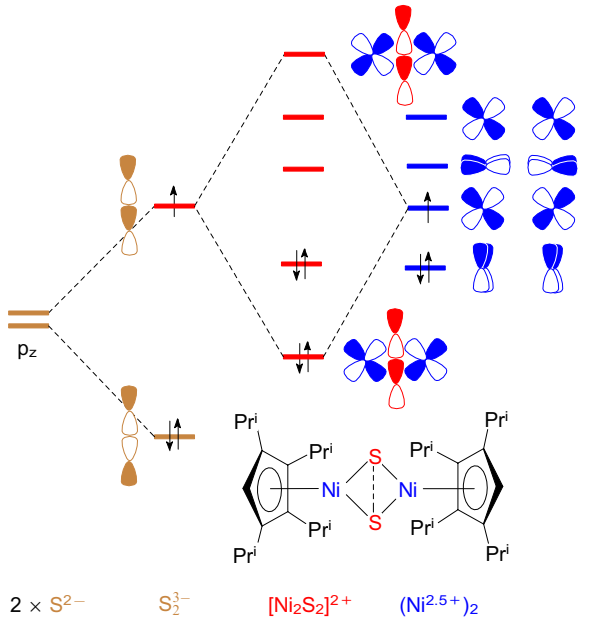


Figure 45. Fragment of the MO diagram of the $Cp^*_2Ni_2S_2$ cluster representing the covalent interaction between the σ*-orbital of the S–S moiety and nickel orbitals.[147]
Other interactions between Ni_2-S_2 and π-orbitals of the cyclopentadienyl anion are not shown.

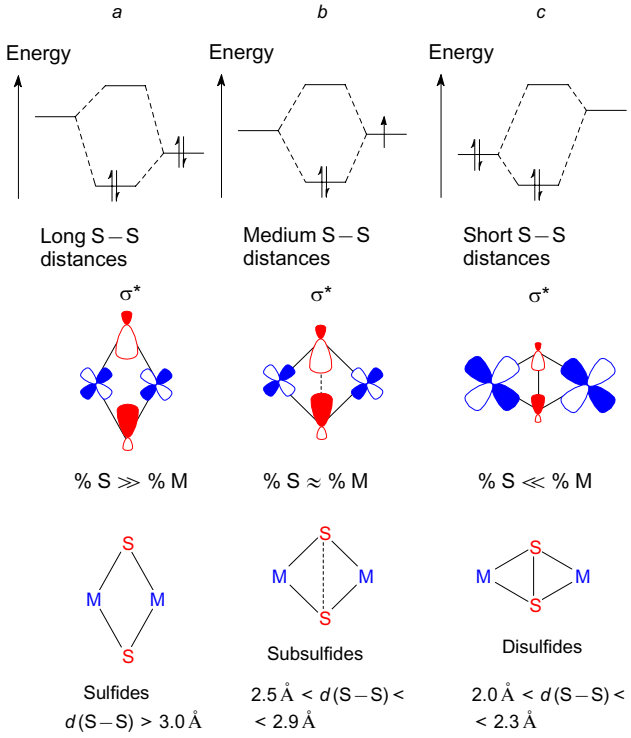
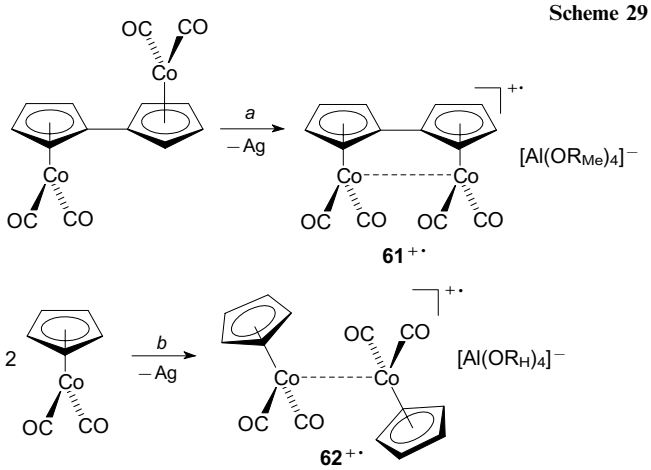


Figure 46. Electronic properties [metal–sulfur interactions (top); occupied orbitals and contributions of S and M orbitals to the MOs (middle)] and structural features (bottom) for sulfide (*a*), subsulfide (*b*) and disulfide (*c*) complexes.[147]

Figure 46 presents a diagram of electronic and structural properties of sulfide ($2 \times S^{2-}$), subsulfide (S_2^{3-}) and disulfide (S_2^{2-}) complexes.

Scheme 29



(*a*) $Ag[Al(OR_{Me})_4]$, 0 °C; (*b*) $Ag[Al(OR_H)_4]$, 0 °C;
$OR_{Me} = OC(CF_3)_2Me$, $OR_H = OC(CF_3)_2H$

A publication of 2015[161] describes the radical cation clusters $[Co_2Cp_2(CO)_4]^{+\bullet}$ with Co∴Co bonds formed upon single-electron oxidation of the starting multinuclear complexes (Scheme 29), either bridged (**61**$^{+\bullet}$) or non-bridged (**62**$^{+\bullet}$). The structures of complexes **61**$^{+\bullet}$ and **62**$^{+\bullet}$ are presented in Fig. 47. As can be seen, the Co–Co bond in the non-bridged complex is even somewhat shorter than in the fulvalenediyl-bridged complex. The oxidation of the starting complexes results in the formation of Co∴Co half bonds. The replacement of the Cp anion by a larger Cp* anion gives a mixture of non-bridged (*anti*-**62**$^{+\bullet}$) and carbonyl-bridged (*trans*-**62**$^{+\bullet}$) complexes (Scheme 30).[161]

Figure 48 shows the molecular structures of complexes *anti*-**63**$^{+\bullet}$ and *trans*-**63**$^{+\bullet}$. As can be seen from Figs 47 and 48, all binuclear cobalt complexes reported by Zheng

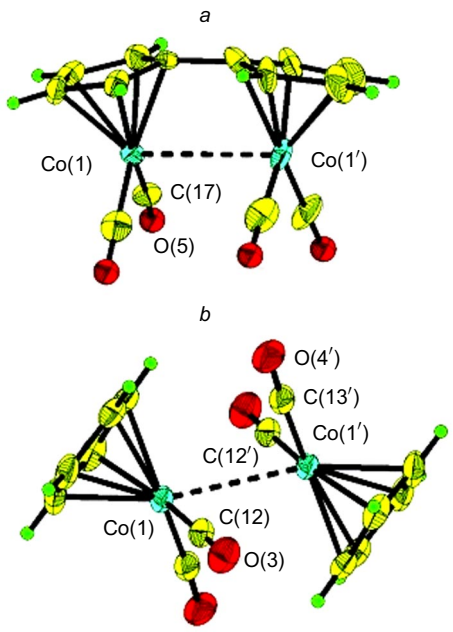
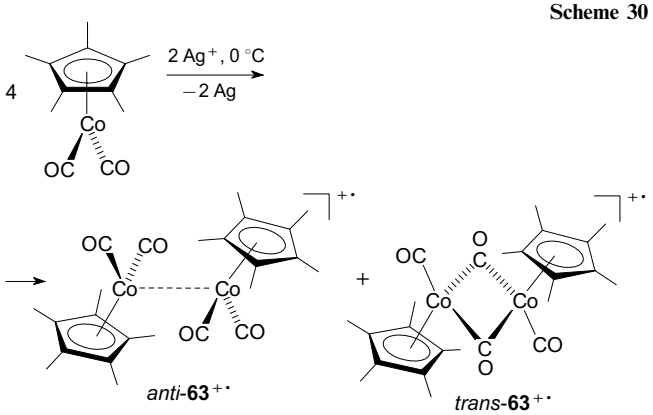


Figure 47. Molecular structures of complexes **61**$^{+\bullet}$ (*a*) and **62**$^{+\bullet}$ (*b*).[161]
Selected bond lengths (Å): for **61**$^{+\bullet}$, 3.0774 [Co(1)–Co(1′)], 1.771 [Co(1)–C(17)], 1.133 [C(17)–O(5)]; for **62**$^{+\bullet}$, 2.9593 [Co(1)–Co(1′)], 1.776 [Co(1)–C(12)], 1.135 [C(12)–O(3)].

Scheme 30



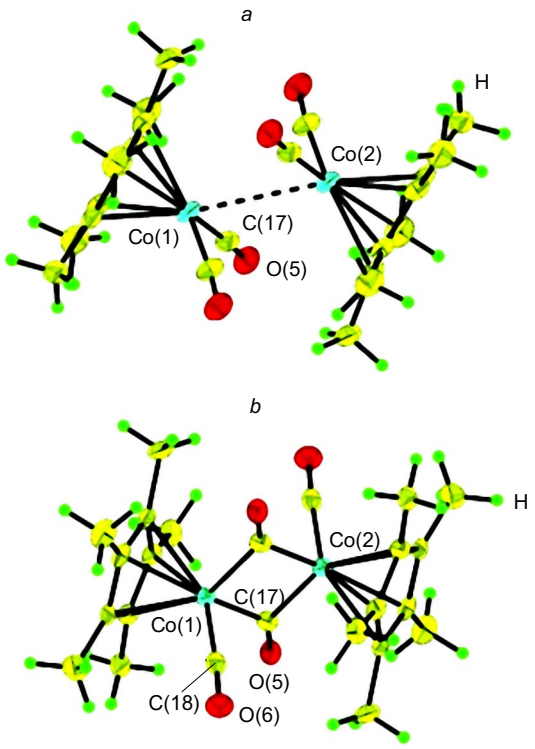


Figure 48. Molecular structures of complexes *anti*-**63**$^{+\bullet}$ (*a*) and *trans*-**63**$^{+\bullet}$ (*b*).[161]
Selected bond lengths and interatomic distances (Å): for *anti*-**63**$^{+\bullet}$, 3.074 [Co(1)–Co(2)], 1.783 [Co(1)–C(17)], 1.133 [C(17)–O(5)]; for *trans*-**63**$^{+\bullet}$, 2.6208 [Co(1)–Co(2)], 1.951 [Co(1)–C(17)], 1.813 [Co(1)– C(18)], 1.158 [C(17)–O(5)], 1.133 [C(18)–O(6)].

et al.[161] contain 2c–3e Co∴Co bonds (15 valence electrons, which corresponds to a d^8-d^7 pair of atoms).

7. Isolated square planar carbon complexes

Since the time of Van't Hoff, the statement of the tetrahedral geometry of carbon bonds has been considered undisputable. The cause for this can be easily understood if the electronic structures of the tetrahedral and square forms of methane are compared. In the case of the tetrahedral structure, the atomic orbitals of carbon are transformed according to irreducible representations (IRR) of T_d group in the following way: 2s orbital is transformed according to the A_1 IRR and three 2p orbitals are transformed according to triply degenerate T_2 IRR. The four-dimensional Γ_4 reducible representation obtained with the basis of four hydrogen 1s orbitals is expanded into IRR in the following way:

$$\Gamma_4 = A_1 \oplus T_2 \qquad (14)$$

By combining the 2s orbital of carbon with the hydrogen group orbital of A_1 symmetry, one gets the a_1 bonding orbital and the a_1^* antibonding orbital of methane. Similarly, by combining the carbon p orbital with hydrogen group orbitals of T_2 symmetric, one gets triply degenerate orbitals: bonding (t_2) and antibonding (t_2^*) ones (Fig. 49).

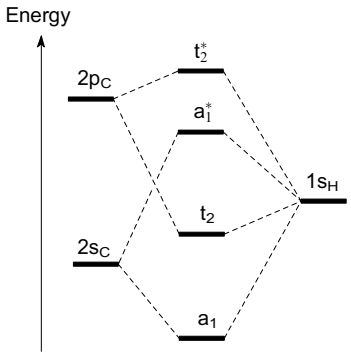


Figure 49. Molecular orbitals of a methane molecule.

Eight electrons occupy the bonding MOs; meanwhile, the electronic configuration of methane is $(a_1)^2(t_2)^6 = A_1$, which corresponds to the formation of four bonds (fully symmetric ground state). In the case of the square structure of methane, the point group of symmetry would be D_{4h}. The carbon AOs are transformed according to D_{4h} group IRRs: A_{1g} for 2s orbital, A_{2u} for $2p_z$ orbital, and E_u for $2p_x$ and $2p_y$ orbitals. The Γ_4 reducible representation obtained with the basis of four hydrogen 1s orbitals is expanded into D_{4h} group IRR in the following way:

$$\Gamma_4 = A_{1g} \oplus E_u \oplus B_{1g} \qquad (15)$$

In this case, the combination of the 2s orbital of carbon with the hydrogen group orbital (A_{1g} symmetry) gives the a_{1g} bonding orbital and the a_{1g}^* antibonding orbital; the combination of $2p_x$ and $2p_y$ orbitals of carbon with the hydrogen group orbitals (E_u symmetry) generates the doubly degenerate e_u bonding level and the corresponding e_u^* antibonding level. The $2p_z$ orbital of carbon gives non-bonding level (A_{2u} symmetry), while the hydrogen group orbital produces one more the non-bonding level (B_{1g} symmetry) (Fig. 50).

Finally, square methane has the following electronic configuration $(a_{1g})^2(e_u)^4(b_{1g})^2 = A_{1g}$. Thus, the bonding MOs contain six electrons and the non-bonding orbital contains two electrons. Since only three bonds are formed, the square structure of methane is much less stable.

The first doubts about the permanent tetrahedral configuration of the four carbon bonds were probably expressed by Hoffmann *et al.*[162] in 1970. On the basis of quantum chemical calculations for model compounds, the authors concluded that the square coordination of carbon is possible in metal clusters. Particular ways to implement this

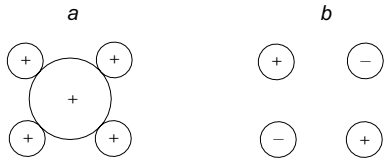


Figure 50. Bonding MO of A_{1g} symmetry (*a*) and B_{1g} non-bonding group orbital (*b*) of hydrogen atoms.

structure were formulated. The square coordination of carbon is addressed in more detail in the review of Minkin, Minyaev and Hoffmann [163] published in 2002. The authors considered seven options to stabilize the square planar coordination of carbon: the use of π-acceptor groups (since the non-bonding A_{2u} orbital is a π-type orbital), annulenes or small rings, organoboron cages, Jahn–Teller effect and sterically strained systems; and the introduction of a carbon atom inside a rigid cage of bonds. The implementation of these methods can be exemplified by an organometallic tantalum complex containing two carbon atoms with a square coordination (Fig. 51).[164]

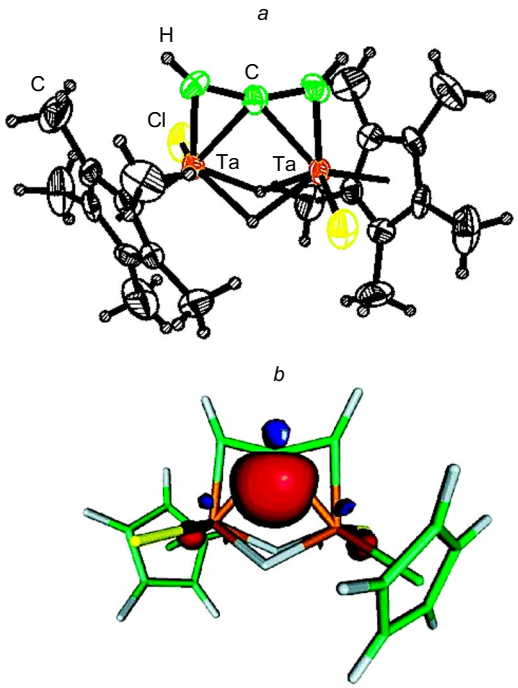


Figure 51. Molecular structure of the binuclear tantalum cluster containing two carbon atoms with a square planar coordination (*a*) and fragment of the structure with the two-electron three-centre Ta–C–Ta bond (*b*).[164]

In 2000, a fundamentally new result was obtained: single square planar carbon clusters were obtained in the gas phase.[165] In particular, it was shown that the $[CAl_4]^-$ and $[CAl_4]^{2-}$ cluster ions are planar in the gas phase. We proposed [166] a simple explanation to this phenomenon. If hydrogen atoms are replaced by p-element atoms (able to form π-bonds), the square form can be stabilized if certain geometric conditions are fulfilled. In particular, the atoms of p-elements should bind not only to carbon, but also to each other. For this purpose, the atoms should be in contact both with the carbon atom and with each other (Fig. 52).

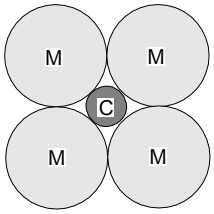


Figure 52. Geometric condition for stability of the planar form of $[CM_4]$.[166]

The contact condition gives the ratio between the carbon and metal atomic radii (R)

$$R_C + R_M = \sqrt{2}\,R_M \quad (16)$$

hence,

$$R_C/R_M = \sqrt{2} - 1\,0.414 \quad (17)$$

When the ratio of the radii is lower, the M–C contact is broken, while when the ratio is higher, the M–M bonds are weakened.

Apart from the geometric conditions, atoms M should be trivalent (each atom forms one bond with carbon and two bonds with neighbouring metal atoms). In the square planar complex, the carbon atom can form three σ-bonds (less strong than the bonds formed by common sp^2-hybridized atoms) and one π-bond. In general, this will lead to energy loss on going from the tetrahedral to the square planar coordination. The loss can be counterbalanced by four-centre M–M–M–M bonds around the perimeter of the complex and a delocalized donor-acceptor π-bond in which carbon serves as the donor. Thus, the geometry of the cluster $[CM_4]$ is determined not by the central atom (carbon), but by the coordinated trivalent atoms.

When the square planar cluster is converted to a tetrahedral one, the M–M distance increases 1.155-fold ($\sin 54.74^\circ/\sin 45^\circ \approx 1.155$, with the M–C bond length being invariable). This would result in a sharp decrease in the M–M bond strength and a considerable energy loss. Table 8 presents the R_C/R_M ratios for trivalent metals (M), where M is a Group 13 or 15 element.

Table 8. Ratios of the atomic radii of trivalent metals and carbon.[166]

M	R_C/R_M (see [a])	M	R_C/R_M (see [a])
B	0.856–0.906	Sc	0.469
Al	0.538	Y	0.429
Ga	0.534	La	0.410
In	0.462	Bi	0.423
Tl	0.449		

[a] The atomic radii of metals were taken from Refs 165 and 167.

As can be seen in Table 8, scandium group elements, especially lanthanum, meet condition (17) best of all. In the case of boron group elements, the formation of stable square carbon clusters is most probable for indium and thallium. For aluminium, this ratio is high (perhaps, for this reason, neutral $[CAl_4]$ is tetrahedral).[165] However, in the $[CAl_4]^-$ and $[CAl_4]^{2-}$ anions, the effective atomic radii increase, which decreases the R_C/R_M ratio to acceptable

values and, hence, the anions can have planar geometry. It was suggested,[167] on the basis of quantum chemical calculations, that the square planar $[CAl_4]^{2-}$ anions may exist in the $\{Na_2[CAl_4]\}_2$ dimeric clusters.

It follows from group theory analysis [166] that the planar clusters $[CM_4]$ have two bonding MOs of A_{1g} symmetry (one five-centre and one four-centre MOs), two bonding MOs of E_u symmetry, four-center bonding MOs of B_{1g} and B_{2g} symmetry (all are σ-bonds); a five-centre bonding π-MO of A_{2u} symmetry, and virtually non-bonding π-MO of E_g symmetry. Therefore, it can be expected that not only the 16-electron planar $[CM_4]$ system, but also the 18-electron $[CM_4]^{2-}$ system will be stable.

This conclusion was confirmed [166] by quantum chemical calculations using the scattered wave method (PB-X_α) in the relativistic approximation for core electrons and non-relativistic approximation for the valence electrons. The calculation results confirmed the idea of importance of the geometric factor. Indeed, the $[CB_4]^{n-}$ clusters are much more stable in the tetrahedral form: the tetrahedral $[CB_4]$ cluster is more stable than the square planar one (the total energy is lower by 7.52 eV; for $[CB_4]^{2-}$, this difference is 6.68 eV). However, tetrahedral clusters based on boron can hardly exist, as their electronic configurations are $(t_2)^2$ for $[CB_4]$ and $(t_2)^4$ for $[CB_4]^{2-}$. Therefore, they are unstable due to the Jahn–Teller effect.

According to the study of Starodub and Ziolkovsky,[166] the square planar form is more stable starting from aluminium for doubly charged clusters and starting from gallium for neutral clusters. The energy difference between the lowest unoccupied and highest occupied MOs in $[CAl_4]^{2-}$ is rather large, about 1.5 eV; therefore, the isolation of crystalline salts with the $[CAl_4]^{2-}$ anion is quite possible (this possibility was also noted by Geske and Boldyrev [167]).

Thus, the geometry of $[CM_4]$ clusters is determined by the combination of four- and five-centre bonds rather than by the carbon atom.

The review by Keese [168] published in 2006 considered the options for stabilization of planar four-coordinate carbon complexes; however, all of them were already discussed by Minkin *et al.*[163] Recent publications [169–172] attest to significance of this problem. However, the approach that we proposed was implemented only in 2012 by Castro *et al.*[173] without reference to our publication.[166] The mentioned paper [173] confirmed out key conclusion for $[CM_4]^{2-}$ (M = Al, Ga, In, Tl), while our paper [166] demonstrated the possibility of existence of square planar anionic $[CM_4]^2$ (M = Al, Ga, In, Tl, Sc, Y, Bi) and neutral $[CM_4]$ clusters for all trivalent elements starting from gallium.

8. Conclusion

This review considers only some important aspects of the modern chemical bond theory — multiple bonds between Group 13–15 elements, unusual triple bond geometry in these compounds, unusually short distances between covalently non-bonded atoms, two-centre three-electron bonds and square planar carbon clusters. The review does not cover other important areas of modern chemistry such as single-electron bonds,[174] halogen, chalcogen and pnictogen bonds,[175, 176] planar hypercoordinated compounds,[177] relativistic effects in chemistry, in particular, so-called aurophilic interactions.[178–181] The aspects of the modern chemical bond theory considered in this review do not exhaust the diversity of new revolutionary phenomena, but nevertheless they give the idea of this theory as a continuously developing area.

References

1. W.Heitler, F.London. *Z. Phys.*, **44**, 455 (1927)
2. L.Pauling *The Nature of the Chemical Bond*. (Ithaca, NY: Cornell University Press, 1939)
3. N.V.Sidgewick, H.M.Powell. *Proc. R. Soc. London, Ser. A*, **176**, 153 (1940)
4. R.J.Gillespie, R.S.Nyholm. *Quart. Rev. (London)*, **11**, 339 (1957)
5. *Chemistry of Hypervalent Compounds*. (Ed. K.-y.Akiba). (New York: Wiley-VCH, 1998)
6. V.A.Starodub. *Obshchaya Khimiya. (Uchebnoe Posobie dlya studentov Vysshykh Uchebnykh Savedenii)*. [General Chemistry. (Textbook for University Students)]. (Kharkov: Folio, 2007)
7. J.-S.Ming, M.-C.Yang, M.-D.Su. *ACS Omega*, **3**, 76 (2018)
8. N.Arnold, H.Braunschweig, R.D.Dewhurst, W.C.Ewing. *J. Am. Chem. Soc.*, **138**, 76 (2016)
9. M.Arrowsmith, J.Böhnke, H.Braunschweig, M.A.Celik, Ch.Claes, W.C.Ewing, I.Krummenacher, K.Lubitz, Ch.Schneider. *Angew. Chem., Int. Ed.*, **55**, 11271 (2016)
10. Y.Wang, G.H.Robinson. *Organometallics*, **26**, 2 (2007)
11. Y.Wang, G.H.Robinson. *Inorg. Chem.*, **50**, 12326 (2011)
12. H.Braunschweig, R.D.Dewhurst. *Angew. Chem., Int. Ed.*, **52**, 3574 (2013)
13. Y.Wang, G.H.Robinson. *Inorg. Chem.*, **53**, 11815 (2014)
14. J.Brand, H.Braunschweig, S.S.Sen. *Acc. Chem. Res.*, **47**, 180 (2014)
15. H.Braunschweig, I.Krummenacher, C.Lichtenberg, J.D.Mattock, M.Schäfer, U.Schmidt, C.Schneider, T.Steffenhagen, S.Ulrich, A.Vargas. *Angew. Chem., Int. Ed.*, **56**, 889 (2017)
16. M.Arrowsmith, H.Braunschweig, T.E.Stennett. *Angew. Chem., Int. Ed.*, **56**, 96 (2017)
17. L.Xi, H.-F.Zhang, L.-S.Wang, G.D.Geske, A.I.Boldyrev. *Angew. Chem., Int. Ed.*, **36**, 3630 (2000)
18. S.G.Shore, K.W.Böddeker. *Inorg. Chem.*, **3**, 914 (1964)
19. D.J.Grant, D.A.Dixon. *J. Phys. Chem. A*, **110**, 12955 (2006)
20. M.Sugie, H.Takeo, C.Matsumura. *Chem. Phys. Lett.*, **64**, 573 (1979)
21. K.W.Böddeker, S.G.Shore, R.K.Bunting. *J. Am. Chem. Soc.*, **88**, 4396 (1966)
22. M.Sugie, H.Takeo, C.Matsumura. *J. Mol. Spectrosc.*, **123**, 286 (1987)
23. Y.Kawashima. *J. Chem. Phys.*, **87**, 6331 (1987)
24. E.Bulak, G.E.Herberich, I.Manners, H.Mayer, P.Paetzold. *Angew. Chem., Int. Ed. Engl.*, **27**, 958 (1988)
25. R.Islas, E.Chamorro, J.Robles, T.Heine, J.C.Santos, G.Merino. *Struct. Chem.*, **18**, 833 (2007)
26. P.Paetzold, C.von Plotho. *Chem. Ber.*, **115**, 2819 (1982)
27. H.Nöth. *Angew. Chem., Int. Ed. Engl.*, **27**, 1603 (1988)
28. J.Kiesgen, J.Münster, P.Paetzold. *Chem. Ber.*, **126**, 1559 (1993)
29. H.-U.Meier, P.Paetzold, E.Schroder. *Chem. Ber.*, **117**, 1954 (1984)
30. P.Paetzold, C.von Plotho, G.Schmid, R.Boese, B.Schrader, D.Bougeard, U.Pfeiffer, R.Gleiter, W.Schafer. *Chem. Ber.*, **117**, 1089 (1984)
31. K.-H.van Bonn, T.von Bennigsen-Mackiewicz, J.Kiesgen, C.von Plotho, P.Paetzold. *Z. Naturforsch., Sect. B*, **43**, 61 (1988)
32. P.Paetzold, A.Richter, T.Thijssen, S.Würtenberg. *Chem. Ber.*, **112**, 3811 (1979)
33. P.Paetzold, T.von Bennigsen-Mackiewicz. *Chem. Ber.*, **114**, 298 (1981)
34. K.Delpy, H.-U.Meier, P.Paetzold, C.von Plotho. *Z. Naturforsch., Sect. B*, **39**, 1696 (1984)

35. P.Paetzold, C.von Plotho, G.Schmid, R.Boese. *Z. Naturforsch., Sect. B*, **39**, 1069 (1984)
36. Ph.P.Power, A.Moezzi, D.C.Pestana, M.A.Petrie, S.C.Shoner, K.M.Waggoner. *Pure Appl. Chem.*, **63**, 859 (1991)
37. D.A.Dixon, M.Gutowski. *J. Phys. Chem. A*, **109**, 5129 (2005)
38. D.A.Dixon, D.J.Grant. *J. Phys. Chem. A*, **109**, 10138 (2005)
39. J.E.Douglas, B.S.Rabinovitch, F.S.Looney. *J. Chem. Phys.*, **23**, 315 (1955)
40. J.-S.Lu, M.-C.Yang, M.-D.Su. *Phys. Chem. Chem. Phys.*, **19**, 8026 (2017)
41. K.B.Wiberg. *Tetrahedron*, **24**, 1083 (1968)
42. J.-S.Lu, S.-H.Su, M.-C.Yang, X.-T.Wen, J.-Z.Xie, M.-D.Su. *Organometallics*, **35**, 3924 (2016)
43. J.Huheey, E.Keiter, R.Keiter. *Anorganische Chemie: Prinzipien von Struktur und Reaktivität*. (2 Auflage). (Berlin, New York: De Gruyter, 1995)
44. J.-S.Lu, M.-C.Yang, M.-D.Su. *Chem. Phys. Lett.*, **686**, 60 (2017)
45. J.-S.Lu, M.-C.Yang, M.-D.Su. *New J. Chem.*, **42**, 6932 (2018)
46. A.Stock, W.Sütterlin, F.Kurzen. *Z. Anorg. Allg. Chem.*, **225**, 225 (1935)
47. E.Kaufmann, P.von R.Schleyer. *Inorg. Chem.*, **27**, 3987 (1988)
48. A.Moezzi, M.M.Olmstead, Ph.P.Power. *J. Am. Chem. Soc.*, **114**, 2715 (1992)
49. R.A.Godfroid, T.G.Hill, T.P.Onak, S.G.Shore. *J. Am. Chem. Soc.*, **116**, 12107 (1994)
50. Y.Shoji, T.Matsuo, D.Hashizume, M.J.Gutmann, H.Fueno, K.Tanaka, K.Tamao. *J. Am. Chem. Soc.*, **133**, 11058 (2011)
51. H.Klusik, A.Berndt. *Angew. Chem., Int. Ed. Engl.*, **20**, 870 (1981)
52. A.Moezzi, R.A.Bartlett, Ph.P.Power. *Angew. Chem., Int. Ed. Engl.*, **31**, 1082 (1992)
53. H.Nöth, J.Knizek, W.Ponikwar. *Eur. J. Inorg. Chem.*, 1931 (1999)
54. W.J.Grigsby, Ph.P.Power. *Chem. Commun.*, 2235 (1996)
55. W.J.Grigsby, Ph.P.Power. *Chem. – Eur. J.*, **3**, 368 (1997)
56. A.B.Burg, H.I.Schlesinger. *J. Am. Chem. Soc.*, **59**, 780 (1937)
57. W.Gordy, H.Ring, A.B.Burg. *Phys. Rev.*, **78**, 512 (1950)
58. P.Paetzold, P.Böhm, A.Richter, E.Scholl. *Z. Naturforsch., Sect. B*, **31**, 754 (1976)
59. H.Bock, L.Cederbaum, W.von Niessen, P.Paetzold, P.Rosmus, B.Soiouki. *Angew. Chem., Int. Ed. Engl.*, **28**, 88 (1989)
60. M.Groteklaes, P.Paetzold. *Chem. Ber.*, **121**, 809 (1988)
61. A.Skancke, J.F.Liebman. *J. Phys. Chem.*, **98**, 13215 (1994)
62. M.Finze, E.Bernhardt, A.Terheiden, M.Berkei, H.Willner, D.Christen, H.Oberhammer, F.Aubke. *J. Am. Chem. Soc.*, **124**, 15385 (2002)
63. A.F.Wells. *Structural Inorganic Chemistry*. (Oxford: Clarendon Press, 1984)
64. G.W.Bethke, M.K.Wilson. *J. Chem. Phys.*, **26**, 1118 (1957)
65. J.Gebicki, J.Liang. *J. Mol. Struct.*, **117**, 283 (1984)
66. R.L.Timms. *J. Am. Chem. Soc.*, **89**, 1629 (1967)
67. T.R.Burkholder, L.Andrews. *J. Chem. Phys.*, **95**, 8697 (1991)
68. S.-D.Li, H.-J.Zhai, L.-S.Wang. *J. Am. Chem. Soc.*, **130**, 2573 (2008)
69. H.B.Gray. *Electrons and Chemical Bonding*. (New York: W.A.Benjamin, 1965)
70. D.L.Yeager, J.A.Nichols, J.T.Golab. *J. Chem. Phys.*, **97**, 8441 (1992)
71. F.Mélen, I.Dubois, H.Bredohl. *J. Phys. B*, **18**, 2423 (1985)
72. H.-J.Zhai, L.-M.Wang, S.-D.Li, L.-S.Wang. *J. Phys. Chem. A*, **111**, 1030 (2007)
73. M.Osiac, J.Röpcke, P.B.Davies. *Chem. Phys. Lett.*, **344**, 92 (2001)
74. K.A.Peterson, R.C.Woods. *J. Chem. Phys.*, **90**, 7239 (1989)
75. J.Baker, R.H.Nobes, L.Radom. *J. Comput. Chem.*, **7**, 349 (1986)
76. P.Pyykkö. *Mol. Phys.*, **67**, 871 (1989)
77. F.J.Lovas, D.R.Johnson. *J. Chem. Phys.*, **55**, 41 (1971)
78. B.J.Ransil. *Rev. Mod. Phys.*, **32**, 239 (1960)
79. S.Fraga, B.J.Ransil. *J. Chem. Phys.*, **36**, 1127 (1962)
80. R.K.Nesbet. *J. Chem. Phys.*, **40**, 3619 (1964)
81. W.M.Huo. *J. Chem. Phys.*, **43**, 624 (1965)
82. R.K.Nesbet. *J. Chem. Phys.*, **43**, 4403 (1965)
83. A.J.Sadlej. *Theor. Chim. Acta*, **47**, 205 (1978)
84. H.A.Kurtz, K.D.Jordan. *Chem. Phys. Lett.*, **81**, 104 (1981)
85. L.Laaksonen, D.Sundholm, P.Pyykkö. *Int. J. Quantum Chem.*, **27**, 601 (1985)
86. K.-Q.Zhang, B.Guo, V.Braun, M.Dulick, P.F.Bernath. *J. Mol. Spectrosc.*, **170**, 82 (1995)
87. F.Fantuzzi, Th.M.Cardozo, M.A.C.Nascimento. *J. Phys. Chem. A*, **119**, 5335 (2015)
88. Th.J.Tague Jr., L.Andrew. *J. Am. Chem. Soc.*, **116**, 4970 (1994)
89. L.B.Knight Jr., K.Kerr, P.K.Miller, C.A.Arrington. *J. Phys. Chem.*, **99**, 16842 (1995)
90. D.Scheschkewitz. *Angew. Chem., Int. Ed.*, **47**, 1995 (2008)
91. M.P.Mitoraj, A.Michalak. *Inorg. Chem.*, **50**, 2168 (2011)
92. A.Stoy, J.Böhnke, J.O.C.Jiménez-Halla, R.D.Dewhurst, T.Thiess, H.Braunschweig. *Angew. Chem., Int. Ed.*, **57**, 5947 (2018)
93. M.Arrowsmith, J.Böhnke, H.Braunschweig, M.A.Celik, Th.Dellermann, K.Hammond. *Chem. – Eur. J.*, **22**, 17169 (2016)
94. J.Böhnke, H.Braunschweig, Th.Dellermann, W.C.Ewing, Th.Kramer, I.Krummenacher, A.Vargas. *Angew. Chem., Int. Ed.*, **54**, 4469 (2015)
95. J.Böhnke, M.Arrowsmith, H.Braunschweig. *J. Am. Chem. Soc.*, **140**, 10368 (2018)
96. Ph.Bissinger, H.Braunschweig, A.Damme, Th.Kupfer, I.Krummenacher, A.Vargas. *Angew. Chem., Int. Ed.*, **53**, 5689 (2014)
97. H.Braunschweig, R.D.Dewhurst, Ch.Hörl, A.K.Phukan, F.Pinzner, S.Ullrich. *Angew. Chem., Int. Ed.*, **53**, 3241 (2014)
98. H.Braunschweig, Ch.Hörl. *Chem. Commun.*, **50**, 10983 (2014)
99. W.Lu, Y.Li, R.Ganguly, R.Kinjo. *J. Am. Chem. Soc.*, **139**, 5047 (2017)
100. W.Lu, Y.Li, R.Ganguly, R.Kinjo. *J. Am. Chem. Soc.*, **140**, 1255 (2018)
101. T.E.Stennett, J.D.Mattock, I.Vollert, A.Vargas, H.Braunschweig. *Angew. Chem., Int. Ed.*, **57**, 4098 (2018)
102. S.R.Wang, M.Arrowsmith, H.Braunschweig, R.D.Dewhurst, M.Dömling, J.D.Mattock, C.Pranckevicius, A.Vargas. *J. Am. Chem. Soc.*, **139**, 10661 (2017)
103. M.Zhou, Q.Xu, Z.-X.Wang, P.von R.Schleyer. *J. Am. Chem. Soc.*, **124**, 14854 (2002)
104. M.Zhou, N.Tsumori, Z.Li, K.Fan, L.Andrews, Q.Xu. *J. Am. Chem. Soc.*, **124**, 12936 (2002)
105. M.Zhou, L.Jiang, Q.Xu. *Chem. – Eur. J.*, **10**, 5817 (2004)
106. H.-S.Wu, H.Jiao, Z.-X.Wang, P.von R.Schleyer. *J. Am. Chem. Soc.*, **125**, 4428 (2003)
107. S.-D.Li, C.-Q.Miao, J.-C.Guo, G.-M.Ren. *J. Comput. Chem.*, **26**, 799 (2005)
108. H.Braunschweig, R.D.Dewhurst, K.Hammond, J.Mies, K.Radacki, A.Vargas. *Science*, **336**, 1420 (2012)
109. H.Braunschweig, Th.Dellermann, R.D.Dewhurst, W.C.Ewing, K.Hammond, J.O.C.Jimenez-Halla, Th.Kramer, I.Krummenacher, J.Mies, A.K.Phukan, A.Vargas. *Nat. Chem.*, **5**, 1025 (2013)
110. H.Braunschweig, Th.Dellermann, W.C.Ewing, Th.Kramer, Ch.Schneider, S.Ullrich. *Angew. Chem., Int. Ed.*, **54**, 10271 (2015)
111. H.Braunschweig, Ph.Constantinidis, Th.Dellermann, W.C.Ewing, I.Fischer, M.Hess, F.R.Knight, A.Rempel, Ch.Schneider, S.Ullrich, A.Vargas, J.D.Woollins. *Angew. Chem., Int. Ed.*, **55**, 5606 (2016)
112. L.J.Bellamy. *The Infrared Spectra of Complex Molecules*. (New York: Wiley, 1975)

113. J.Böhnke, H.Braunschweig, Th.Dellermann, W.C.Ewing, K.Hammond, J.O.C.Jimenez-Halla, Th.Kramer, J.Mies. *Angew. Chem., Int. Ed.*, **54**, 13801 (2015)
114. M.Arrowsmith, J.Böhnke, H.Braunschweig, M.A.Celik. *Angew. Chem., Int. Ed.*, **56**, 14287 (2017)
115. Ch.Hering-Junghans. *Angew. Chem., Int. Ed.*, **57**, 6738 (2018)
116. K.Müller-Dethlefs, P.Hobza. *Chem. Rev.*, **100**, 143 (2000)
117. S.Schulze, S.Köster, U.Geldmacher, A.C.T.van Scheltinga, W.Kihlbrandt. *Nature (London)*, **467**, 233 (2010)
118. D.A.Dougherty. *Acc. Chem. Res.*, **46**, 885 (2013)
119. R.Bertermann, H.Braunschweig, Ph.Constantinidis, Th.Dellermann, R.D.Dewhurst, W.C.Ewing, I.Fischer, Th.Kramer, J.Mies, A.K.Phukan, A.Vargas. *Angew. Chem., Int. Ed.*, **54**, 13090 (2015)
120. O.N.Temkin, R.M.Flid. *Kataliticheskie Prevrashcheniya Atsetilenovykh Soedinenii v Rastvorakh Kompleksov Metallov*. (Catalytic Transformations of Acetylenic Compounds in Solutions of Metal Complexes) (Moscow: Nauka, 1968)
121. H.Braunschweig, Th.Dellermann, R.D.Dewhurst, B.Hupp, Th.Kramer, J.D.Mattock, J.Mies, A.K.Phukan, A.Steffen, A.Vargas. *J. Am. Chem. Soc.*, **139**, 4887 (2017)
122. Ph.Bissinger, H.Braunschweig, A.Damme, Th.Kupfer, A.Vargas. *Angew. Chem., Int. Ed.*, **51**, 9931 (2012)
123. Ph.Bissinger, A.Steffen, A.Vargas, R.D.Dewhurst, A.Damme, H.Braunschweig. *Angew. Chem., Int. Ed.*, **54**, 4362 (2015)
124. A.K.Swarnakar, Ch.Hering-Junghans, M.J.Ferguson, R.McDonald, E.Rivard. *Chem. Sci.*, **8**, 2337 (2017)
125. T.Araki, M.Hirai, A.Wakamiya, W.E.Piers, Sh.Yamaguchi. *Chem. Lett.*, **46**, 1714 (2017)
126. X.-W.Li, W.T.Pennington, G.H.Robinson. *J. Am. Chem. Soc.*, **117**, 7578 (1995)
127. J.Su, X.-W.Li, R.C.Crittendon, G.H.Robinson. *J. Am. Chem. Soc.*, **119**, 5471 (1997)
128. Y.Wang, G.H.Robinson. *Chem. Commun.*, 5201 (2009)
129. Y.Xie, R.S.Grev, J.Gu, H.F.Schaefer III, P.von R.Schleyer, J.Su, X.-W.Li, G.H.Robinson. *J. Am. Chem. Soc.*, **120**, 3773 (1998)
130. N.Takagi, M.W.Schmidt, S.Nagase. *Organometallics*, **20**, 1646 (2001)
131. H.Grützmacher, T.F.Fässler. *Chem. – Eur. J.*, **6**, 2317 (2000)
132. R.J.Wright, M.Brynda, P.P.Power. *Angew. Chem., Int. Ed.*, **45**, 5953 (2006)
133. N.Wiberg, W.Niedermayer, G.Fischer, H.Noth, M.Suter. *Eur. J. Inorg. Chem.*, 1066 (2002)
134. A.Sekiguchi, R.Kinjo, M.Ichinohe. *Science*, **305**, 1755 (2004)
135. M.Takahashi, Y.Kawazoe. *Organometallics*, **27**, 4829 (2008)
136. M.Stender, A.D.Phillips, R.J.Wright, Ph.P.Power. *Angew. Chem., Int. Ed.*, **41**, 1785 (2002)
137. N.Takagi, S.Nagase. *Organometallics*, **20**, 5498 (2001)
138. A.D.Phillips, R.J.Wright, M.M.Olmstead, Ph.P.Power. *J. Am. Chem. Soc.*, **124**, 5930 (2002)
139. L.Pu, B.Twamley, Ph.P.Power. *J. Am. Chem. Soc.*, **122**, 3524 (2000)
140. D.E.Goldberg, P.B.Hitchcock, M.F.Lappert, K.M.Thomas, A.J.Thorne. *J. Chem. Soc., Dalton Trans.*, 2387 (1986)
141. N.Wiberg, H.-W.Lerner, S.-K.Vasisht, S.Wagner, K.Karaghiosoff, H.Nöth, W.Ponikwar. *Eur. J. Inorg. Chem.*, 1211 (1999)
142. H.Preut, F.Huber. *Z. Anorg. Allg. Chem.*, **419**, 92 (1976)
143. E.D.Jemmis, P.N.V.Pavan Kumar, N.R.Sreenivas Kumar. *J. Chem. Soc., Dalton Trans.*, 271 (1987)
144. D.Gau, R.Nougué, N.Saffon-Merceron, A.Baceiredo, A.De Cózar, F.P.Cossío, D.Hashizume, T.Kato. *Angew. Chem., Int. Ed.*, **55**, 14673 (2016)
145. Q.Zhang, W.-L.Li, L.Zhao, M.Chen, M.Zhou, J.Li, G.Frenking. *Chem. – Eur. J.*, **23**, 2035 (2017)
146. L.Pauling. *J. Am. Chem. Soc.*, **53**, 3225 (1931)
147. J.F.Berry. *Acc. Chem. Res.*, **49**, 27 (2016)
148. F.M.Bickelhaupt, A.Diefenbach, S.P.de Visser, L.J.de Koning, N.M.M.Nibbering. *J. Phys. Chem. A*, **102**, 9549 (1998)
149. D.K.Maity. *J. Phys. Chem. A*, **106**, 5716 (2002)
150. T.Drews, K.Seppelt. *Angew. Chem., Int. Ed. Engl.*, **36**, 273 (1997)
151. B.Cordero, V.Gómez, A.E.Platero-Prats, M.Revés, J.Echeverría, E.Cremades, F.Barragán, S.Alvarez. *Dalton Trans.*, 2832 (2008)
152. T.G.Castner, W.Känzig. *J. Phys. Chem. Solids*, **3**, 178 (1957)
153. V.S.Vavilov, N.A.Ukhin. *Radiatsionnye Defekty v Poluprovodnikakh i Poluprovodnikovykh Priborakh*. (Radiation Defects in Semiconductors and Semiconductor Devices) (Moscow: Atomizdat, 1969)
154. F.A.Cotton, M.Matusz, R.Poli, X.J.Feng. *J. Am. Chem. Soc.*, **110**, 1144 (1988)
155. J.F.Berry, E.Bothe, F.A.Cotton, S.A.Ibragimov, C.A.Murillo, D.Villagrán, X.Wang. *Inorg. Chem.*, **45**, 4396 (2006)
156. J.F.Berry, E.Bill, E.Bothe, F.A.Cotton, N.S.Dalal, S.A.Ibragimov, N.Kaur, C.Y.Liu, C.A.Murillo, S.Nellutla, J.M.North, D.Villagrán. *J. Am. Chem. Soc.*, **129**, 1393 (2007)
157. E.C.Brown, J.T.York, W.E.Antholine, E.Ruiz, S.Alvarez, W.B.Tolman. *J. Am. Chem. Soc.*, **127**, 13752 (2005)
158. S.Alvarez, R.Hoffmann, C.Mealli. *Chem. – Eur. J.*, **15**, 8358 (2009)
159. K.Isobe, Y.Ozawa, A.V.de Miguel, T.-W.Zhu, K.-M.Zhao, T.Nishioka, T.Ogura, T.Kitagawa. *Angew. Chem., Int. Ed. Engl.*, **33**, 1882 (1994)
160. T.Nishioka, H.Kitayama, B.K.Breedlove, K.Shiomi, I.Kinoshita, K.Isobe. *Inorg. Chem.*, **43**, 5688 (2004)
161. X.Zheng, X.Wang, Z.Zhang, Y.Sui, X.Wang, Ph.P.Power. *Angew. Chem., Int. Ed.*, **54**, 9084 (2015)
162. R.Hoffmann, W.Alder, C.F.Wilcox. *J. Am. Chem. Soc.*, **92**, 4992 (1970)
163. V.I.Minkin, R.M.Minyaev, R.Hoffmann. *Russ. Chem. Rev.*, **71**, 869 (2002)
164. J.-H.Huang, J.J.Luci, T.-Y.Lee, D.C.Swenson, J.H.Jensen, L.Messerle. *J. Am. Chem. Soc.*, **125**, 1688 (2003)
165. X.Li, H.-F.Zhang, L.-S.Wang, G.D.Geske, A.I.Boldyrev. *Angew. Chem., Int. Ed.*, **39**, 3630 (2000)
166. V.A.Starodub, D.V.Ziolkovskii. *J. Struct. Chem.*, **47**, 8 (2006)
167. G.D.Geske, A.I.Boldyrev. *Inorg. Chem.*, **41**, 2795 (2002)
168. R.Keese. *Chem. Rev.*, **106**, 4787 (2006)
169. Z.-h.Cui, V.Vassilev-Galindo, J.L.Cabellos, E.Osorio, M.Orozco, S.Pan, Y.-h.Ding, G.Merino. *Chem. Commun.*, 138 (2017)
170. P.R.Remyaab, C.H.Suresh. *Dalton. Trans.*, **45**, 1769 (2016)
171. O.Yanez, A.Vásquez-Espinal, R.Pino-Rios, F. Ferraro, S.Pan, E.Osorio, G.Merino, W.Tiznado. *Chem. Commun.*, **53**, 12112 (2017)
172. E.Lewars. *Can. J. Chem.*, **97**, 154 (2019)
173. A.C.Castro, M.Audiffred, J.M.Mercero, J.M.Ugalde, M.A.Méndez-Rojas, G.Merino. *Chem. Phys. Lett.*, **519 – 520**, 29 (2012)
174. D.W.O.de Sousa, M.A.C.Nascimento. *Acc. Chem. Res.*, **50**, 2264 (2017)
175. A.Brown, P.D.Beer. *Chem. Commun.*, **52**, 8645 (2016)
176. L.Brammer. *Faraday Discuss.*, **203**, 485 (2017)
177. L.-M.Yang, E.Ganz, Z.Chen, Z.-X.Wang, P.von R.Schleyer. *Angew. Chem., Int. Ed.*, **54**, 9468 (2015)
178. P.Pyykko. *Chem. Rev.*, **88**, 563 (1988)
179. P.Pyykko. *Annu. Rev. Phys. Chem.*, **63**, 45 (2012)
180. H.Schwarz. *Angew. Chem., Int. Ed.*, **42**, 4442 (2003)
181. G.Moreno-Alcántar, G.Romo-Islas, M.Flores-Álamo, H.Torrens. *New J. Chem.*, **42**, 7845 (2018)